Design and Installation of Precast Ultra-High Performance Fiber Reinforced Jackets for Seismic Retrofitting Concrete Piers

Roberto Salazar Gonzalez

A Thesis Submitted to the Faculty of Graduate Studies

in Partial Fulfillment of the Requirements

for the Degree of Master of Applied Science

Graduate Program in Civil Engineering

York University

Toronto, Ontario

January 2025

©Roberto Salazar, 2025

Abstract

Ultra-high performance fiber-reinforced concrete (UHPFRC) has emerged in the last decade as a new alternative material for retrofitting reinforced concrete structures such as buildings and bridges. One of the most common applications of UHPFRC today is restoring bridge decks and construction joints. UHPFRC can also be applied to the retrofit of principal structural components, such as beams and columns. Decks are repaired by the addition of UHPFRC overlays, whereas columns can be retrofitted with UHPFRC by applying a new layer on the original cross-section, or by removing the concrete cover and replacing it with UHPFRC. This technique is known as jacketing, and it is an attractive solution due to the outstanding mechanical properties of UHPFRC and the fact that the retrofit may be limited to the length of the critical regions and does not have to cover the total height of the column. Specifically, with regards to UHPFRC Jacketing, research on UHPFRC has been conducted when used as a cast-in-place solution. In this research, UHPFRC jacketing is studied as a seismic retrofit alternative, to quantify the jacket's contribution to the various mechanisms of resistance (flexure, shear, reinforcement anchorage capacity, and the confinement effectiveness of the jacket in enhancing the strength and deformation capacity of encased concrete). With confinement effectiveness being the primary knowledge gap, the study included an extensive experimental component, where rectangular concrete prisms modeling concrete columns were jacketed with precast UHPFRC jackets. The objective of the experimental study was to test the proof of concept of jacketing with precast jackets made of UHPFRC, and to also shed light on the contribution of the jackets to the deformation capacity of encased concrete in order to quantify the jacket's effectiveness. As part of the research, the method of connection of the jacket segments and characterization of the materials were designed and optimized through testing. Two possible connectors were designed and tested, providing good results. Several columns were tested under monotonic and cyclic loading, after assembling the precast jackets designed and fabricated for the needs of the study. Parameters of investigation included two jacket thicknesses (i.e. 25 mm and 37.5 mm), the type of connectors between precast components, the loading method (monotonic or cyclic compression load on the encased concrete) and the method of jacketing (cast in situ vs. attaching precast jackets). Finite element modeling was included to understand the lateral resistance to dilation of the encased concrete imparted by the jackets. The

deformation capacity of the columns was enhanced substantially . The findings in this research aim to provide a valuable understanding of UHPFRC as a retrofit solution in the form of jacketing.

Acknowledgments

First of all, I would like to thank my supervisor Dr. Stavroula Pantazopoulou for her patience, teachings, guidance and continuous support for the last two years during my master's program. This thesis could not have been possible without your expertise, encouragement and constant feedback. I am truly grateful for all the time you invested in reviewing my research. This has been by far the most demanding two years of my life. It has been an honor to be your student.

My sincere appreciation goes to my professor and committee member Dr. Liam J. Butler; your comments and feedback were always accurate and constructive, especially in the experimental program. I want to thank Ms. Sindy Mahal for her essential support during these two years, being there to assist me more than once. I want to express my gratitude to the professors from the Civil Engineering Department at York University for their valuable feedback.

Gratitude also goes to my friends and colleagues from York University, with whom I shared laughs, tears, pizzas, coffees and lots of after-hours in the lab. This research would not have been possible without Buddhi Daraniyagala Arachchilage, Sandi Abdelrehim, Farah Dameh and Zoi Ralli. I am sincerely grateful for the assistance of Riad Rajab and Kunjan Rupakheti, our lab technicians, that made it possible for me more than once. Furthermore, I want to thank my friends Mena Morcos, Marco Calcagno, Austin Martins and Mario Antoun for their help. Special thanks to Inner Sun, Tool, Soen, Bon Jovi, Sodom, Death, Iron Maiden and so many others that made my typing and lab days better. There are also many Latin friends I have made along the way that I want to thank, always been there for me when I needed them.

I am extremely grateful for the support of my spouse Merian Vargas. Meri, you have been my support, energy, and strength even before coming to Canada. There is no better partner than you. I could not have done this thesis without you. Thank you for being here with me, and especially for believing in me all this time.

Last but not least, special thanks to my family back in Costa Rica, starting with my parents, Patricia and Fernando who had always supported and pushed me to achieve my goals. Thanks to both my sisters, Adiana and Silvia, for their guidance and constant support. I think about you all every day.

Table of Contents

Abstract ii

Acknowledgments iv

Table of Contents v

List of Tables ix

List of Figures x

Chapter 1: Introduction 1

1.1 Background 1

1.2 Brief Introduction to Precast Jacketing with UHPFRC 4

1.3 Objectives and Scope of the Thesis 5

1.4 Thesis Structure 7

Chapter 2: Literature Review 10

2.1 UHPFRC Properties 10

2.1.1 Compression Strength 12

2.1.2 Tensile Strength 14

2.1.3 Flexure Strength 15

2.1.4 Modulus of Elasticity 15

2.2 UHPFRC Jackets as a Retrofit Material 16

2.3 Review of Experimental Evidence on Columns Jacketed with UHPFRC 17

2.3.1 Performance of Experimental Evidence: Jacket Index 21

2.4 Alternative Arrangements of UHPFRC Jacketing Systems 23

2.4.1 Comparison of Performance of the Retrofit Schemes Presented in Figure 2.8 24

2.4.2 Gaps of the Research 26

Chapter 3: Modelling of Jacket Contribution 27

3.1 Confining Pressure, Strength, and Deformation Capacity of Encased Concrete 28

3.2 Contribution of the UHPFRC Jacket to Flexural, Shear and Lap Splice Strength 31
3.2.1 Flexural Strength Increase 31
3.2.2 Shear Strength Increase of the Jacketed Column.. 34
3.2.3 Lap Splice Strength.. 35
3.3 Limitation of the Deformation Capacity of Jackets Bearing on the Footing...................... 38
3.4 Flexure-Dominated Response.. 38
3.5. Recommended Performance Limits for Retrofit Design with UHPFRC Jackets 39
Chapter 4: Material Testing for Characterization of UHPFRC Mix... 42
4.1 Introduction.. 42
4.2 Materials and Casting 42
4.3 Mechanical Tests 45
4.3.1 Compression Test.. 45
4.3.2 Modulus of Elasticity and Poisson’s Ratio 47
4.3.3 Stress-Strain Behaviour in Uniaxial Compression 49
4.3.4 Direct Tension Test.. 51
4.4 Results.. 55
Chapter 5: Experimental Program for Retrofitted Columns with Precast UHPFRC Jackets and Connection Devices 56
5.1 Introduction... 56
5.2 Optimization of the Connection Device Geometry for the Precast Jacket 56
5.2.1 Finite Element Analysis for the Connection Device Geometry.................................. 56
5.2.2 Preliminary Key Specimens... 61
5.2.3 Precast curved UHPFRC key with 10M rebar... 68
5.2.4 Cast-in Place Lap Splice Key 71
5.3 Casting the Unreinforced Rectangular Concrete Column Specimens 74

5.4 Precast UHPFRC Jacket Fabrication 76
5.4.1 Precast C-Shaped UHPFRC Jackets for Lap Splice Connection 78
5.4.2 Precast C-Shaped UHPFRC Jackets for Precast Curved Key 79
5.4.1 Precast C-Shaped UHPFRC Jackets for Flexure Testing 80
5.5 Assembly of Retrofitted Columns 81
5.5.1 Retrofitted Column with Cast-in-Place Jacket 82
5.5.2 Retrofitted Columns with Precast UHPFRC Jacket with Curved Key 83
5.5.3 Retrofitted Columns with Precast UHPFRC Jacket and Lap Splice Connection 84
5.6 Testing the Retrofitted Columns with the UHPFRC Precast Jackets 86
5.6.1 Retrofitted Columns - Monotonic Tests 87
5.6.2 Retrofitted Columns - Cyclic Tests 98
5.7 Mechanical Interaction on Retrofitted Columns 105
5.7.1 Sandwich Specimen for Interlocking Testing 105
Chapter 6: Finite Element Modelling of Columns with Precast UHPFRC Jackets 108
6.1 3-D Column Model 108
6.1.1 Model Geometry and Boundary Conditions 108
6.2 Material Properties for 3-D Column Models 110
6.3 Results from the 3D Column Models 112
6.4. Cast-in Place Results 115
Chapter 7: Summary and Conclusions 117
7.1 Mechanical Properties 118
7.1.1 Cylinder Compression Strength Tests 118
7.1.2 Direct Tension Testing for CEK2 118
7.1.3 Direct Tension Testing for Connection Devices 119
7.1.4 Flexural Testing for Precast C-Shapes 119

7.2 Database of UHPFRC Jackets & Modelling of the Jacket Contribution 120

7.3 Precast UHPFRC Jackets for Retrofitting Concrete Columns... 121

7.4 Finite Element Models.. 122

7.5 Recommendations and Future Work 122

References.. 125

List of Tables

Table 2.1. Empirical relationships for Modulus of Elasticity of UHPFRC (adapted from Ismail, 2023 ... 16

Table 2.2. Specimens and references for C-Specimens and R-Specimens collected from literature. ... 18

Table 4.1. Mix design proportions of the UHPFRC Mix *CEK2* ... 43

Table 4.2. Compressive strength results for CEK2. ... 47

Table 4.3. Modulus of Elasticity and Poisson's ratio obtained data. ... 48

Table 4.4. Compressive strength vs strain results (CEK Mix). ... 51

Table 4.5. Results of direct tension testing for CEK2. ... 53

Table 5.1. Shell stresses for the different key geometries for given applied lateral force. ... 60

Table 5.2. Direct tension data for the curved UHPFRC keys with 10M rebars. ... 70

Table 5.3. Direct tension data for the lap splice specimens. ... 73

Table 5.4. Mix design proportions for column concrete mix. ... 75

Table 5.5. Testing scheme for the retrofitted columns. ... 76

Table 5.6. Flexural capacity of the precast C-Shaped UHPFRC jacket specimens. ... 81

Table 5.7. Compressive strength results of material cube or cylinder samples during monotonic and cyclic loading. ... 87

Table 5.8. Summary of Retrofitted Columns under Monotonic Tests. ... 87

Table 5.9. Summary for all the monotonic loading tests performed on seven Retrofitted Columns. ... 96

Table 5.10. Summary of Retrofitted Columns under Cyclic Tests. ... 98

Table 5.11. Cyclic loading regime programmed on *Controls Pilot*. ... 99

Table 5.12. Summary for all the cyclic loading tests performed on six Retrofitted Columns. . 103

Table 6.1. Model geometry details for 3-D ATENA GiD ® models. ... 109

Table 6.2. Main mechanical properties used for the *SOLIDConcrete* materials for models. 112

Table 6.3. Monitor points used for recording displacements data. ... 114

Table 6.4. Stresses in the YY direction of the Cast-in Place Model. ... 116

List of Figures

Figure 1.1. Different UHPFRC applications around the world:(a,b,c,d,e) Bridges (f) Facade (Azmee & Shafiq. 2018; Amran et al., 2022). 5

Figure 2.1.Tensile stress-strain diagrams for: a) THFRC and b)TSFRC (Fig U3, reproduced from Annex U of CSA-A23.1). 11

Figure 2.2. Classification and behavior of UHPFRC (adapted from Naaman & Reinhardt, 2006). 12

Figure 2.3.Compression model for UHPFRC (Ismail et al., 2022) 13

Figure 2.4. Envelope curves for THFRC in a) tension; b) compression (Wu et al. 2016) (adapted from Ismail, 2023) 15

Figure 2.5. Details of a) C- and b) R-Specimens, regarding parameters and experimental configuration (adapted from Ralli et al., 2024)... 18

Figure 2.6. Drift capacity and milestone points of the response curve used in the Database...... 21

Figure 2.7. Ultimate drift ratio of (a) C-; (b) R-Specimens plotted against J_i and C_i. 22

Figure 2.8. Possible arrangement of UHPFRC Jackets and developed stresses: (a) Gap between footing and jacket, (b) Cold joint between footing and jacket, and (c) Extension of Jacket into the footing; (d) State of stresses in the Jacket in case (a); (e) Stresses on the jacket in the compression zone of case (b); (e and f) Stresses in the jacket in the compression and tension zone of case (c) (adapted from Ralli et al., 2024).. 24

Figure 2.9. (a) Moment-Curvature; (b) Lateral Load-Drift responses of the retrofitted column using the jacket arrangements of Figure 2.7 for axial load ratio v=0.1. The NJ curves cannot be realized after lap splices failures shown by the dashed line in the left. 25

Figure 2.10. (a) Moment-Curvature; (b) Lateral Load-Drift responses of the retrofitted column using the jacket arrangements of Figure 2.7 for axial load ratio v=0.2. The NJ curves cannot be realized after lap splices failures shown by the dashed line in the left. 25

Figure 3.1. Definition of the confining pressure exerted by the UHPFRC Jackets on encased concrete: (a) Circular and (b) Rectangular encased cross sections, (c) effectively confined region and definition of terms. 28

Figure 3.2. (a) Flexural resistance provided by the jacket near failure (after formation of localized crack) affects the rate of post-peak degradation of the encased concrete stress-strain response; (b), (c) Crack pattern in experimentally tested jacketed short columns (Tsiotsias, 2024). 29

Figure 3.3. Circular jacketed cross section – equilibrium of forces at yielding. (a) Cross section, (b) lengthwise slices of length dy: left before jacketing, and right after jacketing. 32

Figure 3.4. Rectangular jacketed cross section – equilibrium of forces at yielding. (a) Cross section, (b) lengthwise slices of length *dy*: left before jacketing, and right after jacketing.......... 32

Figure 3.5. Normalized depth of compression zone against longitudinal reinforcement ratio for v=0.1 and v=0.2, in the original state and after jacketing with the nuanced setups of Figure 2.8.34

Figure 3.6. Models for estimation of the contribution of the UHPFRC Jacket to (a) flexural and (b) shear strength for Figure 2.8 (b) and 2.8 (c); (c) Kinematic relationship between slip of tension bars and compressive strain increment in the jacket. 35

Figure 3.7. (a) Anchorage strain ductility capacity versus the required anchorage length for steel category S500, two values for hardening modulus (Esh=1% and 5% of Es=200GPa), five concrete strengths (fc'=12, 16, 20, 25, 30 MPa) and two bond conditions (Good bond conditions: fb max=2.5√fc'(MPa); All other bond conditions: fb max=1.25√fc'(MPa)). 37

Figure 3.8. Behavior of flexural strength as V_{peak}/V_{flex} of all specimens against the geometric Jacket Index J_i (%). 39

Figure 3.9. Performance limit states in retrofitting systems with UHPFRC Jackets. 40

Figure 4.1. An illustrative flowchart of the UHPFRC CEK2 mixing procedure. 43

Figure 4.2. UHPFRC CEK2 flow test. 44

Figure 4.3.CEK2 specimens immediately after casting. 45

Figure 4.4. Specimen surface detail with acrylic smooth plate on top (adapted from Development of Alternative Test for Tensile Characterization of UHPC, Ralli, 2024). 45

Figure 4.5. Compressive strength test setup. 46

Figure 4.6. (a) Cylindrical specimens after testing, (b) specimen setup with strain gauges....... 49

Figure 4.7. Stress-Strain response of cylinders in uniaxial compression (CEK2 Mix). 50

Figure 4.8. Direct tension specimen setup ready for testing in the MTS.................................. 51

Figure 4.9. Stress-Strain Response for the direct tension prismatic specimens.......................... 54

Figure 4.10. Cracking Pattern for the prismatic direct tension specimens. 54

Figure 5.1. Initial sketches for (a) the retrofitted concrete column jacketed with independent horizontal strips, and (b) the geometry of the key. 57

Figure 5.2. Finite element analysis for the (a) & (d) *Y* geometry, (b) & (e) *T* geometry, and (c) & (f) *dogbone* geometry in SAP2000. All dimensions in mm.. 58

Figure 5.3. Different material properties were applied to the three geometry models. 59

Figure 5.4. Stress-Strain curve for the UHPFRC used in SAP2000 for the key models. 59

Figure 5.5. Stress distribution along the *dogbone* geometry perimeter. 60

Figure 5.6. Initial *dogbone* key dimensions for the (a) UHPFRC key and (b) mild steel key. All dimensions in mm with a 15 mm thickness.. 61

Figure 5.7. Preliminary stage of the key preparation involving (a) an in-house 2 L mixer, (b) steel molds for the keys, (c) the first keys created, (d) the first UHPFRC precast jacket shell, and (e) the first key assembly. 62

Figure 5.8. Improving the alignment to the first UHPFRC key and UHPFRC jacket shells by (a) & (b) adding 3D inserts, (c) placing the keys, and (d) securing the keys with *Sikadur* ® epoxy. 63

Figure 5.9. The first set of UHPFRC keys (a) before testing, (b) & (c) after peak. 63

Figure 5.10. A third set of UHPFRC keys (a) incorporating a 125 mm threaded, (b) ready to place on the UHPFRC jacket shell and (c) & (d) specimens ready for direct tension testing, (e) & (f) after peak load.. 64

Figure 5.11. Fourth set of (a) curved UHPFRC keys with 10 M rebar, (b) fourth set of precast UHPFRC jacket shell.. 65

Figure 5.12. Direct tension specimen setup for the fourth and Lap Splice specimens for testing in the MTS. 66

Figure 5.13. Fourth set of UHPFRC keys (a) specimens ready for direct tension testing (b) & (c) mode of failure. 67

Figure 5.14. Mild steel key specimen tested under direct tension in MTS machine. 68

Figure 5.15. Fifth set of (a) & (b) round head curved UHPFRC keys with 10 M rebar, (c) fifth set of precast UHPFRC jacket shell specimen. 69

Figure 5.16. Fifth curved UHPFCR key specimen (a) ready for testing, (b) & (c) & (d) mode of failure after testing for CKT1, CKT2, and CKT3 respectively. 70

Figure 5.17. Direct tension testing for curved UHPFRC key with 10M rebar specimens. 70

Figure 5.18. Lap Splice key specimen sketch. 71

Figure 5.19. Lap Splice Specimens (a), (b) & (c) lab production and (d) final specimens. 72

Figure 5.20. Lap splice specimens (a) ready for testing and (b), (c) & (d) after testing. 73

Figure 5.21. Direct tension testing for curved UHPFRC key with 10M rebar specimens. 73

Figure 5.22. (a) Column molds before casting, (b) columns after casting, (c) columns in the curing tank, and (d) concrete cylinder tested at 28 days of age. 75

Figure 5.23. C-shaped inserts used to create the precast C-shaped UPHFRC jackets (a) without and (b) with a layer of large 5/16 in bubble wrap. These "chairs" with the bubble wrap were placed inside the steel molds in order to formulate the precast jacket components as depicted in Fig. 5.24. 77

Figure 5.24. Precast C-Shaped UHPFRC Jackets for Lap Splice Solution (a) & (b) preparation, (c) & (d) after demolding. 79

Figure 5.25. Precast C-Shaped UHPFRC Jackets for Precast Curved Key (a) & (b) preparation, (c) & (d) after demolding. 80

Figure 5.26. C-Shaped UHPFRC Jackets (a) setup and (b), (c) & (d) after flexure testing. 81

Figure 5.27. White Kilz primer used for coating the specimen's surfaces and Rust-Oleum black spray used for speckles. 82

Figure 5.28. Final Retrofitted Columns with Cast-in-Place UHPFRC Jacket (a) fabrication and (b) & (c) specimens prior to painting. 83

Figure 5.29. Retrofitted Columns with Precast UHPFRC Jackets and Curved Key (a) & (b) when pouring the non-shrink grout and (c) the specimens prior to painting.. 84
Figure 5.30. Retrofitted Columns with Precast UHPFRC Jackets and Lap Splice Connection (a) prior to pouring the UHPFRC 3%, (b) & (c) prior to pouring the non-shrink grout, and (c) the final specimens before painting.. 85
Figure 5.31. Steel loading plates used on top and bottom of the Retrofitted Columns. 86
Figure 5.32. Set up for monotonic testing when testing (a) C4 specimen with all instrumentation, (b) C13 specimen with the instrumentation, and (c) bottom steel plate placed below column. ... 88
Figure 5.33. Scheme showing the position of the instruments relative to the top and bottom plate of the Controls ® when (a) testing the Cast-in Place Retrofitted Columns and (b) the remaining Retrofitted Columns.. 89
Figure 5.34. Specimen C4, cast-in place UHPFRC Jacket, after testing. 90
Figure 5.35. Specimen C6, precast UHPFRC Jacket with Curved Key, after testing. 91
Figure 5.36. Specimen C13, precast UHPFRC Jacket with Curved Key, after testing. 92
Figure 5.37. Specimen C12, precast jacket with Lap Splice Connection, after testing. 92
Figure 5.38. Rotation of specimen C8 due to dimensions and space limitations. Only DTs were place on the front and back face of the Retrofitted Column, the LVDTs remain in position....... 93
Figure 5.39. Specimen C8, cast-in place jacket, after testing. 93
Figure 5.40. Specimen C11, precast jacket with curved key, after testing. 94
Figure 5.41. Specimen C1, precast jacket with lap splice connection, after testing. 95
Figure 5.42. Stress-strain curves for the seven Retrofitted Columns under monotonic loading tests. 96
Figure 5.43. Stress-strain curves for the uniaxial compression for NSC1 and NSC2. 97
Figure 5.44. Stress-Strain of all monotonic test compared to the NCS results. 97
Figure 5.45. NSC1 and NSC2 after being tested in uniaxial compression. 97
Figure 5.46. Specimen C7, cast-in place jacket, after testing. 100
Figure 5.47. Specimen C5, cast-in place jacket, after testing. 100
Figure 5.48. Specimen C3, precast jacket with Lap Splice connection, after testing. 101

Figure 5.49. Specimen C10, cast-in place jacket, after testing. 101

Figure 5.50. Specimen C9, precast jacket with curved key, after testing. 102

Figure 5.51. Specimen C2, precast jacket with Lap Splice Connection, after testing. 103

Figure 5.52. Stress-strain curves for the six Retrofitted Columns under cyclic loading tests. .. 104

Figure 5.53. Stress-strain curves of all cyclic tests compared to the NSC results. 104

Figure 5.54. Sandwich Specimens for interlocking testing. 106

Figure 5.55. Results for the Sandwich Specimens for interlocking testing……………………106

Figure 5.56. Sandwich Specimens after testing under axil load at the top surface of the non-shrink grout………………………………………………………………………………….... 107

Figure 6.1. Outline of 3-D model and layer details of the Final Retrofitted Column Model (a) with the precast UHPFRC curved key, (b) with the lap splice connection and (c) cast-in place alternative. 109

Figure 6.2. Location of monitor points on the 3-D models to capture displacements for (a) the precast UHPFRC curved key, (b) the lap splice connection and (c) cast-in place alternative. .. 113

Chapter 1: Introduction

1.1 Background

Reinforced concrete (RC) is one of the most commonly used materials in civil engineering. We have been relying on RC structures, such as buildings and bridges, for many decades now due to the versatility and strength that concrete provides. However, there is a large number of older bridges and buildings that are considered substandard in terms of seismic resistance owing to lack of reinforcement detailing. Brittle behavior marked by inadequate resistance in shear and in lap splices due to sparse stirrups is compounded by environmental impact, aging and use of older versions of building codes in existing structures. Different jacketing techniques with various confining methods have always been a method of preference in retrofitting columns and piers. Those techniques started by incorporating additional layers of normal strength reinforced concrete, leading to larger cross-sectional areas, by encasing the original cross section of the pier. An alternative was achieved with the introduction of fiber-reinforced polymers (FRP) jackets in the late 1990s which was hailed for the advantages it brought (no change in geometry, very effective in enhancing ductility), however, several issues have been raised with regards to durability of these retrofits. Proper surface preparation is crucial for effective bonding between the FRP and the concrete. Inadequate surface preparation can lead to poor adhesion, which compromises the effectiveness of the retrofit. While FRP materials are generally durable, they can be susceptible to environmental degradation over time, especially when exposed to UV radiation, fire conditions, moisture, and temperature fluctuations. A new and emerging material of choice today for jacketing retrofit techniques is the Ultra-High Performance Fiber Reinforced concrete (UHPFRC). Its material properties include high compressive strength, ductility and durability, with the ability to support tension in the hoop direction of the jacket even beyond cracking.

UHPFRC is an ideal solution in retrofitting through jacketing of concrete members, because it provides significant durability to the retrofit owing to its low permeability and high density; it combines the advantage of not significantly altering the geometrical dimensions of the encased member, because based on experimental evidence, it can be a very effective solution even when used in very thin layers. It can be used on main structural members such as bridge piers and girders. Several other jacketing options can be found and further explored. Those include normal concrete jacketing by adding a layer that may involve removing the existing cover; steel plate jacketing by encasing the cross-section with steel plates (often welded or bolted together); fiber-reinforced polymer (FRP) jacketing in strips or sheets made of materials such as carbon, glass or aramid fibers; prestressed jacketing that combines concrete with prestressed tendons; shotcrete jacketing (sprayed concrete); all any hybrid method combing the above techniques mentioned.

UHPFRC has been used for the last few years primarily for repairing and enhancing bridge decks, joints and rehabilitation works in many structural members (*Yang et al. 2021, Doiron 2017*). Even though UHPFRC has been known to possess outstanding material properties, its use is not yet supported by sufficient clauses on the current design code (*Islam 2022).* It is noted that when using UHPFRC for new designs, the required cross sectional of the member may be significantly reduced due to its high strength and the limited amount of design transverse reinforcement due to the fiber content and the bridging effect (*Hu et al. 2020*). Because the tensile properties of UHPFRC are essential in the design, the most critical question in current related research is the dependable tensile strength and strain capacity of the material when cast under controlled conditions and how much reduced these properties are when the material is cast in the field. Several researchers have conducted experiments for the characterization of the mechanical and durability properties of UHPFRC to fully understand its behavior, which involves a complex setup for direct tension testing as well as bending testing (Del Zoppo et al., 2021; Farzad et al., 2019; Graybeal, 2014; Mohammed, 2023). Field application is accounted for, usually, by introducing attenuation factors to the values obtained by the characterization experiments; this is in acknowledgement of the fact that in field application, fiber orientation, which is responsible for the materials' resilience in tension, is not optimally controlled as it would be in the lab. In addition, casting of UHPFRC in the field is not always easy, as it requires special mixing equipment, and leak-tight formwork particularly when the material needs to be cast in thin layers, because in such conditions it must be particularly flowable. To address these practical difficulties, precasting of the required UHPFRC elements is a promising alternative. For example developing precast jacketing elements for columns appears to be a practical solution to the need of onsite casting of very thin layers not exceeding 2 inches over the side face of a column. To develop this solution a number of practical details need to be addressed: these include the following: (a) Casting of precast elements in sizes that can be handled during assembly (b) Addressing the bonding requirement between the added jacket components and the encased members; (c) providing the details of connectivity between precast elements so that the jacket may develop their tensile and compressive strengths.

In the present thesis jacketing with thin layers of UHPFRC is explored first by analyzing the available experimental evidence, with the objective to determine the effects of this method of retrofit, on the overall member response. It is found that a critical unknown is the effectiveness of the jacket confining pressure in enhancing the deformation (axial compressive strain) capacity of the encased concrete. Expressions are developed and tested against the collective database of available experiments for strength in flexure, shear, and anchorage of the embedded column reinforcement when subjected to lateral load resembling seismic action. UHPFRC's exceptional behavior has become a topic of increasing interest in research for the last couple of decades, with a notable body of knowledge already in published literature (Farzad et.al., 2019; Yuan et.al., 2021; Yuan et.al., 2022; Zhou et.al., 2023; Zohrevand et.al., 2010; Aviram et.al., 2014; Chan et.al., 2020; Guan et.al., 2021; Hung et.al., 2021; Guan et.al., 2021; Reggia et.al, 2020, 2020; Li et.al., 2017; Tong et.al., 2018; Del Zoppo et.al., 2018; Pereiro Barcelo et.al., 2021; Cho et.al., 2012; Ichikawa et.al., 2016; Tsiotsias et.al., 2024; Hong et.al., 2021; Habel et.al., 2018; Shao et.al., 2021; Wang et.al., 2022; Zhang et.al., 2022; Tian et.al., 2021; Del Zoppo et.al., 2021; Dagenais et.al., 2017)). The published literature used in this research is summarized in Table 2.2.

To understand the concept of UHPFRC jacket components, an experimental study is undertaken to develop a complete solution for design, fabrication, application and assessment of this UHPFRC-jacket retrofit for columns. An objective of the proposed research is to develop all the essential elements of a new type, precast jacket that may be post-installed for strengthening or repair on the lateral surface of rectangular columns. The work presented encompasses the design of the connectors, application procedures to ensure adequate interaction and proof of concept. Thin UHPFRC precast jackets reinforced with 2 percent fiber content are considered in the proof of concept study. The confinement effectiveness of the retrofit solution is gauged by the increase in strength and deformation capacity of the encased concrete. The experimental program considered two different jacket layer thicknesses (of 25mm and 37.5mm). While the tensile strength of conventional concrete is neglected, UHPFRC jackets as precast elements are an attractive and innovative retrofit technique because they have high tensile strength – over 9 MPa, which enables them to support very large levels of tensile strain, and may accelerate the process for restoring important structural characteristics. A total of thirteen column tests are conducted, where, apart from jacket thickness, a parameter of study was the connector installed to join the jacket components and the type of axial loading applied (monotonic to failure or cyclic). Results are explored with particular emphasis on the effectiveness of jacket confinement on the strength and deformation capacity of the encased concrete, so as to provide necessary data for future development of pertinent confinement models.

1.2 Brief Introduction to Precast Jacketing with UHPFRC

Ultra-high-performance fiber-reinforced concrete (UHPFRC) is an emerging composite material that has gained increasing popularity in civil engineering construction, specifically to restore bridge decks and construction joints. However, its use can easily be expanded to the retrofit of structural members due to its favorable characteristics. UHPFRC possesses very high compressive strength, durability, impermeability and post-peak ductility due to the dense fiber distribution. The behavior of the descending branch in the post-peak region engages effective crack bridging mechanisms caused by the fiber reinforcement. UHPFRC is described in the Annex 8.1 of CSA S6 (2019) as a "*cementitious material with enhanced compressive strength and durability compared to high performance concretes and having a minimum compressive strength of 120 MPa".* In addition, UHPFRC is classified as *tension-hardening* (TH) or *tension-softening* (TS) according to Annex U of CSA A23.1 (2019). In the present study, only TH materials are considered on account of their inherent ductility.

UHPFRC is a concrete mixture that contains fine aggregate (sand), silica fume, slag, ground quartz, Portland cement, a water-reducer admixture known as superplasticizer, water (in lower water/cement ratios than conventional concrete) and fibers. Since the early 1990's, UHPFRC has become popular among civil engineering applications for restoration and retrofitting concrete structures such as bridge decks and construction joints. The first bridge to be constructed with UHPFRC in Canada is the Sherbrooke pedestrian bridge in 1999 (Blais et at., 1999). After it, more applications followed across the world, for example, France, Germany, South Korea, Switzerland, Czech Republic and USA. UHPFRC can be used also in seismic engineering for repairing concrete columns, bridge piers, architectural elements, hydraulic components and power plant facilities (Azmee et at., 2018). Some of these UHPFRC structural and non-structural applications are shown in Figure 1-1.

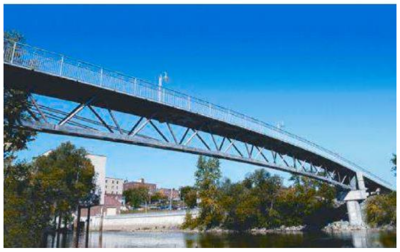

(a) Sherbrooke Pedestrian Bridge, Canada

(b) Mars Hill Bridge, USA

(c) Celakovice Pedestrian Bridge, Czech Republic

(d) Jean Bouin Stadium, France

(e) Seonyu Bridge, South Korea

(f) Rabat-sale Airport, Morocco

Figure 1.1. Different UHPFRC applications around the world:(a,b,c,d,e) Bridges (f) Facade (Azmee & Shafiq. 2018; Amran et al., 2022).

1.3 Objectives and Scope of the Thesis

Nowadays, there are many older bridges and buildings that are considered substandard in terms of seismic resistance owing to lack of reinforcement detailing. Different jacketing techniques with various confining methods have always been a method of preference in retrofitting columns and piers. Those techniques started by incorporating additional layers of normal strength concrete, leading to larger cross-sectional areas and/or replacement of the original concrete cover, all of these by encasing the original cross section of the pier. UHPFRC is an ideal solution in this retrofitting application because it provides significant durability to the retrofit owing to its low permeability and high density. However, some practical problems hinder the widespread application of UHPFRC in the construction industry: there is a knowledge gap regarding several design issues in the Codes – for example in Canada, the attempt to develop a code for design with UHPFRC is still at the informational (not enforced) state (Annex 8, CHBDC Code 2019). Practical issues such as the need of qualified personnel to ensure proper results, is a motivation to explore precasting alternatives that can be done in controlled settings.

As was mentioned in Section 1.2, this research study includes both experimental and analytical components. The experimental program focuses in creating a retrofit technique for concrete columns in the form of jacketing, where the jacket that encases the concrete member comprises as assembly of connected precast components. When the jacket is prepared in the fabrication facility, the risk of having errors such as the fiber orientation, fiber distribution, and casting method are reduced. A set of characterization experiments conducted on UHPFRC tension and compression samples help to understand the tensile strength, flexural capacity, and post-peak behavior of this class of material. The UHPFRC material under study is reinforced by fine steel fibers; jackets were made using a 2% volumetric ratio of fibers in two thicknesses (25mm and 37.5mm). A 3% fiber ratio was also used in the connection regions or to make the connection keys between precast components. The material used is a nano-fibre reinforced premix. For the mixes made, the material's compressive strength was above 150 MPa, the tensile strength was over 6 MPa, and the strain capacity at the onset of localization was more than 0.002. The elastic modulus was over 50 GPa.

The rectangular concrete columns, made from normal unreinforced concrete, studied in this research are to be retrofitted with precast jackets made with UHPFRC. These precast jackets needed to be connected to each other with a particular connector device. The rectangular columns once under compression loads, will dilate and therefore produce passive transverse tension in the precast jackets. Therefore, high tensile strength is required, so the tensile stress that may develop in the connected precast jacket reaches the tensile and deformation capacity of the UHPFRC material used in the jackets.

The experimental program is divided into three parts: the first part focuses on designing and fabricating connectors with high tensile strengths to join and hold the precast jackets in the assembled position; the second part focuses on creating the rectangular concrete specimens and all the precast jacket components with adequate dimensions and inserts; the third part focuses on assembling the column with the precast jackets and connectors to carry out the final monotonic and cyclic testing for proof of concept. The analytical program is divided into two parts: the first part focuses on finite element non-linear analysis to study the behavior of the connector and optimize its final shape before starting the experimental program; the second part focuses on developing non-linear finite element analysis for the final retrofitted column specimens to correlate the experimental data obtained and validate the models derived during the research.

In addition, an extensive review of the available experimental literature was conducted, prior to embarking on the experimental part of the study, to understand the effectiveness of jacketing on complete member response particularly for seismic applications and to identify the open issues in terms of our ability to estimate the contribution of the jacket to member resistance, drift capacity and the effectiveness of its performance as a confining system.

The main objectives of this research are summarized as follows:

1. To assemble and analyze a database based on previous experimental work from the published literature that incorporates UHPFRC as an alternative to retrofit concrete columns in the form of jacketing.
2. To create special connectors to join the precast UHPFRC Jackets that have the ability to carry out high tensile strengths, so that the tensile stress experienced on the encased concrete column are transferred through the connectors to the jacket.
3. To create a retrofit jacketing technique for concrete columns with precast elements made with UHPFRC materials.
4. To conduct material and connector characterization tests in support of the technology development of precast UHPFRC jackets
5. To conduct monotonic and cyclic compression tests on columns encased with precast jackets, for proof of concept of the proposed technology.
6. To correlate and validate the experimental data with a non-linear finite element model to estimate the confinement effectiveness contributed by the precast jackets.

1.4 Thesis Structure

The thesis is organized into eight chapters. Each chapter is summarized as follows:

*Chapter 1 – Introduction***:** This chapter provides a brief introduction and background to UHPFRC, its application in the form of Jacketing and practicability in the use of this novel material. Scope of the thesis, main objectives and the outline of the research are also detailed in this Chapter.

Chapter 2 – Literature Review: This chapter presents a review of several experiments from the published literature involving reinforced and/or non-reinforced concrete columns retrofitted with UHPFRC Jackets. Mechanical properties and important factors of UHPFRC are described. Experiments involving UHPFRC retrofits in the form of jacketing are analyzed, deriving several mathematical expressions that quantify the contribution of the jackets to lateral load strength and drift capacity of retrofitted columns. The database study is also used to explore the evidence regarding the effectiveness of the jacket as a confining devise for encased concrete.

Chapter 3 – Modelling of Jacket Contribution: The database tests are analyzed to extract mathematical expressions that can be used to predict the lateral confinement pressure, strength and deformation capacity for a concrete member with either circular or rectangular cross section, subjected to lateral sway representative of earthquake action. Moreover, the flexural strength, shear strength, and lap-splice strength increase provided by the UHPFRC Jacket are related to the mechanical properties of the jacket material.

Chapter 4 – Material Testing for Characterization of UHPFRC Mix: The experimental program performed to obtain the real mechanical properties of the UHPFRC Premix provided for the research is presented in this chapter. The main tests performed for the characterization of the material include direct tension, flexural and compression tests. Important parameters that influence the behavior of the material include the type of fiber used as well as the fiber content in the mix, mixing procedure and casting methodology.

Chapter 5 – Experimental Program for Retrofitted Columns with Precast UHPFRC Jackets and Connection Devices: This chapter explains how the design of the connecting elements was developed in support of the methodology development. By performing non-linear finite element modeling, different shapes of the possible connectors for the Precast UHPFRC Jackets were studied. Three kinds of connectors were developed based on the geometry and the stress concentrations generated around the key. Optimization of the shape for the connectors was performed with the objective to reduce stress concentrations in the connected components. A specific shape was selected from this research, which was used as a basis to start the fabrication of the precast components in the laboratory. The experimental program is described in this chapter by analyzing, preparing, casting and testing the final Precast UHPFRC Jacket specimens as well as the rectangular columns that were used for proof of concept. Description of the casting methodology, mix design, specimens' assembly and results for all the retrofitted columns are listed in this chapter.

Chapter 6 – Finite Element Modelling of Columns with Precast UHPFRC Jackets: This chapter includes the non-linear finite element modeling used to predict the confinement behavior obtained from the experiments presented in the previous chapter. Three models were considered, one for the UHPFRC Jacket when is a Cast-in-Place solution and two for the UHPFRC Jacket as a Precast Element added to the concrete column. The main difference between the finite element models for the Precast Elements is the connection method. Correlations between the models and the experimental results are drawn.

Chapter 7 – Summary and Conclusions: This chapter presents a brief summary of the thesis followed by the conclusions of the research work done. In addition, challenges and difficulties during the course of work related to the experimental and analytical program are outlined, including recommendations for future extension of this research.

Chapter 2: Literature Review

This literature review starts by reviewing the properties of UHPFRC and the main factors influencing its behavior, followed by experimental data and observations regarding mechanical properties, performance and post-cracking response explored by other researchers. A comprehensive evaluation of several experiments involving UHPFRC as a retrofit technique in the form of Jacketing is conducted, with an emphasis on concrete columns. The objective of this review is to identify and highlight the characteristics of the response of encased concrete and the knowledge gaps regarding this method of retrofitting. In addition, this chapter reviews the opportunities and challenges of extending the jacketing procedures to precasting of the jacketing layers, as an alternative retrofit method.

2.1 UHPFRC Properties

Experimental programs have been developed around the world that support derivation of models regarding the uniaxial stress-strain response of the material in compression (Ismail et al., 2023). However, more work needs to be done to totally define the material behavior under different states of stress, so that it can be used for the development of design provisions.

UHPFRC is a mix that includes Portland cement, fine sand, silica fume, high-range water reducer or *superplasticizer*, water, chemical additives (in some scenarios), small amounts of water and reinforcing fibers (PVA, carbon or steel fibers). Like any other emerging and promising material, UHPFRC needs to be fully understood before it can be used in seismic applications and for repair/retrofit applications. Different mix designs, variation in the quantities of the aggregates, mixing procedures, casting method, fiber orientation, fiber content, fiber distribution, flowability of the mix and curing methods are just some of the factors that influence the outcome of UHPFRC. Canadian standards for UHPFRC are established in Annex 8.1 of CSA-S6 (2019) and Annex U of CSA A23.1 (2019) where it is stated that a minimum compressive strength *(f_c')* of 120 MPa is required for a material to be classified as UHPFRC. The material's response in uniaxial tension has been categorized as tension hardening (THFRC) or tension softening (TSFRC) depending on the characteristics of the tensile stress-strain response after cracking. In terms of tension, the minimum tensile strength *($f_{cr,U}$)* is 4.0 MPa for TSFRC and 6.5 MPa for THFRC (a lower limit of $0.6\sqrt{f'_{c,U}}$ has been set by Annex 8 of CSA-S6 2019). The corresponding stress-strain diagrams provided by Annex U of CSA A23.1 and a general classification of UHFRC for tension hardening stress-strain behavior are depicted in Figure 2.1 and Figure 2.2 below, respectively.

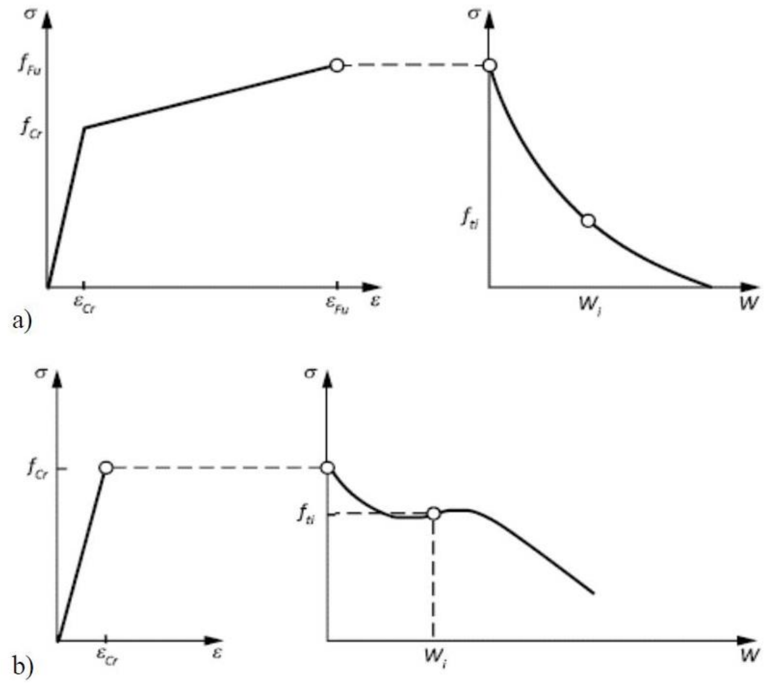

Figure 2.1.Tensile stress-strain diagrams for: a) THFRC and b)TSFRC (Fig U3, reproduced from Annex U of CSA-A23.1).

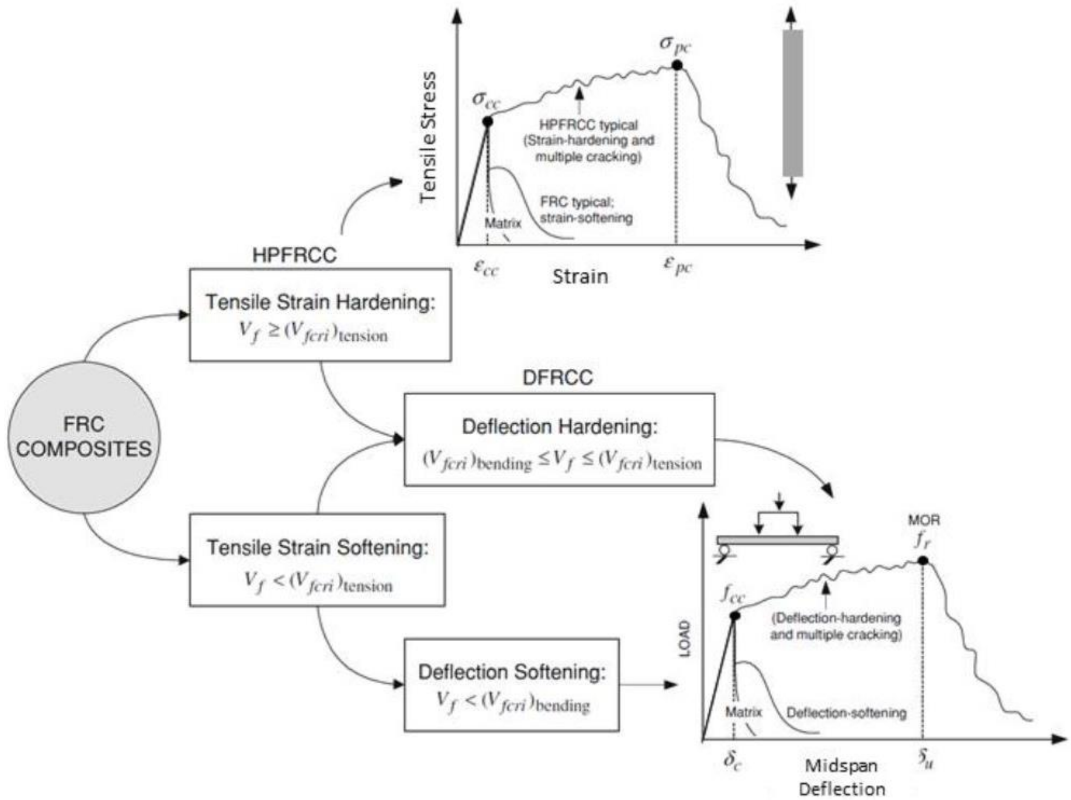

Figure 2.2. Classification and behavior of UHPFRC (adapted from Naaman & Reinhardt, 2006).

Figure 2.2 refers to a persistent conundrum that hampers experimental definition of the properties of the material in tension: depending on the characterization test conducted, tension hardening response may be implied, as for example in flexural prism tests - without necessarily being reproducible in direct tension tests. Therefore, the values measured are dependent on the test setup used. In fact, the type of characterization testing used for UHPFRC is still considered an open issue, introducing a great degree of bias in terms of the true values of the tension properties, the relationship between the values obtained between different test setups and the relevance of these values with the properties occurring in the field casting.

2.1.1 Compression Strength

UHPFRC can achieve high levels of compression strength due to its integrity and its dense matrix thanks to the bond occurring by particle packing. The volumetric fiber ratio incorporated in the mix, results in a more ductile lateral strain capacity (Naeimi & Moustafa, 2021). It may seem that with the addition of fibers, the compressive strength of the mixture is to be increased, however there is no significant increment when using 2% to 4% fiber content (Wang et al., 2020). It has been determined that UHPFRC mixes may reach up to 70 MPa of compressive strength at such an early age, as 2 days (Graybeal, 2005). According to Annex 8.1 of CSA S6:19 (2019), as a requirement, the minimum compressive strength of the concrete mix needs to be 120 MPa for the material to be classified as UHPFRC. A compression model for UHPFRC consisting of four branches was proposed by Ismail et al. (2022) and it is shown in Figure 2.3 below. The ascending branch is defined by the equation proposed by Thorenfeldt, Tomaszewicz & Jensen (1987) (Eq. 2.1). Parameter *n* is adjusted so that the slope of the ascending branch matches the initial tangent modulus of elasticity and parameter *k* =1 for compressive strains $\varepsilon_a < \varepsilon_{cc,o}$; this line is shown as a dashed line in Figure 2.3 for simplicity (Tsiotsias, 2023).

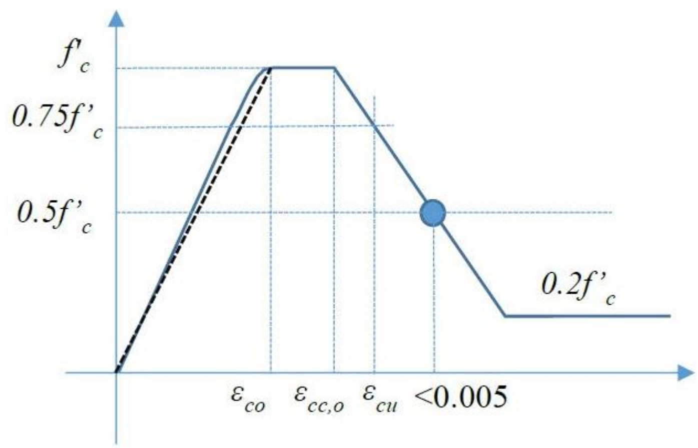

Figure 2.3.Compression model for UHPFRC (Ismail et al., 2022)

$$\sigma_a = f'_{c,U} \cdot \left[\frac{n \cdot (\varepsilon_a/\varepsilon_{co})}{n - 1 + (\varepsilon_a/\varepsilon_{co})^{nk}}\right] \tag{2.1}$$

$$\varepsilon_{co} = f'_{c,U}/E_{c,U} \tag{2.2}$$

$$E_{c,U} = 4070 \cdot \sqrt{f'_{c,U}} \tag{2.3}$$

$$q_{f,lat} = \varphi_c \cdot f_{td} \tag{2.4}$$

$$\varepsilon_{cc,o} = \varepsilon_{co}\left(1 + 6\left(\frac{q_{f,lat}}{f'_{c,U}}\right)\right) \tag{2.5}$$

$$\varepsilon_{cu} = \varepsilon_{co}\left(1 + 20\left(\frac{q_{f,lat}}{f'_{c,U}}\right)\right) \geq 0.004 \tag{2.6}$$

The strain at peak stress ε_{cc} and the modulus of elasticity may be calculated from Eq. 2.2 and Eq. 2.3. The internal confining pressure provided by the dispersed fiber reinforcement is represented by parameter $q_{f,lat}$ and it is estimated from Eq. 2.4. The material resistance factor φ_c used is set as 0.75 in Annex 8 of CSA-S6. The strain $\varepsilon_{cc,o}$ is calculated from Eq. 2.5. When having a 25% drop in the descending branch, the strain capacity ε_{cu} can be calculated with Eq. 2.6.

2.1.2 Tensile Strength

In structural members made of concrete, the tensile strength is always neglected and taken equal to be zero in flexural analysis. But with UHPFRC emerging as a new material that can be used for both new-built structures and for retrofitting purposes, the tensile strength and ductility in tension of concrete due to its significant post-cracking behavior is an essential attribute that guides the design of the retrofit. The bridging effect provided by fiber reinforcement allows the material to reach high tensile strains after cracking. According to the provisions of the AASHTO T 397, 2022 which is now adopted in the revised Annex 8 that is to be issued in 2025, the tensile properties of UHPFRC are obtained by conducting uniaxial direct tension tests on prismatic specimens having a cross-sectional area of 50 mm by 50 mm and 400 mm length. Even though direct tension is the recommended method for determining the uniaxial tensile strength of UHPFRC, it is a difficult test to perform (Naaman & Reinhardt, 2006) due to the procedure, implements, tools and other setup limitations that are not practical and palatable for most commercial labs today. In addition, imperfections on the surfaces of the prisms, fiber distribution, fiber orientation, incorrect test rates, non-uniform stress concentrations, misalignment of the specimen, boundary conditions and slippage are just some of the challenges faced during direct tension testing (Ismail, 2023). Other methods and specimen geometries for calculating tensile properties have been used in the past by many researchers (e.g., Graybeal & Baby, 2013; Yang et al., 2021); for example the flexural prism test when the specimen is loaded at the third points was recommended by older standards for FRC (e.g ACI 544.4R-88, 1999). Short steel fibers were used in this research study (13mm length and 0.2mm diameter), where the bond between the fibers and the matrix is improved due to the compressive strength and cohesion of the fine-grained matrix (López, 2017).

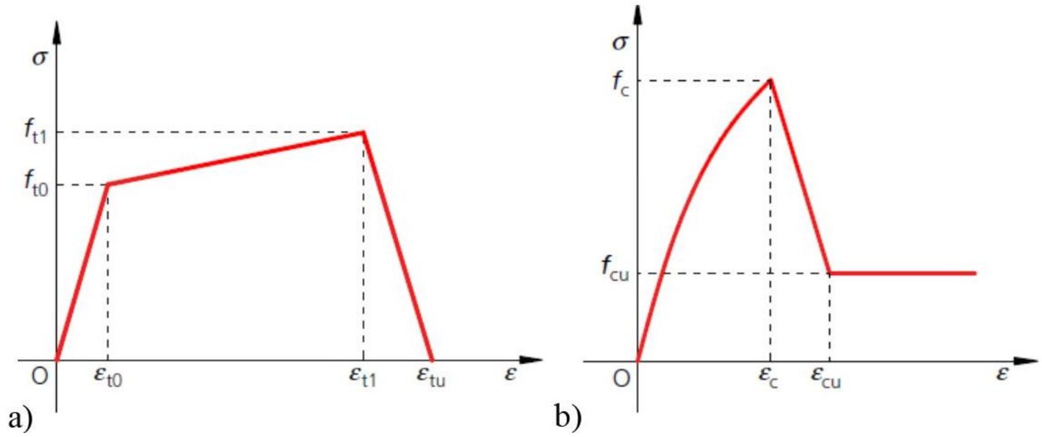

Figure 2.4. Envelope curves for THFRC in a) tension; b) compression (Wu et al. 2016) (adapted from Ismail, 2023)

2.1.3 Flexure Strength

It was stated earlier that flexural tests have been used in the past as an alternative method for characterizing the tensile strength of UHPFRC. This type of test is relatively easier to conduct than direct tension, albeit it is also hampered by its own practical difficulties none the least being the sensitivity of the test results to the exact details of the end and loading shafts (see Yang et al. 2021). Another challenge is that the experimental data obtained from flexural tests need to be processed with an inverse analysis procedure for appropriate interpretation of the direct tensile behavior of UHPFRC (Ismail, 2023); currently there is no universally accepted procedure for conducting the inverse analysis in order to extract the direct tension properties from flexural prism tests.

2.1.4 Modulus of Elasticity

Annex U of the standard CSA A23.1 (2019) recommends the parameters and procedures established in ASTM C469/C469M (2014) for calculating the static modulus of Elasticity and Poisson's ratio of UHPFRC. When sufficient data is not available, mathematical expressions can be employed to estimate the modulus of elasticity based on the uniaxial compressive strength, $f'_{c,U}$. Considering that the value of $f'_{c,U}$ varies among mix designs and commercial premixes available, Table 2.1 shows the more relevant empirical expressions for calculating the modulus of Elasticity of UHPFRC. The average value for the modulus of Elasticity for the already characterized commercial premixes is the range of 55 GPa to 59 GPa (Graybeal et al., 2013).

Table 2.1. Empirical relationships for Modulus of Elasticity of UHPFRC (adapted from Ismail, 2023

Source	Equation	Note
Graybeal (2012)	$E_c = 4069 \cdot \sqrt{f_c'}$	$97 \leq f_c' \leq 179\ MPa$
Graybeal (2007)	$E_c = 3840 \cdot \sqrt{f_c'}$	$126 \leq f_c' \leq 193\ MPa$
Ma et al. (2004)	$E_c = 19000 \cdot (f_c'/10)^{1/3}$	UHPC without coarse aggregates, $150 \leq f_c' \leq 180\ MPa$
Ma and Schneider (2002)	$E_c = 16365 \cdot (f_c') - 34828$	$f_c' \geq 140\ MPa$
AFGC (2012)	$E_c = 9500 \cdot (f_c')^{1/3}$	Heat-cured UHPC, $f_c' \geq 140\ MPa$

2.2 UHPFRC Jackets as a Retrofit Material

For seismic retrofitting, great potential lies in the use of UHPFRC materials as jacketing systems in piers, providing confinement, deformation capacity, and corrosion protection due to their impermeable microstructure. Significant improvements in strength and ductility are reported whereas this form of jacketing mitigates premature modes of failure (in lap splices and lightly reinforced piers under shear). A good retrofit technique not only restores the structural performance but also mitigates the deterioration mechanism that caused the need of repair in first place. (Ismail, 2023). For example, UHPFRC is an ideal solution in retrofitting of members exposed to corrosive environments, as it provides significant durability to the retrofit owing to its low permeability and dense microstructure. The material is usually reinforced by fine steel fibers at volume ratios in the range of 1.5 to 4%. Generally, the strength in compression is above 120 MPa, and the Elastic Modulus is over 40 GPa. Nevertheless, the attractiveness of the material is not just in the favorable mechanical strength and stiffness under compression, but the high tensile strength (over 5 MPa), strain capacity (in the range of 0.2% or more), and high residual strength. The confinement provided due to sustained tensile strength that hinders the lateral dilation of the encased core, and the development of normal stresses in the cross-section that enhance the flexural and shear component are part of the main mechanisms of the UHPFRC jacket. It has also been shown that in case of jackets with thickness greater than 30 mm, the plastic hinge zone may be relocated outside the jacket after the retrofit (Tsiotsias, 2023). Due to the unique properties described above, UHPFRC jackets have great potential to be used for newly built and for rehabilitation projects and might be considered a mild global intervention as they enhance the seismic performance of RC elements with respect to axial load and deformation capacity, stiffness, shear, and flexural strength (Gonzalez et al., 2023). Moreover, it has been shown that jackets on corroded columns have resulted in superior load capacity, ductility, and cracking (El Joukhadar, 2022). Other options, explored earlier, such as steel jackets are not recommended for piers with rectangular cross-section mainly due to the reduced efficiency and the risk of localized corrosion at the corners in aggressive environmental exposure (Priestly et al., 1994). On the other hand, Carbon-fibre-reinforced-polymers (CFRP) wraps have very small jacket thickness because of the great tensile strength, which is provided by the fibers, also making CFRP wrapping suitable for circular piers (Lavorato et al., 1194). For a rectangular shape pier retrofitted with CFRP wraps, rupture of the CFRP fibers generally occurs at the corners of the pier and this is followed by great strength loss and brittle failure load (Tastani et al., 2019). In either case, CFRP wrapping is only suitable as a local intervention (enhancing deformability of the column, but neither stiffness nor strength) (Gonzalez et al., 2023). Another mechanism by which concrete jackets contribute is by means of developing normal stresses in the cross section of the structural member and therefore enhance the flexural and the shear strength of the component. Although the thickness is small in the case of UHPFRC, the total active area of jacket material in the tension and compression zones of the member produce significant stress resultants, and because they occur in the extreme zones of the cross section, these forces have significant lever arm, thereby contributing both to the sectional equilibrium and the flexural strength. Thus, even such small jacket thicknesses cause a notable increase in column flexural strength and stiffness (Ismail, 2024).

2.3 Review of Experimental Evidence on Columns Jacketed with UHPFRC

In order to derive design provisions for seismic retrofit with UHPC jacketing, a large database with experimental results for circular and rectangular cross-section columns was assembled and used in the present study (Gonzalez et al., 2023); tests considered comprised beam-column elements that were subjected to a reversed cyclic lateral displacement history of increasing amplitude simulating the effects of earthquakes on open storey columns of buildings or on bridge piers. Axial load representing the overbearing action of dead loads supported by the columns were applied prior to the application of the lateral load, however a range of values were considered in the various tests. In all cases the specimens the lateral load history introduced constant shear to the columns. Where the column was modeled as a cantilever, the moment diagram varied linearly from the tip to the maximum moment at the base; where the full length of the column was modelled then a point of inflection occurred at the column midheight (symmetric fixity against rotation was applied in both ends). The assembled database comprises a total of 78 specimens of which 21 had a circular cross-section (denoted as C-specimens), and the remaining 57 had a rectangular cross-section (denoted as R-specimens). All specimens and the source references are listed in Table 2.2. Figure 2.5 summarizes the key details of the respective specimens.

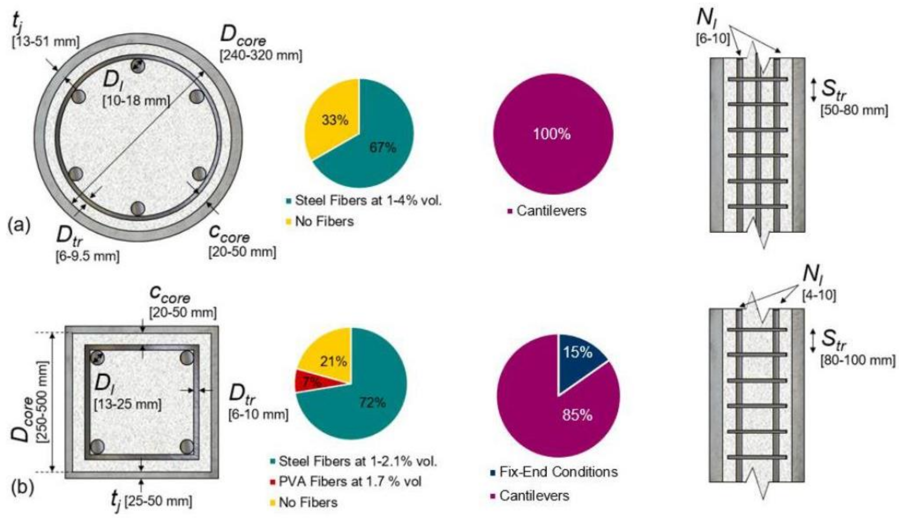

Figure 2.5. Details of a) C- and b) R-Specimens, regarding parameters and experimental configuration (adapted from Ralli et al., 2024)

Table 2.2. Specimens and references for C-Specimens and R-Specimens collected from literature.

Paper's Name	Publication Year	Cross-Section Type	Specimen's ID
Retrofitting of Bridge Columns Using UHPC	2019	C-specimen	A-U2-0-F A-U2-102-F S-U2-102-F S-N02-64-N S-U4-64-N S-U4-64-F S-U4-64-F
Cyclic Performance of RC bridge piers retrofitted with UHPC Jackets: Experimental Investigation	2021	C-specimen	URC1 URC2
Cyclic Loading Test for RC Bridge Piers Strengthen with UHPC Jackets in a corrosive environment	2022	C-specimen	URC4 URC5 URC6
Cyclic Performance of severely earthquake damaged RC bridge columns repaired with grouted UHPC Jackets	2023	C-specimen	MM-R MH-R MHE-R
Cyclic Performance of severely	2010	C-specimen	RUHPC CFFT

earthquake-damaged RC bridge columns repaired with grouted UHPC Jacket			
High-Performance Fiber-Reinforced Concrete Bridge Columns under Bidirectional Cyclic Loading	2014	C-specimen	S1: HPFRC S2: HPFRC
Precast Seismic Bridge Column Connection Using UHPC Lap Splice	2020	C-specimen	CIP40 CIP25
Seismic Performance of Precast Concrete Columns with Prefabricated UHPC Jackets in the Plastic Hinge	2021	R-specimen	Specimen PC 1 Specimen PC2
Cast-in-Place and Prefabricated UHPC Jackets for Retrofitting Shear Deficient RC Columns with different Axial Load Levels	2021	R-specimen	L-UHPC L-R/UHPC H-NC H-UHPC H-R/UHPC H-P/UHPC
Development and seismic behavior of a novel UHPC-shell strengthened prefabricated concrete column	2021	R-specimen	USPCC-1 USPCC-2 USPCC-3
Experimental Study of a reinforced concrete column of 1:4 Scale	2020	R-specimen	Specimen 1:4 Scale
Cyclic Behavior of damaged reinforced concrete columns repaired with high-performance fiber-reinforced cementitious composite	2017	R-specimen	C0-300-R C0-500-R C120-300-R C120-500-R
Seismic Retrofitting of Rectangular Bridge Piers using UHPRFC Jackets	2018	R-specimen	Pier R400 Pier R850
Comparative Analysis of Existing RC Columns Jacketed with CRFP or FRCC	2018	R-specimen	CL_FRPa CL_FRP_B CM_FRPa CM_FRPb CL_FRCC
Cyclic response of precast column to foundation connection using UHPC and Ni-Ti SMA reinforcements in columns	2021	R-specimen	Z1 Z2 Z3 Z4
Cyclic Responses of reinforced concrete composite columns strengthened in the plastic hinge region by HPFRC mortar	2012	R-specimen	HPFC-RC-0 HPFC-RC-1 HPFC-RC-2
Seismic Resistant Bridge Columns Using UHPC Segments	2016	R-specimen	RC-UHPC HY-UHPC

Cyclic Testing of UHPC Retrofitted Columns	2024	R-specimen	CT1-15M-R CT1-15M-S CT2-20M-R CT2-20M-S CS3-15M-R CS3-20M-R
Seismic Strengthening of Concrete Columns By UHPFRC Jacketing	2021	R-specimen	U-30 UCT-30 UGT-30 U-45 UCT-45 UGT-45
Seismic performance of full scale UHPC Jacket strengthened RC columns under high axial loads	2022	R-specimen	URC1-a URC1-b URC2-a URC2-b URC3-a URC3-b
Mechanical behavior of RC columns strengthened with thin UHPC jacket under cyclic loads	2022	R-specimen	U2-RC1 U1-RC2 RU2-RC2 U2-RC2 U2RC3
Experimental and Numerical Investigation on the Seismic Performance of concrete-filled UHPC tubular columns	2021	R-specimen	U50 U50H U20H
Opportunities of light jacketing with fibre reinforced cementitious composites for seismic retrofitting of existing RC columns	2021	R-specimen	F_0.1R S_0.1R S_0.2R
Seismic Retrofitting of Rectangular Bridge Piers with UHPC Materials	2017	R-specimen	S1 S2 S3 S4

It is noted that for C specimens, the only type of fibers used were brass-coated straight steel fibers with a length of 13 mm, diameter of 0.2 mm having a Young's Modulus of 200 GPa. The yielding and ultimate stress of longitudinal and transverse reinforcements were in the range of 335-570 MPa and 637-779 MPa, respectively.

Contrary to C-specimens, where only steel fibers had been used, the experimental database for R-specimens includes cases with hybrid mixes of PVA fibers and steel fibers. The PVA fibers had a tensile strength of 1600 MPa and a modulus of Elasticity of 43 GPa, whereas the steel fibers had a tensile strength of 2800 MPa and a modulus of Elasticity of 205 GPa. Drift capacity and strength increase achieved over the nominal flexural strength of the columns prior to jacketing are used in this study, for specimens of either cross-section type, to gauge the effectiveness of the retrofit. Lateral load and drift ratio coordinates at milestone points of the response curves as shown in

Figure 2.6, were collected for all the specimens listed in Table 2.2, for reported values at yielding, peak, and ultimate.

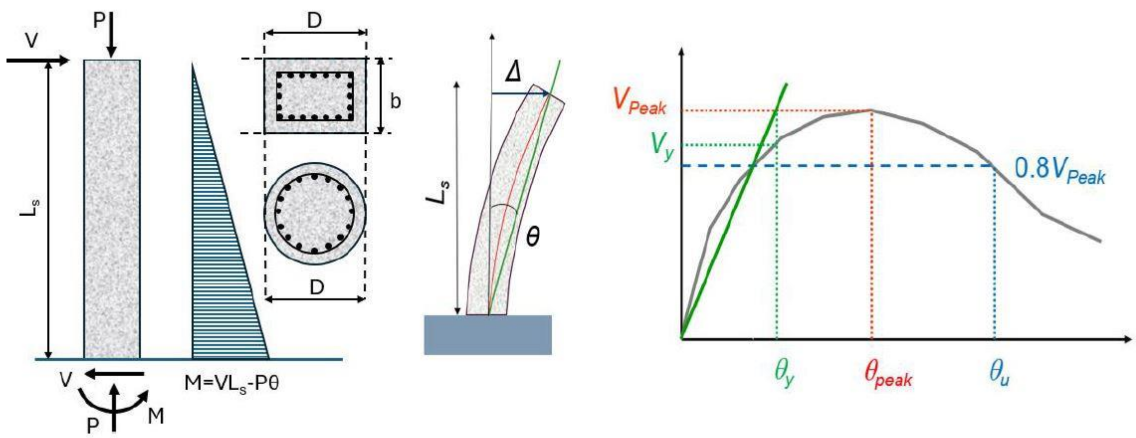

Figure 2.6. Drift capacity and milestone points of the response curve used in the Database.

The ultimate deformation capacity was defined as the post-peak point in the envelope of the hysteretic response curve, which corresponds to 80% of the peak load (meaning a drop of 20% after peak load). The drift ratio θ was defined as the lateral displacement Δ divided by the shear span L_s of each experiment. The shear span for C and R-specimens was in the range of 1300-1800 and 600-2650 mm, respectively. Another important design parameter was the aspect ratio (a), calculated as the ratio of the shear span, (L_s) divided by the diameter of the C-Specimen or by the depth of the R-Specimen cross-section (D). Some of the Specimens did not report yielding values. For such cases, notional yielding was assigned to the displacement and corresponding strength pair of values, which were defined by the intersection of the radial green line at 80% of the envelope with a horizontal line drawn at peak load in Figure 2.6.

2.3.1 Performance of Experimental Evidence: Jacket Index

The analysis of the experimental evidence assembled in the Database provides insights regarding the confinement of the encased concrete behavior, the deformation capacity, and the attainment of flexural strength, and can be used to support design recommendations for this retrofitting method. Considering that the hoop stress in the jacket is proportional to the fiber content (v_f) a geometric index is used to organize the experimental data. This is referred to as Jacket Index, J_i, and it is calculated according to Eq. 2.7, to account for the role of the important variables that influence the lateral confining pressure exerted on the encased member, namely, the jacket thickness to encased diameter ratio, and the volumetric ratio of fibers. It is noted however that for a random distribution of fibers (random casting) the value for J_i may be as low as 75% to 35% of the value given below. For this present study, as the method of casting is unknown, J_i is considered a nominal indicator.

$$J_i = \frac{100 \cdot t_j \cdot v_f}{D_{core}} \quad (2.7)$$

Subsequently, it is observed that there are certain design variables of the original column designs that may either hinder or enhance the deformation capacity. Generally, the presence of large amounts of longitudinal reinforcement increases the lateral force demand required to cause flexural yielding of the column, whereas high axial load ratios and low aspect ratios compromise the deformation capacity, while the presence of transverse reinforcement has a positive impact on that property. Similar is the effect of these parameters on the characteristics of the mode of column failure even after jacketing. Therefore, in the same manner, a Composite Index (C_i) is used to classify the experimental values of the ultimate drift capacity and is described by Eq. 2.8. C_i is proportional to transverse reinforcement ratio (ρ_{tr}) and aspect ratio of the column (a=L_s/D), inversely proportional to the longitudinal reinforcement ratio (ρ_{sl}, here all the longitudinal reinforcement ratio is implied, assuming a symmetrically reinforced column). Parameter C_i decays linearly with increasing axial load ratio ($v=P/(A_g f_c')$). The influence of both indices on θ_u is illustrated in Figure 2.7.

$$C_i = \mathrm{a} \cdot (1 - v) \frac{\rho_{tr}}{\rho_{sl}} \quad (2.8)$$

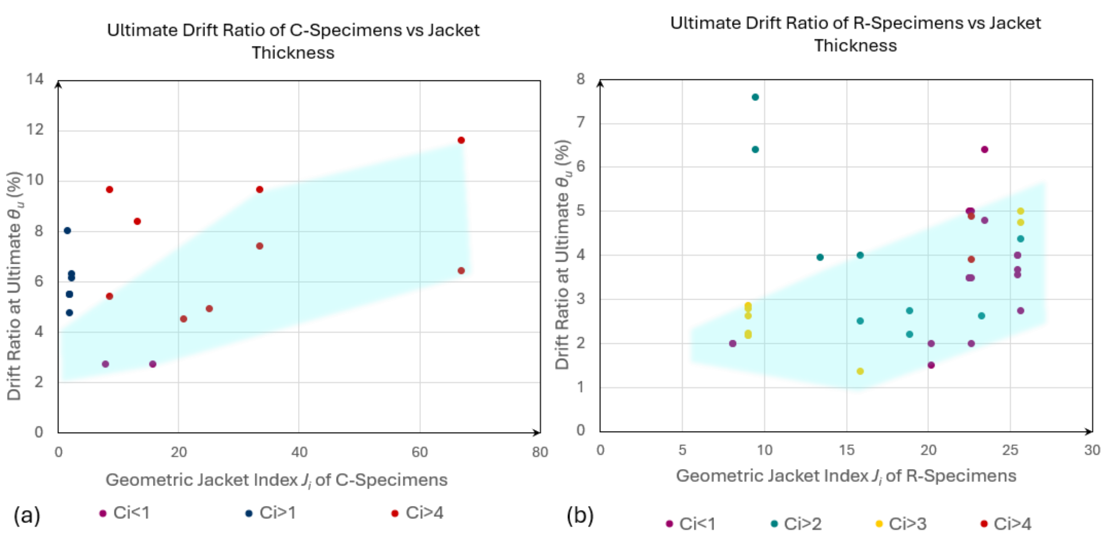

Figure 2.7. Ultimate drift ratio of (a) C-; (b) R-Specimens plotted against J_i and C_i.

It is noted that C sections generally attained higher amounts of θ_u (more than 4%) as compared to the R sections (a lower limit was 2%), the value of θ_u showing a relatively mild increase and significant dispersion with increasing magnitude of the index C_i. The volume of the available data is still limited to support derivation of a detailed analytical expression; however, the proposed index is effective in reproducing the experimental trend which is shown by the light cloud color.

2.4 Alternative Arrangements of UHPFRC Jacketing Systems

The application of UHPFRC jackets in retrofitting of piers may be implemented using three different alternative arrangements organized in the order of increasing extent of invasiveness and efficiency of intervention: (i) jacketing in the plastic hinge zone but allowing a non-contact gap between jacket and footing (Figure 2.8(a)), (ii) jacketing directly on the pier, thereby forming a cold joint connection between existing concrete (footing) and jacket (Figure 2.8(b)), and (iii) penetration of the jacket into the footing (Figure 2.8(c)). In all three arrangements, the UHPFRC jacket exerts some confining pressure on the encased concrete member. In the first case, the jacket provides only confinement to the encased concrete (Figure 2.8(d)) with the gap between jacket and footing enabling some minimal strain spreading within the gap length and adjacent spreading above and below the gap; the objective in this detail is to prevent the localization of the strain of the bars in tension. In the cold joint arrangement, besides the confinement, the jacket participates in the compressive zone and therefore in the sectional equilibrium of the critical section (Figure 2.8(e)). In the last arrangement, with the extension of the jacket into the footing, the jacket participates in sectional equilibrium by stress results both in the compression and tension regions of the critical section (Figure 2.8(e and f)). This arrangement aims to decrease permanent damage at the column-footing connection owing to strain localization at the critical section, which would also lead to large strain penetration in the upper part of the bars inside the footing (Aviram et al., 2014; Farzad et al., 2019; Tazarv, 2015;Yuan et al., 2022; Del Zoppo et al., 2018). In the cases of cold joint and penetration in the footing, it is recommended to introduce bond breakers (also known as sleeves by placing PVC conducts) in the lower end of the jacket (at the connection with the footing) to enable strain penetration over an adequate length and prevent local bar fracture (El-Joukhadar et al., 2024; Shao et al., 2022).

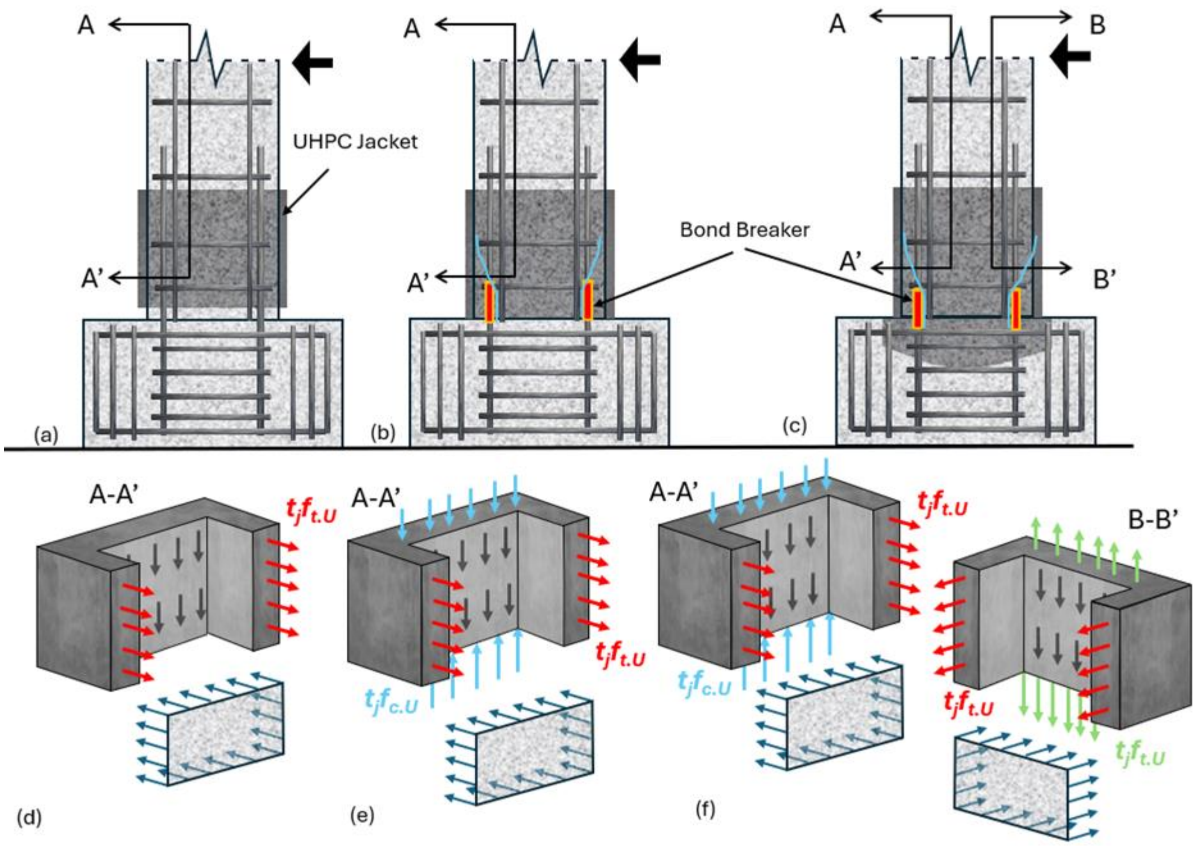

Figure 2.8. Possible arrangement of UHPFRC Jackets and developed stresses: (a) Gap between footing and jacket, (b) Cold joint between footing and jacket, and (c) Extension of Jacket into the footing; (d) State of stresses in the Jacket in case (a); (e) Stresses on the jacket in the compression zone of case (b); (e and f) Stresses in the jacket in the compression and tension zone of case (c) (adapted from Ralli et al., 2024).

2.4.1 Comparison of Performance of the Retrofit Schemes Presented in Figure 2.8

To illustrate the implications of the nuances in the retrofit details depicted in Figure 2.8, the sensitivity of the response of a typical bridge pier column case is considered in this section. The pier model has a circular cross section with diameter D=1.2 m, and a total height of 9.0 m; under lateral sway the pier develops double – curvature, with a shear span L_s=4.5 m. Monotonic moment curvature responses of the critical section are plotted in Figure 2.9(a) and 2.10(a), whereas the theoretical lateral force – lateral drift ratio are plotted in Figure 2.9(b) and 2.10(b) for two different axial load ratios. Details of the analysis are as follows: $f'_{c,U}$=25 MPa, longitudinal reinforcement ratio ρ_{sl}= 1.6% comprising 30-M bars, f_y=400 MPa steel, and lapped above the base over a length equal to $30D_b$; transverse hoop volumetric ratio is taken as 0.5% (10 M hoop bar at 180 mm spacing); axial load stress v= 2.5 MPa and 5 MPa (i.e, axial load ratio v= 0.1 and 0.2, respectively).

A 100 mm TH-UHPFRC jacket is used (ratio $t_j/D = 0.085$), having $f'_{c,U}$=150 MPa, with $f'_{t,U}$=11 MPa and tensile strain at the onset of crack localization $\gamma_F \varepsilon_{t,U}$=0.002. Note that on account of the specimen size a fiber alignment coefficient is assumed, γ_F=0.75 (i.e., the tensile strength is taken as the $\min(f^U_{t,cr} = 0.6(f'_{c,U})^{0.5};\ \gamma_F f'_{t,U})$). For the sake of comparison, all material factors φ are taken =1 in the present analysis. Figures 2.9 and 2.10 illustrate the moment-curvature and corresponding lateral load-displacement curves for axial load ratio of 0.1 and 0.2, respectively. Term NJ refers to the non-jacketed column.

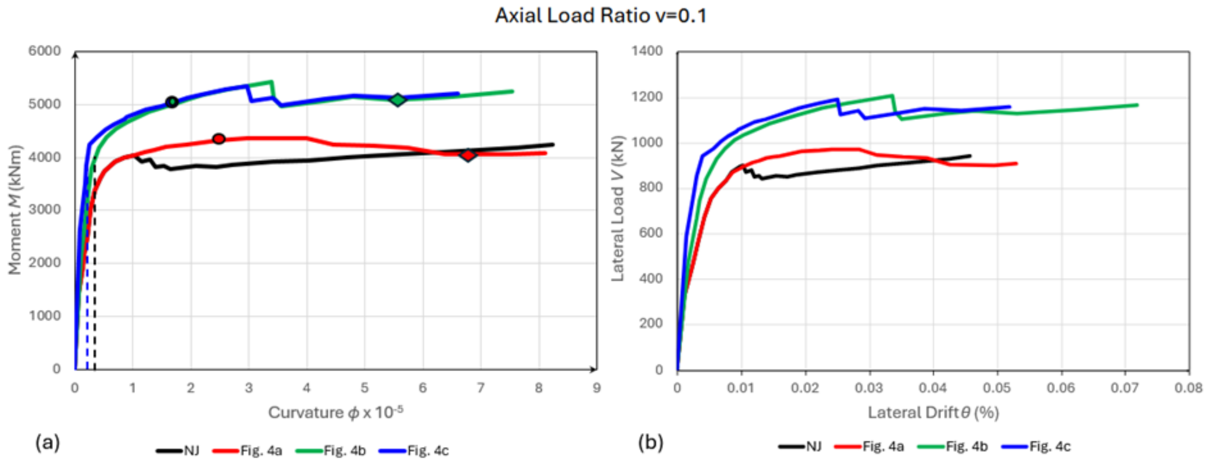

Figure 2.9. (a) Moment-Curvature; (b) Lateral Load-Drift responses of the retrofitted column using the jacket arrangements of Figure 2.8 for axial load ratio v=0.1. The NJ curves cannot be realized after lap splices failures shown by the dashed line in the left.

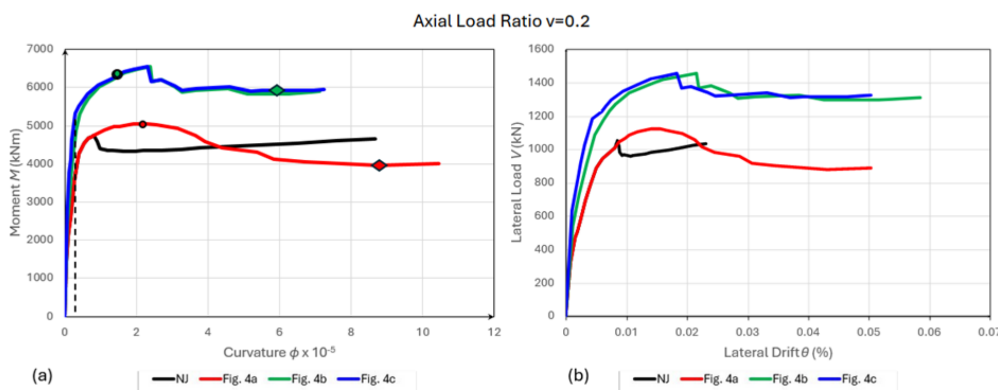

Figure 2.10. (a) Moment-Curvature; (b) Lateral Load-Drift responses of the retrofitted column using the jacket arrangements of Figure 2.8 for axial load ratio v=0.2. The NJ curves cannot be realized after lap splices failures shown by the dashed line in the left.

Results of the analyses illustrated that there are practically negligible differences in the theoretical flexural response of the original (NJ) and the jacketed column corresponding to the scheme of Figure 2.8 (a). One reason for the low effect on the Moment strength is the relatively low axial load ratio acting on the pier – which however is representative of bridge pier loading conditions; however, this is also due to the low effect that passive confining pressures have on the strength. Much more important is the effect of the jacketing on mitigating failures (a) due to web shear, (b) along the lap splices, and (c) in preventing buckling of longitudinal compression reinforcement, which are essential for the theoretically extensive nonlinear range of the response to be possible.

It is also observed that there is practically no difference in the flexural response of cases 2.8 (b) and 2.8 (c) although both represent a 33% increase in flexural strength over the NJ and 2.8 (a) cases. The practical coincidence of the results of these two analyses suggests that on account of the low axial load ratio, the extreme part of the jacketed cross section within the tension zone of the circular section exceeds its tensile strain capacity, $\gamma_F \varepsilon_{t,U}$=0.002, before the attainment of the flexural strength of the cross section. Therefore, for the large size pier sections examined here, the flexural strength increase is primarily dominated by the compressed part of the jacketed section, and the performance limit states for design of the retrofit would need to be linked to the maximum compression strain attainable with controlled degree of damage by the UHPFRC jacket. Similar response is observed in case of axial load ratio of 0.2 (Figure 2.10). The main differences are that the increased axial load significantly decreased the ductility of the NJ column, as expected, whereas the flexural enhancement observed in cases 2.8 (b) and 2.8 (c) are greater than in case 2.8 (a).

2.4.2 Gaps of the Research

This research studies UHPFRC as a precast alternative to retrofit rectangular concrete columns in the form of jacketing. This scenario is shown in Fig 2.8 (b), where the jacketing technique has no gap between the jacket and the footing. The other two alternatives could be further studied analytically and experimentally. The same approach can be used to study circular cross-sectional columns, where a different and new connection method can be implemented. The UHPFRC used in this research used steel fibers with a volumetric ratio of 2% for the precast jackets and 35 for the connection method; these two con be further studied in an experimental program.

Chapter 3: Modelling of Jacket Contribution

This chapter extends the basic behavioral models that have been developed in the past to interpret the contribution of reinforced concrete jackets to encase member strength, by modifying the contribution of the jacket stress results in order to consider the tensile strain ductility and post cracking strength of the UHPFRC layer. A point of reference in this regard has been the work of Thermou et al. (2017).

Similar to conventional jackets, the material placed on the lateral surface of a jacketed reinforced concrete member is engaged in actions that are supported by the confining pressure exerted on the encased core. The peak magnitude of this pressure, σ_{lat}, is calculated as in all cases of jacketing, as described from the equilibrium model depicted in Figure 3.1. It has been shown that the clamping action provided by the confining jacket pressure enhances the frictional bond between the jacket which represents the shear flow at the interface between jacket and encased member and is described by Eq. 3.1 (Thermou et al. 2007).

$$\tau = c_o + tan\phi \cdot \sigma_{lat} \quad (3.1)$$

where c_o is the cohesion and ϕ is the angle of internal friction. Interfacial tests between UHFRPC layers and concrete have shown ϕ to be around 62^o (El-Joukahadar et al., 2024). The coefficient of friction is $tan\phi$ =μ=1.8.

The shear flow that develops at the jacket-encased member interface is responsible for the monolithic action of the jacketed part of the member, and thus, for the engagement of the jacket in sectional equilibrium. The weakest section of the retrofitted member is at the gap, or at the cold joint formed between the jacket and footing, where longitudinal normal stresses in the jacket are either zero (Figure 2.8(a) and 2.8(d)) or can only be developed under bearing -i.e., only in the compressed part of the cold joint (Figure 2.8 (b) and 2.8 (e)).

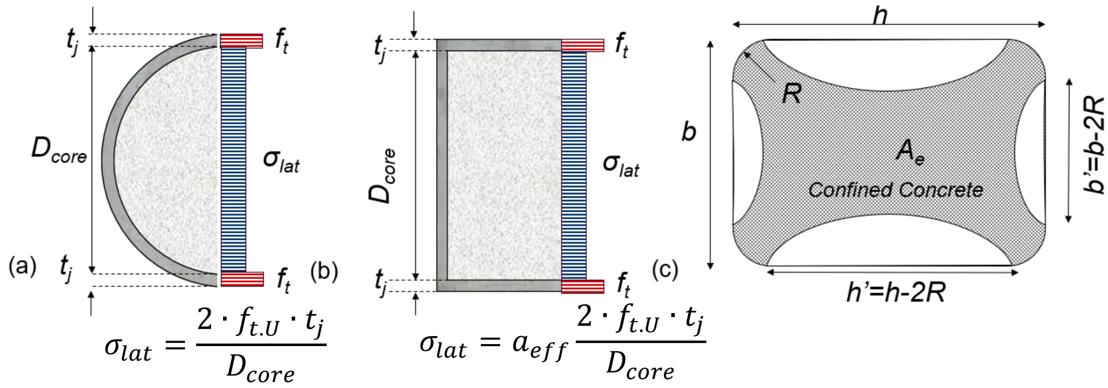

Figure 3.1. Definition of the confining pressure exerted by the UHPFRC Jackets on encased concrete: (a) Circular and (b) Rectangular encased cross sections, (c) effectively confined region and definition of terms. The red rectangles show the tensile strength and the blue rectangle shows the confining lateral pressure.

In the case of the extended jacket into the footing, the longitudinal tensile ($t_j f_{t,U}$) and compressive stresses ($t_j f_{c,U}$) that develop in the jacket walls participate in the flexural action of the critical section as depicted in Figure 2.8 (c) and 2.8 (e) for the compression part, and in Figure 2.8 (f) for the tension part of the critical section.

3.1 Confining Pressure, Strength, and Deformation Capacity of Encased Concrete

The simplest model describing the confining action of a UHPFRC jacket is used here to estimate the average lateral confining pressure, σ_{lat}, (Figure 3.1), where t_j is the jacket thickness, $f_{t,U}$ is the tensile strength of the jacketing material and $f_{y,j}$ is the yield strength of any horizontal reinforcement added in the jacket at a volumetric ratio $\rho_{j,tr}$ and bar spacing s_j.

$$\sigma_{lat}^{U} = \frac{2 \cdot (\alpha_{eff}^{U} \cdot f_{t,U} + \rho_{j,tr} s_j \cdot f_{y,j}) \cdot t_j}{D} \quad (3.2)$$

Eq. 3.2 is adapted from (Ralli et al., 2023). Thus, as in the case of fibre-reinforced polymer (FRP) wrapping, the confining pressure exerted by UHPFRC jackets, σ_{lat}^{U}, is proportional to the thickness t_j and to the maximum hoop stress available in the jacket – i.e., the material tensile strength, $f_{t,U}$. From Figure 3.1 it is evident that the pressure is also inversely proportional to the section size, D. In the context of the present work, $f_{t,U}$ could denote the cracking stress (conservatively), $f_{t,cr}$, or could be taken equal to a fixed fraction of the peak tensile strength, $f_{t,U}$, (e.g., $f_{t,U} = \varphi \gamma_f f_{t,U}$ where

φ is the material safety factor, and γ_f is the fiber orientation factor proposed to be taken equal to 0.75 for UHPFRC materials, (Annex 8.1 of CSA-S6, 2019)). The confinement effectiveness, α_{eff}^U, for a circular cross-section is equal to 1; for rectangular cross-sections the effectiveness coefficient, representing the fraction of the encased area that may be assumed to sustain uniform confining pressure, has been shown to take a similar form to what is proposed for other external jackets (see Figure 3.1(c)) (Ismail et al., 2023; Tsiotsias, 2022; Tsiotsias, 2024):

$$\alpha_{eff}^U = 1 - \frac{(b-2R)^2 + (h-2R)^2}{3bh(1-\rho_g)} \tag{3.3}$$

The above simplistic interpretation of the role of UHPFRC jacketing as a confining device overlooks the significant flexural stiffness of the jacket layer against lateral outwards bending. This flexural stiffness is engaged by the outwards pressure exerted by the dilating encased concrete as it approaches failure (Figure 3.2(a)). This is an aspect of the confining effectiveness that will be explored in the experimental part of the present thesis.

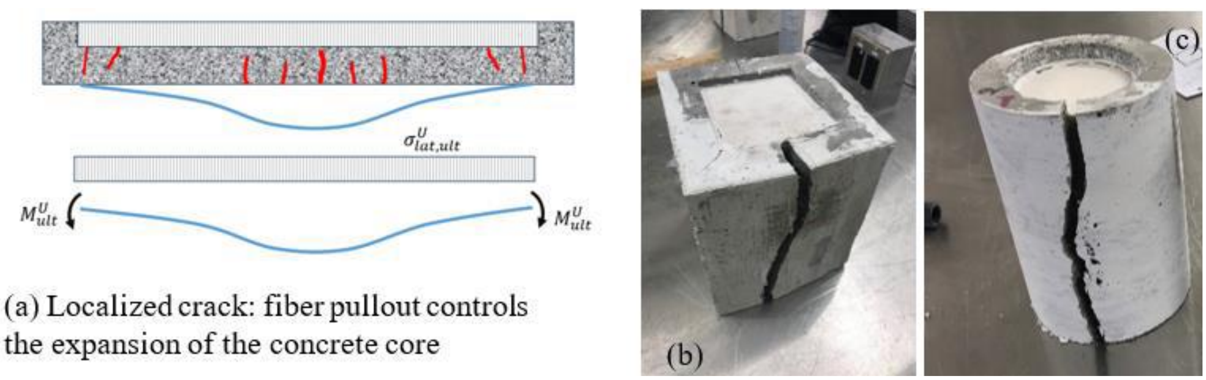

Figure 3.2. (a) Flexural resistance provided by the jacket near failure (after formation of localized crack) affects the rate of post-peak degradation of the encased concrete stress-strain response; (b), (c) Crack pattern in experimentally tested jacketed short columns (Tsiotsias, 2024).

Experimental evidence on TH-UHPFRC encased cylindrical and prismatic short columns has shown that whereas the strength increase is marginal – consistent with the passive nature of the exerted confinement, the relative deformation capacity increase is extensive – and it is actually more evident in rectangular rather than in circular sections. To address this effect, Tsiotsias (Tsiotsias, 2024) proposed different confinement factors for peak compressive strength f'_{cc} and ultimate deformation capacity, ε_{cc}, of TH-UHPFRC – encased concrete as per the following expressions:

$$f'_{cc} = K_\sigma \cdot f'_c; \qquad \varepsilon_{cc,u} = K_\varepsilon \cdot \varepsilon_{c,u} \tag{3.4}$$

$$K_\sigma = 1 + \lambda_\sigma \bar{\sigma}_{lat}, and\ \ K_\varepsilon = 1 + \lambda_\varepsilon \bar{\sigma}_{lat} \tag{3.5}$$

In Eq. 3.5, $\bar{\sigma}_{lat} = \sigma_{lat}/f'_c$ is the total normalized lateral pressure (which includes contributions from the UHPFRC material layer and any other form of transverse reinforcement either pre-existing in the member or added in the jacket. Here, ρ_{vol}^{tr} is the volumetric ratio of transverse steel reinforcement, α_{eff}^{tr} is the confinement effectiveness, and $f_{y,tr}^{st}$ the yield strength of transverse steel reinforcement; in the remainder, the presence of jacket horizontal reinforcement (Eq. 3.2) is neglected for simplicity because it is mostly used in TS-UHPFRC cases:

$$\sigma_{lat} = \sigma_{lat}^U + \sigma_{lat}^{st} = \sigma_{lat}^U = \frac{2 \cdot \alpha_{eff}^U \cdot f_{t,U} \cdot t_j}{D_{core}} + 0.5\alpha_{eff}^{tr}\rho_{vol}^{tr} f_{y,tr}^{st} \tag{3.6}$$

Values for the λ_σ and λ_ε coefficients were calibrated by Tsiotsias (Tsiotsias, 2024) against experimental results as follows: $\lambda_\sigma = 3$ and $\lambda_\varepsilon = 20$. To model the complete uniaxial compressive stress – strain response of encased concrete, the Hognestad parabola (Hognestad E, 1951), which is used for conventional concrete is used to describe the ascending part of the response up to the point with coordinates $(f_{cc}(\varepsilon_{co}) = f'_c,\ \varepsilon_{co})$ that correspond to peak strength of plain concrete. (The reason for this is to ensure that confined concrete has at least the same initial stiffness as unconfined concrete). Thus:

$$f_{cc}(\varepsilon) = f'_c \left(2\frac{\varepsilon}{\varepsilon_{co}} - \left(\frac{\varepsilon}{\varepsilon_{co}}\right)^2 \right) \quad for \ \ \varepsilon \le \varepsilon_{co} \tag{3.7}$$

A linear segment is used to model the response from that point up to peak strength of the TH-UHPFRC confined concrete, with coordinates ($f'_{cc}, \varepsilon_{cc,o}$), where the strain $\varepsilon_{cc,o}$ at the attainment of the confined strength, f'_{cc} is given by (Imran et al., 1996; Richard et al., 1928):

$$\varepsilon_{cc,o} = \varepsilon_{co} \cdot 5 \cdot \left[\frac{f'_{cc}}{f'_c} - 0.8\right] \le \varepsilon_{cc,u} \tag{3.8}$$

therefore,

$$f_{cc}(\varepsilon) = f'_c\big(1 + \lambda_\sigma \bar{\sigma}_{lat}(\varepsilon - \varepsilon_{co})\big) \le f'_{cc} \quad for \ \ \varepsilon_{co} < \varepsilon \le \varepsilon_{cc,o} \tag{3.9}$$

The stress model includes a plateau at constant strength equal to f'_{cc} up to attainment of the ultimate strain $\varepsilon_{cc,u}$ (which is determined from Eq. (3.4) considering that for conventional concrete $\varepsilon_{c,u} = 0.0035$). To model the post peak response, a descending branch is assumed, which corresponds to the degrading response of the jacket in tension after localization of failure along a vertical crack which is the usual manner by which jackets fail (Figure 3.2(b), 3.2 (c)). Tsiotsias (Tsiotsias, 2024) recommended a linear decay to a residual (constant) stress of $0.25f'_{cc}$ at a strain that is 3 (for prisms) to 4 (for circular sections) times the value of $\varepsilon_{cc,o}$.

3.2 Contribution of the UHPFRC Jacket to Flexural, Shear and Lap Splice Strength

3.2.1 Flexural Strength Increase

For cases where the jacket participates in the equilibrium of normal stress results of the cross section, (Figure. 2.8 (b) and 2.8 (c)) an approximate expression to assess the flexural strength increase is derived by considering the additional force component that develops in the part of the jacket which falls within the compression zone of the jacketed cross section. It was found that for low axial load ratios (similar is the case for low amounts of longitudinal reinforcement) the tensile strains that develop in the tension zone quickly exceed the nominal tensile strain capacity of the jacket (which is in the order of 0.002). Figure 3.3 and 3.4 depict a circular and a rectangular cross section after addition of a thin UHPFRC jacket layer. Forces are depicted as required for equilibrium under the simultaneous action of a compressive axial force, P, and a flexural moment, M. Parameter x denotes the depth of the compression zone of the cross section, T_y is the tensile force resultant (at yielding) of the tension reinforcement, and the various components C represent compressive stress resultants ($C_{c,con}$ is the force in the encased concrete that lies within the compression zone, $C_{c,s}$ is the compression force resultant of the reinforcement in the compression zone, and $C_{c,U}$ is the compression force resultant in the jacket layer). Letter Δ in front of terms denotes the change in the respective variable after addition of the jacket layer.

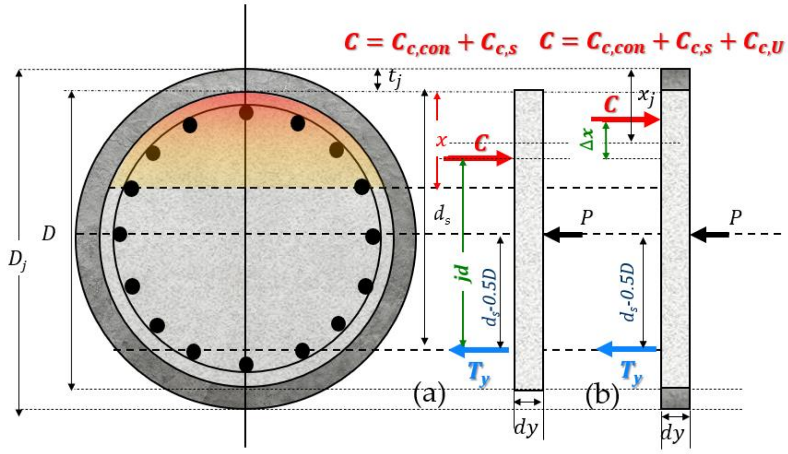

Figure 3.3. Circular jacketed cross section – equilibrium of forces at yielding. (a) Cross section, (b) lengthwise slices of length dy: left before jacketing, and right after jacketing.

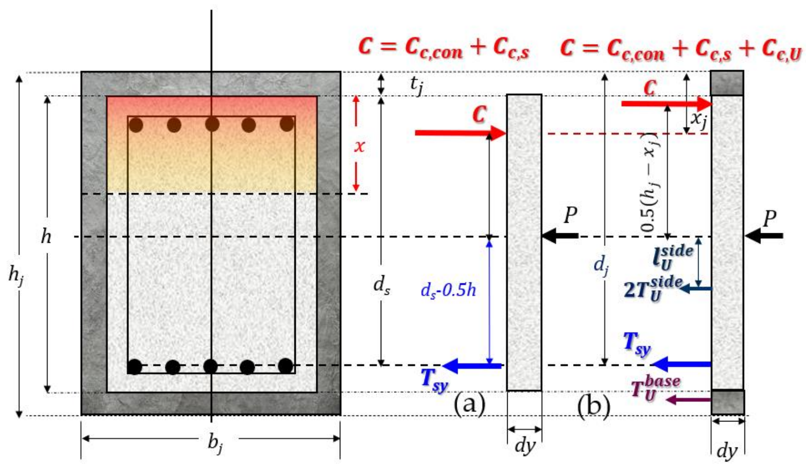

Figure 3.4. Rectangular jacketed cross section – equilibrium of forces at yielding. (a) Cross section, (b) lengthwise slices of length *dy*: left before jacketing, and right after jacketing.

At the end of the linear range of the UHPFRC jacketing material in compression ($\varepsilon_{c,o}^{U}$=0.003) the equilibrium of normal forces in the cross section has the form (Figure 3.3 & 3.4):

$$P + T_y - C_{s,c} - C_c = 0 \ = 0 \quad \rightarrow \quad P + T_y = C_{s,c} + C_{c,con} + C_{c,U} \approx C \qquad (3.10)$$

(where $C_c = C_{c,con} + C_{c,U}$ is the force developing in the compression zone of concrete and the corresponding part of the UHPFRC jacket; these forces are replaced by a single compressive resultant, *C*, which is assumed to act at the midpoint of the depth of compression zone, *x*). Considering that the left-hand side of Equation is practically constant or very mildly affected by the addition of the jacket over the original cross section, it is concluded that the increase in flexural strength of cases of Figure 2.8 (b) and 2.9 (c) over the original unjacketed section is primarily controlled by the increase in the internal lever arm of the compression stress resultant C, about the centroid of the cross section. To check this assumption, the depth of compression zone (normalized with the diameter D of the original cross section) is examined for the pier example in Figure 3.3 for two different values of the axial load ratio ν (ν=$P/(A_g f_c')$)=0.1 and 0.2); the abscissa in the figure is the total longitudinal reinforcement ratio. It is observed that the original depth of the neutral axis was in the range from 0.27D to 0.33 D for ν=0.1, and from 0.36D to 0.4D for ν=0.2, whereas the addition of the jacket has reduced the depth of the compression zone by 0.15D for ν=0.1, to 0.2D for ν=0.2. This reduction effectively is reflected in the flexural moment resistance as:

$$M_j = M_o + \Delta M; \tag{3.11a}$$

$$\Delta M = C \cdot \Delta x = \left(P + T_y\right) \cdot (0.15 + (\nu - 0.1) \cdot 0.5 \cdot) D \; for \;\; 0.1 < \nu \leq 0.2 \tag{3.11b}$$

where ΔM is the flexural moment strength increase effected by the jacket, M_o is the flexural strength of the original cross section, $M_o = \left(P + T_y\right) \cdot jd - P \cdot (d_s - 0.5D)$ where jd the initial lever arm of the unstrengthen cross section ($\approx 0.75D$). Solving for the term:

$$\left(P + T_y\right) = (M_o + P \cdot (d_s - 0.5D))/jd \tag{3.11.c}$$

for the range of axial load ratios considered, a conservative approximation for ΔM is:

$$\Delta M = \frac{1}{0.75}\left(0.15 + \frac{(\nu - 0.1)}{2}\right) \cdot (M_o + P \cdot (d_s - \frac{D}{2})) \tag{3.11.d}$$

$$= (0.2 + \frac{(\nu - 1)}{1.5}) \cdot (M_o + P \cdot (d_s - \frac{D}{2}))$$

This corresponds to the increase in the lateral load flexural resistance of the pier equal to $\Delta V_{flex} = \Delta M_o / L_s$. It is noted here that the increased shear demand in the region above the end of the jacketed section needs to be checked against the available shear strength of the original member.

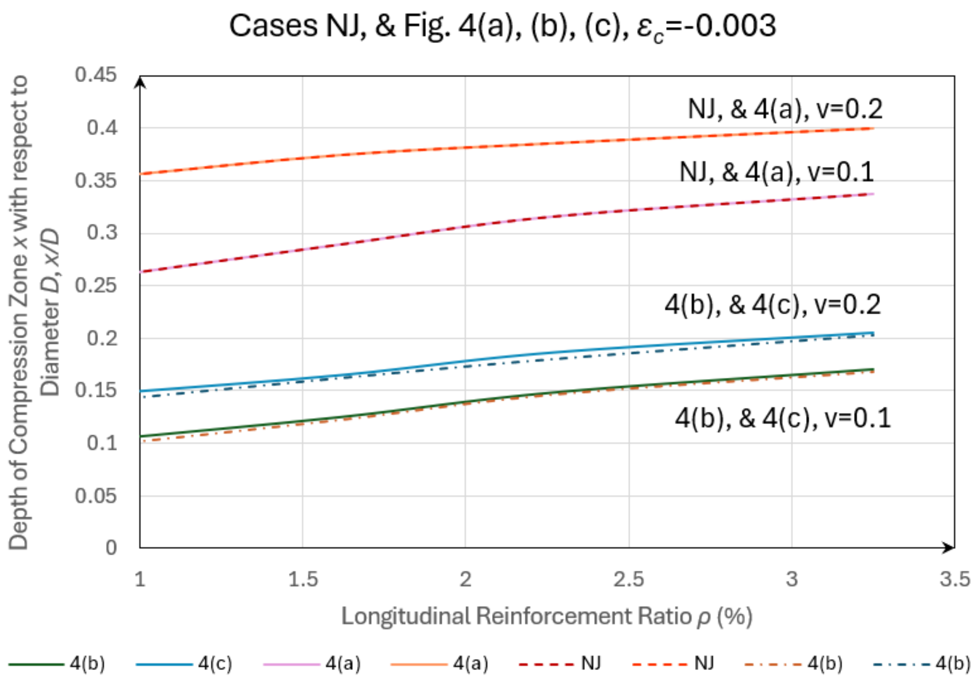

Figure 3.5. Normalized depth of compression zone against longitudinal reinforcement ratio for v=0.1 and v=0.2, in the original state and after jacketing with the nuanced setups of Figure 2.8.

3.2.2 Shear Strength Increase of the Jacketed Column

It is noted that the nominal shear strength of the original cross section is taken (Ang et al., 1986) for circular piers as:

$$V_{shear} = V_{concr} + V_{steel} = 0.185(f_c')^{0.5} \cdot A_{core} + \frac{\pi A_{tr} f_{y,tr} D_{sh} \cot\theta}{2s} \tag{3.12}$$

In the above equation, s the hoop spacing, and A_{tr} is the hoop bar area (a single hoop), D_{sh} is the effective depth of the shear resisting part of the cross section (taken in approximation as $0.8D$) ; θ_a is the angle of diagonal cracks with respect to the longitudinal axis. For columns and piers that bear axial load, cracks occur at an angle θ_a from the longitudinal axis of the member. (Ang et al, 1986) recommended taking θ_a =25° ($cot25° = 2.15$). Based on the collective experimental evidence (Gonzalez et at., 2023; Ralli et al., 2024), it has been observed that the web shear strength increase resulting from the jacket addition mitigates the likelihood of shear failure even after the above flexural strength increase. Eq. 3.13 below is used to determine the enhancement of shear strength contributed by the jacket, where f_{td}, is the design tensile strength of the material, which is taken equal to: $f_{td} = \min\{f^U_{t,cr};\ \gamma_F f'_{t,U}\}$; D_j is the external diameter of the jacketed section).

$$V_{shear} = V_{concr} + V_{steel} + V_j\,; \qquad V_j = 2t_j \cdot f_{td} \cdot (D_j - t_j)cot\theta_a \tag{3.13}$$

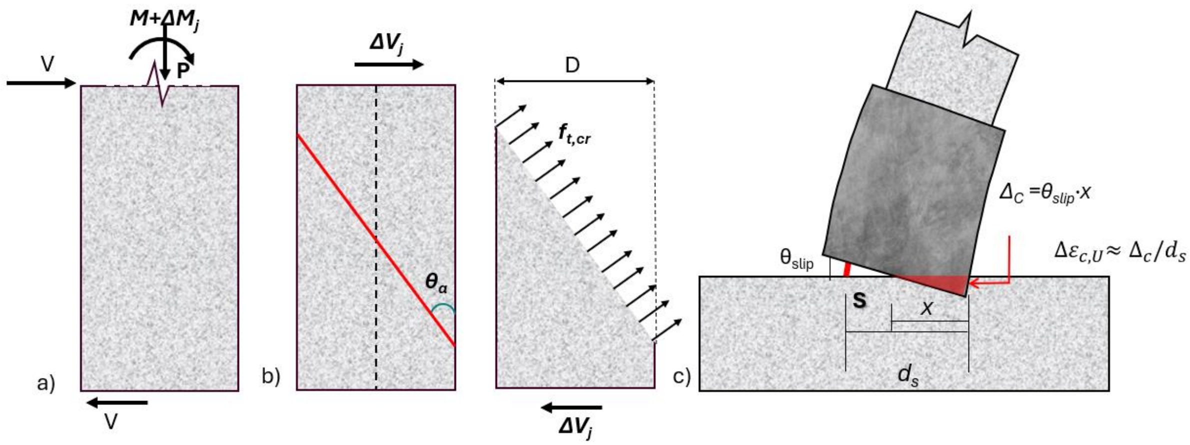

Figure 3.6. Models for estimation of the contribution of the UHPFRC Jacket to (a) flexural and (b) shear strength for Figure 2.8 (b) and 2.8 (c); (c) Kinematic relationship between slip of tension bars and compressive strain increment in the jacket.

3.2.3 Lap Splice Strength

Lateral pressure provided by the cover, and the hoops crossing the development length of lap splices provide the essential clamping action that enables the development of the reinforcing bars. The frictional model expression has been used in the past to quantify the bar development capacity as:

$$F_b = \mu \cdot ((2c + D_b) \cdot f'_t \cdot L_b + \sum A_{tr} f_{y,tr}) \leq \frac{\pi}{4} D_b^2 f_y \tag{3.14}$$

The frictional coefficient, μ for seismic applications is usually taken, $\mu=1$. Also, the clamping contribution provided by the cover is eliminated upon splitting failure, which occurs after bar yielding, and therefore it is usually neglected. In the example considered, Eq. 3.14 results in a maximum developed force of F_b of about 75% of the yielding strength of the bar. Therefore, the vertical dashed line in the left of the moment curvature diagrams of Figure 2.9 (a) and 2.10 (a) represents the limit of lap-splice failure for the circular pier studied. Thus, the benefit of the jacketing option depicted in Figure 2.8 (a) is that it enables bar yielding and development of a significant part of the inelastic range of response in the Moment-Curvature diagram beyond the limiting boundary shown in the plot. The revised expression for the tension bar force resultant after accounting for the jacket contribution is given by Eq. 3.15:

$$F_b = \mu \cdot \left(\sigma_{lat}^{U} \cdot t_j \cdot L_j + \sum A_{tr} f_{y,tr}\right) \tag{3.15}$$

In Eq. (3.15), σ_{lat}^{U} is the lateral confining pressure provided by the jacket (Eq. 3.2) and L_j is the minimum value between the length of the jacket and the available lap-splice length. For the jacket to be adequate the right-hand side term of Eq. 3.14 should exceed at least the yield strength of the bar to provide some capacity for redistribution after yield penetration over part of the lap length. According to the design charts provided (Tastani et al., 2013), for good bond conditions a $30D_b$ anchorage length can support a strain ductility in the reinforcement of the order of 9 (i.e. a nonlinear bar strain in the order of 0.018) for high strain hardening reinforcement; this ductility is increased to 25 for low strain hardening reinforcement (i.e., bar strain in the order of 0.05).

Therefore, although the flexural strength increase by the addition of the jacket according to the scheme of Figure 2.8 (a) is negligible, it is found that it enables the development of the flexural strength up to a large strain limit (depicted with a circular marker in Figure 2.9(a) and 2.10 (a) is the lower case of nonlinear strain of 0.018 and with a rhomb marker for the higher nonlinear strain option of 0.05) - while also mitigating shear failure.

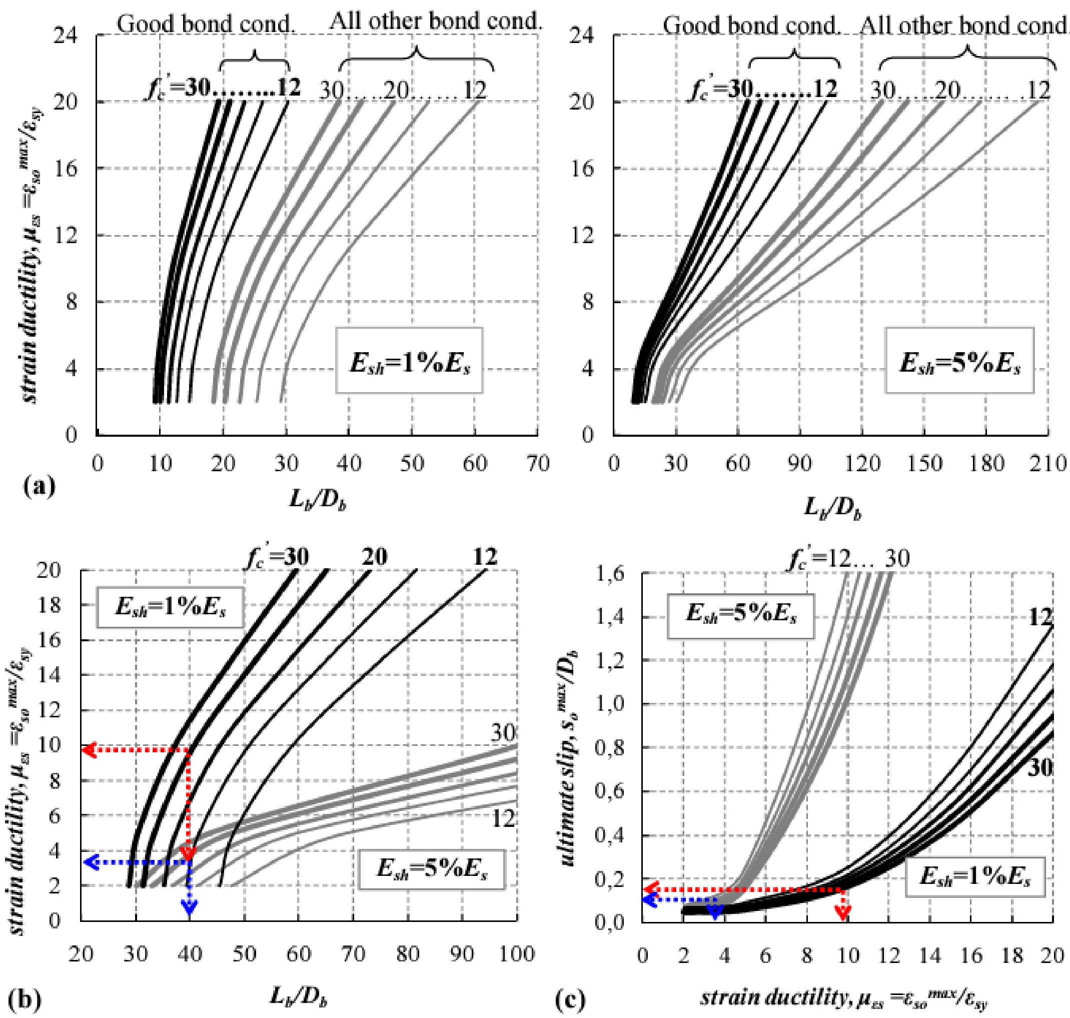

Figure 3.7. (a) Anchorage strain ductility capacity versus the required anchorage length for steel category S500, two values for hardening modulus (E_{sh}=1% and 5% of E_s=200GPa), five concrete strengths (f_c'=12, 16, 20, 25, 30 MPa) and two bond conditions (Good bond conditions: fb max=2.5√f_c'(MPa); All other bond conditions: $f_{b\ max}$=1.25√f_c'(MPa). Adapted from Tastani et al. 2013).

Using design bond strength f_{bd} values (For S500 & D_b≤20 mm: $f_{bd}=2\cdot f_{bo}= 2\cdot n_1n_2n_3n_4(f_c'/20)^{0.5}$ =2.8, 3.2, 3.6, 4.0, 4.4 Mpa for the concrete strengths listed above, where, n_1 =1.8 for ribbed bars, and the other terms are taken equal to 1 for normal concrete and favorable bond conditions): (b) diagrams $\mu_{\varepsilon s}$ - L_b/D_b and (c) charts of the ultimate slip as a function of strain ductility capacity. (From Tastani and Pantazopoulou, 2013).

3.3 Limitation of the Deformation Capacity of Jackets Bearing on the Footing

In the absence of a separating gap above the footing it was found that jacket schemes from Figure 2.8(b) and 2.8(c) enable the attainment of a strength increase in the order of 33% of the original nominal flexural resistance by bearing action directly on the footing. A failure mode that needs to be mitigated by controlling the amount of lateral drift demand in the column is the increased compression strain in the compression zone, effected by the localized reinforcement pullout slip, *s*, that is occurring in the tension zone. The kinematic relationship that relates the localized compression strain increase, $\Delta\varepsilon_{c,U}$ with tension reinforcement pullout is (Syntzirma et al., 2010):

$$\Delta\varepsilon_{c,U} \approx \frac{s}{d_s - x} \cdot \frac{x}{d_s} \tag{3.16}$$

where d_s is the distance of the tension reinforcement from the extreme compression fiber of the jacketed cross section and x is the depth of the compression zone (Figure 3.4). Based on the study presented in the preceding, under good bond conditions as would be provided by the jacket over an anchorage length of $30D_b$ the maximum pullout slip before complete bond failure of the rebar is in the range of $0.3D_b$=*9mm* for the strain ductility of 9 that was determined above assuming a moderate amount of reinforcement strain hardening. Using d_s=1250 mm for the pier example of Chapter 2, and the result for $x \approx 0.12D$=145mm found earlier, this leads to $\Delta\varepsilon_c = 0.00095$ – this strain can accelerate compression failure of the outer layer of the jacket; the increment $\Delta\varepsilon_c$ is exacerbated further with increasing crack opening above the footing in the tension zone rendering the compression failure of the jacket at the toe of the pier a likely contingency for arrangements according with Figure 2.8 (b) and 2.8 (c).

3.4 Flexure-Dominated Response

Using the initial flexural strength of the cross-section and the additional flexural strength provided by the jacket as described in Eq. 3.11.d, the lateral force V_{flex}, for flexure-dominated response can be determined, according to Eq. 3.17:

$$V_{flex} = \frac{M_o + \Delta M_j}{L_s} \tag{3.17}$$

The lateral force that takes into consideration the enhanced flexural strength due to the TH-UHPFRC jacket was compared to the maximum experimental lateral force of each specimen in the aforementioned database. The results are plotted against the geometric jacket index J_i in Figure.

3.8 below. Specimens having V_{peak}/V_{flex} ratios less than one indicate that another form of failure other than extensive flexural yielding may have occurred (e.g. jacket tow crushing or shear failure above the end of the jacketed region), limiting the effectiveness of the retrofit. It is noted that specimens that present J_i of less than 25 % were able to attain strengths at least equal to the nominal Flexural Strength, only when the ρ_{sl} was less than 2%; shear failures were mitigated in these cases. But for higher longitudinal reinforcement ratios and small values of the composite index (e.g., when PVA fibers were used in the jacket, or a high axial load ratio was applied, or an excessive amount of longitudinal reinforcement ratio had been used in the encased member), premature shear failure, or jacket toe crushing due to bar pullout as illustrated by Eq. 3.16 limited the strength increase offered by the jacket whereas the moderate drift capacity comprised a large component of slip and shear deformation components.

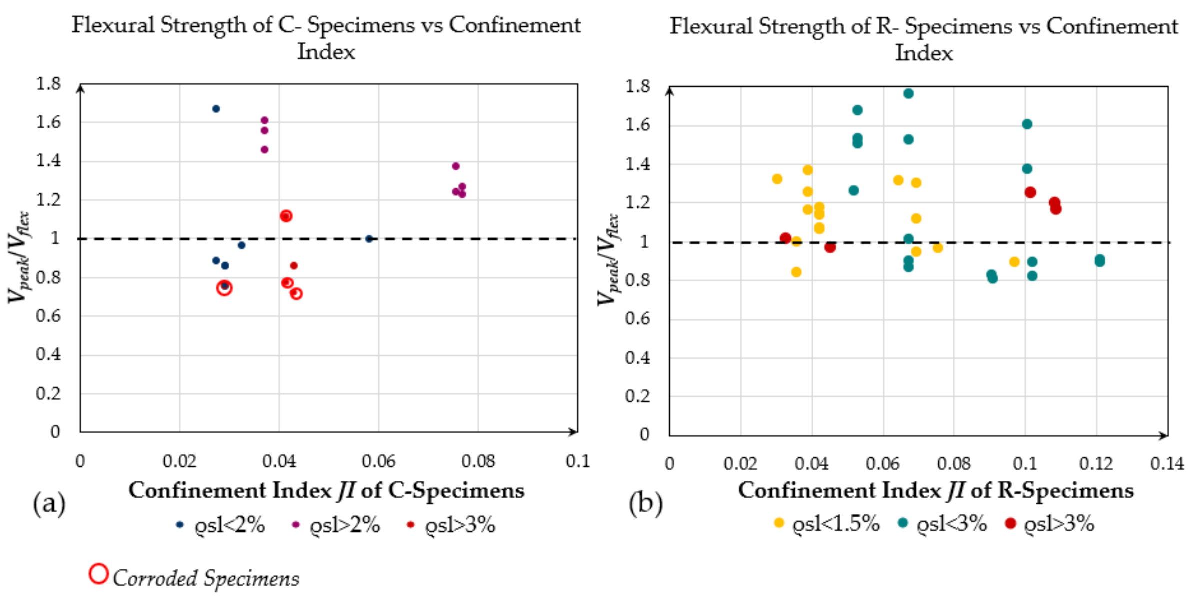

Figure 3.8. Behavior of flexural strength as V_{peak}/V_{flex} of all specimens against the geometric Jacket Index J_i (%).

3.5. Recommended Performance Limits for Retrofit Design with UHPFRC Jackets

Consistent with the prevalent methods of seismic evaluation of existing structures, it is of interest to develop the design of seismic UHPFRC retrofit solutions compatible with a performance-based framework. After detailed evaluation of the available experimental evidence on UHPFRC material characterization and reversed cyclic load testing of UHPFRC Jacketed components (Ismail, 2024;

Ralli et al., 2024; Tsiotsias, 2024) pertinent design provisions refer to three different performance objectives (from Figure 3.9 below) as follows (ASCE, 2017; CSA S6, 2018):

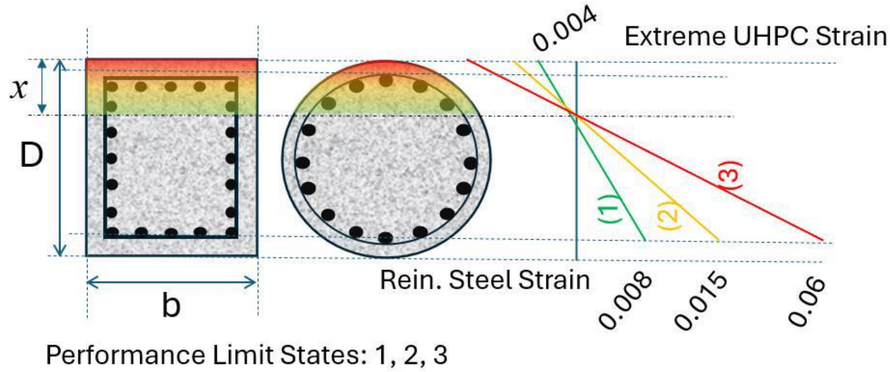

Figure 3.9. Performance limit states in retrofitting systems with UHPFRC Jackets.

- *Minimal Damage*- UHPFRC jacket strain in compression ≤0.004, longitudinal reinforcement tension strain ≤0.008. In the CSA-S6, this refers to cover crushing and delamination in conventional concrete piers as a first indication of notable distress. These two criteria are intended to limit the requirement for repairs under a frequent intensity earthquake (20% probability of exceedance in 50 years) – such as local crushing of the jacket in compression and significant bar pullout from the footing. It is noted that based on the experimental evidence summarized by (Ismail et al., 2023) the UHPFRC attains its uniaxial compressive strength at strains in the range of 0.004 – 0.005. A counterargument to the compression strain limit chosen for the Minimal Damage Limit State is that the enhanced strain capacity of the encased concrete would not be exploited at that stage. It is noted however, that with reference to the frequent earthquake design event, a primary requirement of the retrofit scheme is the continued functionality of the retrofit. In this context, a higher level of damage in the extreme fibers of the compression zone of the jacketed section would not be warranted.
- *Repairable Damage*- The tensile strain in longitudinal reinforcement is limited to 0.015 – this value is extended from what is valid for conventional seismic design of bridge piers for the Repairable Damage performance limit state. It is noted that strain reversal from this strain level has been linked to reinforcement buckling for conventionally confined cross sections, whereas here it was shown that short lap-splices or anchorages may accelerate crushing at the toe of the UHPFRC Jacket on account of pullout rotations for these levels of strain. Therefore, this limit heralds the onset of serious damage beyond which, repair may not be possible.

- *Life Safety Limit*- The damage sustained by the member should not cause crushing of the encased concrete core, whereas the reinforcing steel tensile strains should not exceed a nominal strain of 0.06. It is noted that this is a conservative limit for bar fracture. This limit is necessary for cases where the main reinforcement has been previously embrittled by corrosion. Another reason is that the significant confinement exerted by the jacket has been shown to enhance reinforcement to concrete bond, thereby limiting strain penetration and leading to severe strain localization at the critical section with increased likelihood of bar fracture at high levels of lateral drift.

Chapter 4: Material Testing for Characterization of UHPFRC Mix

4.1 Introduction

This chapter presents the data obtained from experimental work for characterization of the UHPFRC mix used in the experimental component of this research. Specimen dimensions and forms for material characterization were according to the relevant CSA standards (Annex 8.1 CSA-S6, 2019, Annex U of CSA A23.1 (2019) and AASHTO (2022)). Various mechanical tests were performed including compression tests on 75 mm diameter cylinders with a height of 15 0mm to evaluate the peak strength, $f'_{c,U}$ and the compression stress-strain response. In addition, the Modulus of Elasticity *(E)* and Poisson's Ratio *(v)* values were obtained; each experimental variable reported represents the average of at least three identical tests. Tension was evaluated using Direct Tension Tests according with the AASHTO test recommendation. Certain relevant parameters such as fiber orientation, effects of casting and direction of flow are studied with the prisms involved in direct tension.

4.2 Materials and Casting

The UHPFRC used in this research was produced from the prepackaged dry cementitious mix powder. From now onwards this UHPFRC premix material is referred to as *CEK2*, where the integer 2 presents the volume fraction of steel fibers in the mix. The UHPFRC premix is a cement-based powder which contains Portland cement, finely graded aggregates, nanostructured materials, carbon nanofibers (CNFs), a special admixture that functions as a superplasticizer *(SP)* and a solution of nickel II chloride used as an accelerator chemical additive *($NiCl_2$)*. No other superplasticizer nor external material that was not provided by the manufacturer was used. For this research, this UHPC premix falls into the UHPFRC when incorporating steel fibers. The brass coated straight steel fibers used were added at different volumetric ratios in fabricating the Precast Jackets and the Connectors devices, i.e., at 2% and 3% correspondingly. These steel fibers had a 0.2mm in diameter and 13mm in length, categorized as High Carbon Steel (HCS) with a reported tensile strength of about 2,750 MPa. The mix proportions are shown in Table 4.1.

The UHPFRC CEK2 characterization batch was mixed in a large industrial pan type drum mixer with a nominal capacity of 400 L. The premix was first poured into the drum and mixed for 2 minutes, followed by the superplasticizer *SP* admixture combined with the *accelerator* and water for 9 minutes. Lastly, for the last 3 minutes of the mixing procedure the steel fibers were gradually added and mixed. Figure 4.1 illustrates the mixing procedure followed.

Table 4.1. Mix design proportions of the UHPFRC Mix *CEK2*

Mix CEK2	Dry Premix	Admixture SP	Accelerator $NiCl_2$	Water	Steel fibers (2%)
Proportions by weight (g) to produce 1 L	2130	16.7	10.29	167	156

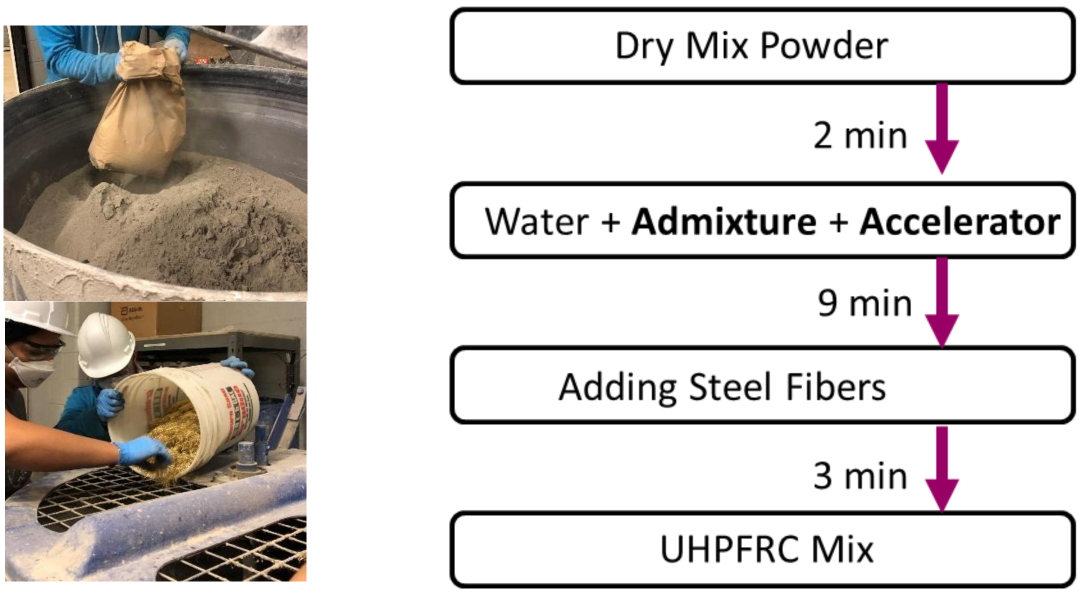

Figure 4.1. An illustrative flowchart of the UHPFRC CEK2 mixing procedure.

The UHPFRC *CEK2* mix produced was flowable and self-consolidating. Immediately after the mixing process, flowability of each mix was determined using a flow test table as per ASTM C1856 (2017) by filling the conical bronze for the flowability test in a single pour up to its max capacity and making with flush with the top edge (Figure 4.2). Once filled, the conical mold was lifted over to allow the cementitious mortar to spread on a circular bronze plate. Flowability was determined using the average diameter of the CEK2 flow which was measured about 120 seconds after lifting the mold (see Figure 4.2). The average flow value for CEK2 was 230 mm which indicated sufficient flowability of the UHPFRC.

Figure 4.2. UHPFRC CEK2 flow test.

Wooden and acrylic molds were used for casting the direct tension test specimens, whereas standard plastic molds were used for casting cylindrical specimens. The cylinders had a diameter of 75 mm with a height of 150 mm. The direct tension specimens were prisms with a square cross section of 50 mm by 50 mm by 430 mm in length; the minimum cross-sectional dimension is limited by the requirement that it ought to be at least 3 to 5 times the fiber length used. These specimens were cast from the end of the mold, according to what is known in the literature as one-way casting (OW). The OW casting was carefully performed by marking the outside of the mold with a marker, to then pour UHPFRC CEK2 from one end to allow the mix to fill the mold thanks to the self-consolidation and self-flowing capability of the fresh material; light tapping with a mallet on the sides of the forms was the only method used to eliminate trapped air in the lateral surfaces of the specimens (see Figure 4.3). All the molds were lightly coated with oil prior to the casting to act as a releasing agent, and the specimens were covered after casting and allowed to harden in a controlled environment before demolding. To help the hydration process and to generate a level surface which is needed for the test setup, the specimens were covered with an acrylic smooth plate (*plexiglass*) (see Figure 4.4). The specimens were demolded after 48 hours from casting and then they were all placed in a curing tank for 28 days.

Figure 4.3.CEK2 specimens immediately after casting.

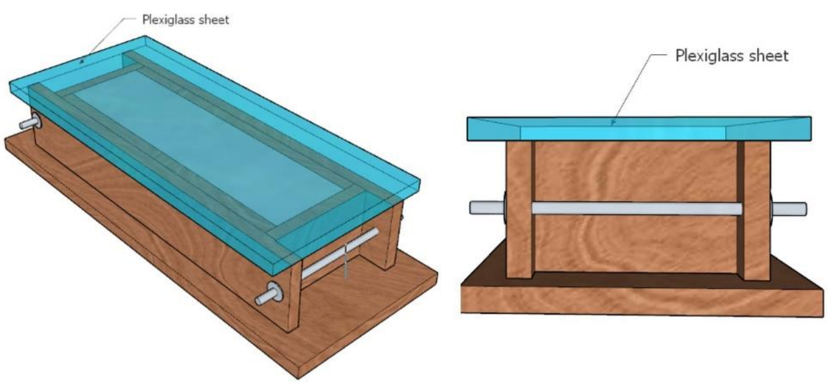

Figure 4.4. Specimen surface detail with acrylic smooth plate on top (adapted from Development of Alternative Test for Tensile Characterization of UHPC, Ralli, 2024).

4.3 Mechanical Tests

4.3.1 Compression Test

To test the cylindrical specimens, a displacement-controlled compression-testing machine (*Controls Pilot)* was used. The specimens had a 75 mm diameter with a 150 mm height and they were tested with a testing rate of 0.0075 mm/min based on the recommendations in Annex U of CSA A23.1 (2019). The main reason of using a displacement-controlled setting instead of a loading-controlled, was in order to obtain the post-peak behaviour of the CEK2 mix. However, some of the cylinders specimens suffered sudden fracture followed by an exploding sound when reaching peak load, which made the machine unable to capture the post-peak behavior. The cylinders were cast in a plastic mold where the inner surface was oiled prior pouring. No consolidation process was performed (tapping rod, tapping mallet nor vibration table) since CEK2 is a self-consolidating and flowable mix in fresh state. Only the top surface of the cylinder was carefully smoothened out with a rod to help the grinding process after demolding. The plastic molds were sealed with the incorporated lid after casting. Prior to casting, a small hole was made at the bottom of the plastic molds with a nail and a hammer, so that the specimens could be demolded with an air pressure gun. The cylinders were demolded 48 hours after casting, and then they were placed into a curing tank in a controlled environment for 28 days. To achieve a smooth surface, the cylinders were grinded on both top and bottom surfaces with a concrete grinding machine to secure an even surface so that the compression stress could be evenly distributed. Figure 4.5 shows the compression test setup. The average compressive strength ($f'_{c,U}$) obtained was 158 MPa. Peak load and $f'_{c,U}$ are summarized in Table 4.2 for a total of six cylindrical specimens. After testing, the CEK2 cylinders held their integrity due to fiber bridging effect crossing the cracks, which were oriented along the longitudinal or inclined relative to the direction of loading.

Figure 4.5. Compressive strength test setup.

Table 4.2. Compressive strength results for CEK2.

Cylinder	Peak Load	Compressive Strength	Average Strength
	(kN)	(MPa)	(MPa)
C1	379.9	86	158
C2	680.4	154	
C3	658.3	149	
C4	799.6	181	
C5	826.1	187	
C6	852.6	193	

4.3.2 Modulus of Elasticity and Poisson's Ratio

The Modulus of Elasticity (*E*) and Poisson's ratio *(v)* were calculated according to the ASTM C469 (2014). Three cylinders (C2, C4, and C5) were prepared with installation of strain gauges on their lateral surface to obtain the strain records in the transverse and longitudinal directions. Foil strain gages were placed on the cylinder surfaces as follows: two 10 mm gauge length strain gages were placed diametrically opposite at the mid height of the cylinder in the longitudinal direction (parallel to loading) to record longitudinal strain values; one 5 mm gauge length strain gage was placed in the transverse direction (horizontally to loading) to capture transverse strain values. The horizontal strain gage was leveled with the mid height of the vertical strain gage. The surface of the cylinder was cleaned of any dust particles with sandpaper and a small brush, and the cylinder was also marked with vertical lines to select an area with no voids. Commercial super glue was used to secure the strain gage, and a non-stick foil was used to place the strain gage before allowing it to dry. The electrical terminals of the strain gages were soldered to the electrical wires by using a lead wire. The strain gages were protected with rubber tubes to avoid damage due to the specimen handling, from the installation station into the Controls Pilot setup. The electrical wires were plugged into a data acquisition unit (DAQ) to record the strain data which was synchronized with the Controls Pilot machine right before the test started. Before starting each test, the wires were secured to the bottom loading plate to avoid twisting of the electrical wires during testing. Moreover, the two electrical terminals of each strain gauge were protected from merging into each other before testing, otherwise the resulting data would be incorrect. Figure 4.6 (a) shows the setup of the cylindrical specimen prepared for calculating *E* and *v*, whereas (b) shows the cylinders after testing. Results for the three cylindrical specimens and their values are shown in Table 4.3. The values of *E* and *v* were calculated with Eq 4.1 and 4.2 respectively, below. Variables σ_1 and σ_2 are the values of compressive strength corresponding to a longitudinal strain of 50 μm/m and at 40% of the compressive strength, respectively. The value for calculating 40% is defined with reference to the average compressive strength from Table 4.2. Terms ε_1 and ε_2 represent a longitudinal strain of 50 μm/m and the longitudinal strain corresponding to σ_2. Parameters ε_{t1} and ε_{t2} represent the transverse strains corresponding to σ_1 and σ_2, respectively. However, the cylinder tests only had one strain gage attached in the transverse direction. Therefore, the value taken is for the transverse strain ε_{t2} ; Table 3.3 shows no values for ε_{t1}. According to the data obtained, the average modulus of elasticity (*E*) was 54.32 GPa and the average Poisson's ratio (*v*) was 0.21.

$$E = \frac{\sigma_2 - \sigma_1}{\varepsilon_2 - \varepsilon_1} \tag{4.1}$$

$$\nu = \frac{\varepsilon_{t2} - \varepsilon_{t1}}{\varepsilon_2 - \varepsilon_1} \tag{4.2}$$

Table 4.3. Modulus of Elasticity and Poisson's ratio obtained data.

Cylinder ID	ε_1 (μm/m)	ε_2 (μm/m)	ε_{t2} (μm/m)	σ_1 (MPa)	σ_2 (MPa)	*E* (MPa)	*v*
C2	50	1201.90	205.66	8.85	61.59	45.78	0.18
	50	1201.67	205.71	8.85	61.60	45.81	0.18
	50	1201.01	205.57	8.85	61.61	45.83	0.18
	Average					**45.81**	**0.18**
C4	50	1236.62	218.99	1.81	59.59	48.69	0.18
	50	1236.97	218.90	1.82	59.60	48.68	0.18
	50	1236.27	218.05	1.82	59.61	48.71	0.18
	Average					**48.69**	**0.18**
C5	50	1065.76	284.41	5.28	74.78	68.49	0.28
	50	1065.28	284.78	5.28	74.80	68.47	0.28
	50	1065.72	284.88	5.28	74.81	68.46	0.28
	Average					**68.47**	**0.28**
	Overall Average					**54.32**	**0.21**

(a) (b)

Figure 4.6. (a) Cylindrical specimens setup with strain gauges to obtain values of compressive strength, Poisson's Ratio and Modulus of Elasticity, (b) mode of failure of the cylindrical specimens after testing in the displacement controlled machine.

Using the average compressive strength from Table 4.2 and Eq 4.3, the modulus of elasticity *E* for CEK2 can be predicted from Eq. 4.3. This expression was proposed for UHPFRC without coarse aggregate while having a compressive strength in the range of 150 MPa to 180 MPa. When using Eq. 4.3, the estimated value of E is equal to 47,710 MPa, which has a 12.17% difference from the experimental value. However, the results given by C5 may be considered as an outlier since they are providing higher values of E relative to the other batches; when ignoring the data given by C5 then, the modulus of elasticity E for the CEK2 is 46.95 GPa and the difference when compared to Eq 4.3 is only 1.61%.

$$E = 19000 \cdot \left(\frac{f_c'}{10}\right)^{\frac{1}{3}} \quad in\ MPa \tag{4.3}$$

4.3.3 Stress-Strain Behaviour in Uniaxial Compression

The same cylindrical specimens from Table 3.3 (C2, C4 and C5) were used to evaluate the full stress-strain response of the CEK2 mix in compression. These are the same specimens that were used to perform modulus of Elasticity and Poisson's ratio test. These tests were performed in the compression testing machine shown in Figure 4.5 (*Controls Automax*) with a load capacity of 3000 kN which was also capable of applying both load-controlled and displacement-controlled loading. The tests were performed with a test rate equal to 0.075mm/min (~0.45MPa/s).The strain gages installed of the sides of the cylinders mentioned above were used to measure the strain readings. The vertical reading was taken as the average from the two vertical strain gage readings to obtain the stress-strain response in uniaxial compression (see Figure 4.7). The cylinders were tested at about 270 days of age. These cylinders were kept under water in a curing tank for the first 28 days after casting, but were then stored in refrigerators to delay or stop further hydration. Excess cylinders that were cast during batching of the mixes were also kept inside a refrigerator to be used for future work. According to the results from Table 4.7, which summarizes the compressive stress-strain response, the average compressive stress corresponding to peak load of the CEK2 mix is 174 MPa with a corresponding average strain of 4.32 mm/m. Mode of failure and crack pattern of the cylindrical specimens is illustrated in Figure 4.6 (a). When the cylindrical specimens reached their peak load, it released the accumulated strain energy with a loud noise. Despite this, the cylinder specimens maintained their integrity and did not completely break apart, holding load even after the peak. This behavior was consistent even with a much slower loading rate of about 0.05 mm/min on other test specimens, including specimens form other UHPFRC mixes that were used as trial. The strain gauges ruptured due to cracks forming at peak stress, preventing them from measuring the post-peak phase. Future studies would need to explore non-contact instrumentation for effective and reliable estimation of the post-peak behavior of UHPFRC in compression.

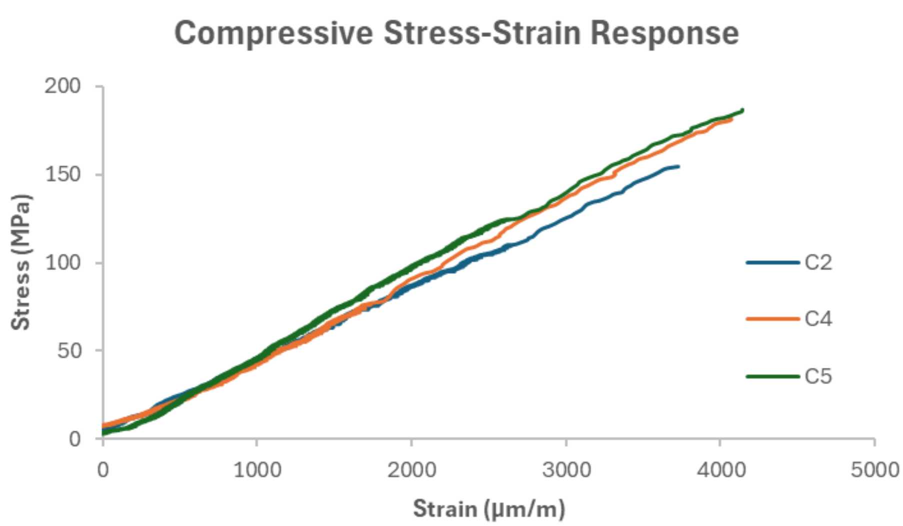

Figure 4.7. Stress-Strain response of cylinders in uniaxial compression (CEK2 Mix).

Table 4.4. Compressive strength vs strain results (CEK Mix).

Specimen ID	Peak Load	Compressive Strength	Strain at Peak Stress
	(kN)	(MPa)	(mm/mm)
C2	743	154	0.00389
C4	803	181	0.00480
C5	827	187	0.00429
Average	**791**	**174**	**0.00432**

4.3.4 Direct Tension Test

The direct tension tests were performed to obtain the tensile properties of the CEK2 mix. The tests were conducted in a displacement-controlled, closed loop universal testing machine MTS. For the characterization of the CEK2 mix, six prismatic specimens were tested (Figure 4.8.).

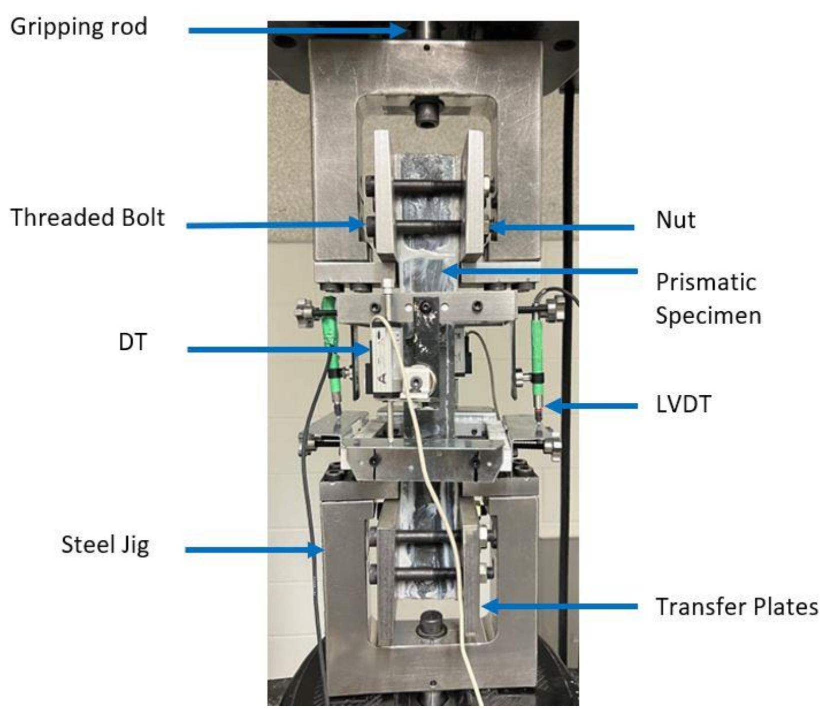

Figure 4.8. Direct tension specimen setup ready for testing in the MTS.

For all the cases, a challenging procedure had to be employed to obtain the proper setup to avoid slippage of the specimen. Prior to any direct tension test, aluminum shims where glued to the original level surfaces of the specimen. These aluminum shims were 150 mm in length by 50 mm width, having a triangular cross-sectional area, generating an angle of 2˚. The thicker side of the shim was glued flush to the edge of the specimen. The shims were glued with a two-part adhesive (*Sikadur-31 Hi-Mod Gel A+B Epoxy ®)*, where the mix ratio of the parts was 1:1. To ensure that the shims were correctly placed and that the glue was hardened, one side of the prismatic specimen was glued 48 hours prior to testing, and the other side the next day, corresponding to 24 hours prior to testing. Mounting of the specimen on the testing frame required first attachment of the transfer plates; this was done 24 hours after gluing the last shim, on a level stainless steel table. By using two even surfaces on each side of the specimen, a thick steel plate with a rectangular hollow section was placed so that the prismatic specimen was hanging to set up the top of the element, always checking that the shims and plates were flush and level. The setup procedure can be divided in two phases: top and bottom. Starting with the top phase, as a first step, two steel transfer loading plates were placed on each aluminum shim and then joined with four steel threaded bolts and nuts. The second step was to secure each bolt with a torque wrench and a socket wrench at 40 N.m. As a third and last step for phase I, once the first four bolts were torqued and secured, the instrumentation frames where placed (see Figure 4.8.). Phase II initiated by flipping the specimen carefully and repeating the same steps to secure again the transfer loading plates on the other end of the prism. As shown in Figure 4.8., two steel loading jigs (top and bottom) were used to hold the prismatic specimen in place, while the jigs were being held by a ¾ in diameter steel rod. The MTS machine was gripping the steel rod, not the specimen itself. Once the specimen was assembled as described in phases I and II, the specimen was placed inside the available space between the top and bottom jigs in the MTS. Results of the uniaxial tensile strength are summarized in Table 4.5. To capture displacement values, four instruments were used, two linear variable differential transformers (LVDTs) and two differential transformers (DTs). The readings were taken by connecting the instruments to a data acquisition system (DAQ), which was then plugged in the computer. All four instruments were placed by implementing a top and bottom instrumentation aluminum frame. Different metal angles were used in these frames, and by using magnets the instruments were secured onto the frame. The average uniaxial tensile strength obtained was 8.11 MPa, and these values are calculated according with Eq. 4.4:

$$\sigma = \frac{F}{A} \tag{4.4}$$

where F is the peak force and A is the average cross-sectional area measured within the gauge length. Figure 4.9 plots the stress-strain responses obtained in uniaxial tension from all the direct tension tests conducted.

Table 4.5. Results of direct tension testing for CEK2.

Specimen ID	Peak Load	Area	Tensile Strength
	(kN)	(mm^2)	(MPa)
BT1	21.56	2279.41	9.46
BT2	18.90	2701.63	6.99
BT3	15.79	2512.10	6.28
BT4	20.77	2626.54	7.91
BT5	15.31	2683.79	5.71
BT6	20.41	2581.53	7.91
		Average	**7.37**

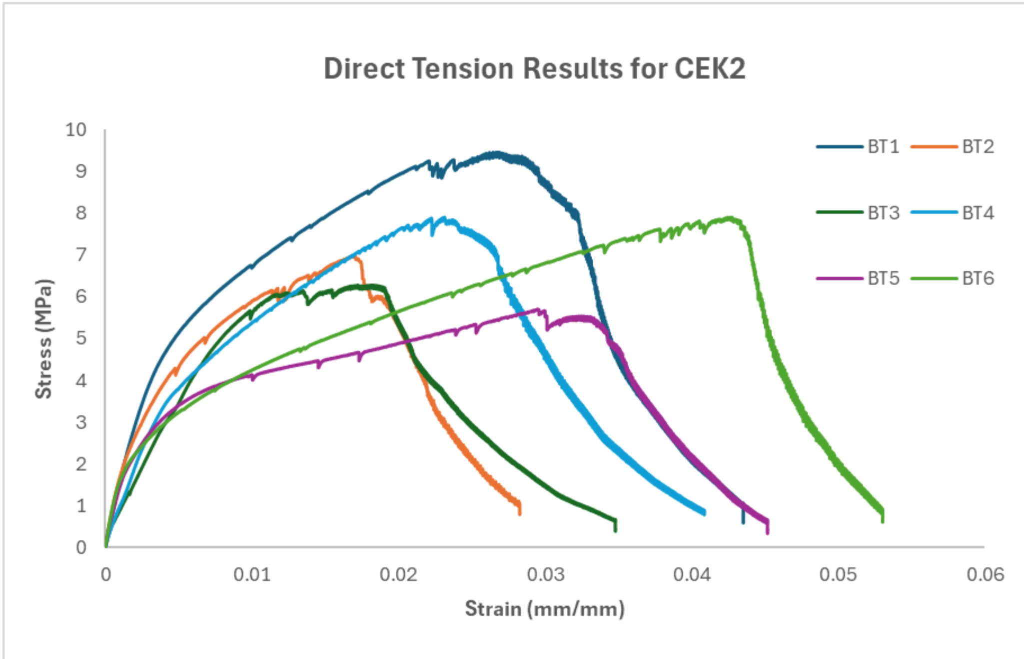

Figure 4.9. Stress-Strain Response for the direct tension prismatic specimens.

(BT1) (BT2) (BT3) (BT4) (BT5) (BT6)

Figure 4.10. Cracking Pattern for the prismatic direct tension specimens.

A desirable failure mode happens when a localized crack forms within the gauge length of the specimen without any out-of-plane bending. The gauge length of the specimen was 140 mm, as shown in Figure 4.8. On the other hand, undesirable failure modes occur when out-of-plane bending is caused by eccentricities at the crack initiation stage, the specimen setup, or irregularities in the specimen's geometry. Additionally, crack localization outside the gauge length or within the aluminum shims is considered undesirable. Figure 4.10 provides evidence regarding the location of the failure cracks for the six prismatic specimens. It is noted here that during testing several fine cracks had formed transversely to the main axis of the prisms, however these cracks closed after localization in one major crack.

Just like any other emering material, UHPFRC has a un unique learning curve. However, UHPFRC needs to be treated with care since it requires special admixtures and strict control when it comes to mixing and casting methodology. The type of UHPFRC dry mix used for this research provided results that may be slightly different than other UHPFRC dry mixes found in the market. This when comparing some mechanical properties such as flowability and fiber segregation that may affect the compression and tensile strength, as well as strains and deformation capacities. The CEK2 batch was noticed to be sensitive to the amount of chemicals added to the mix, where the slightest human error that may occur in the lab (i.e. weighting and aggregates measurements) may affect the results. In despite of this, the CEK2 provided good results in order to be categorized as UHPFRC.

4.4 Results

Material characterization was performed for the mix CEK2 used for this research. Several runs of compression and tension tests were conducted. The major findings from the tests performed for CEK2, prepared with premixed ultra-high performance cementitious material incorporating 13 mm in length brass coated straight steel fibers with a 2 % volume fraction are listed below:

a. Average compressive strength was found to be 158 MPa at 28 days of age.
b. Modulus of Elasticity was found to be 46.95 GPa whereas Poisson’s ratio was about 0.21.
c. Stress-strain responses in compression were obtained where average stress at peak at 250 days from casting was found to be 174 MPa with a corresponding strain of 0.00432 mm/mm.
d. Direct tension tests provided and average tensile strength of 7.37 MPa when one-way casting method was used, with a localized peak strain of 0.029 mm/mm. Cracking strength was however lower, at an average strength of 2.94 MPa.
e. Direct tension testing provided desirable failure modes where all the specimens cracked inside the gauge length.

Chapter 5: Experimental Program for Retrofitted Columns with Precast UHPFRC Jackets and Connection Devices

5.1 Introduction

This chapter presents the experimental program methods used and results obtained, for proof testing the concept of precast jacketing. The first step in this part of the study was the optimization process to obtain the proper geometry of the connector device (keys) that would connect the precast components in assembling the jacket on the lateral surface of a column. This step was supplemented by direct tension tests of simple precast components connected by the designed keys. The second step was implementation of this method on columns with a rectangular cross section; and the last step was conducting proof of concept tests, by subjecting the column specimens under uniaxial compression to failure. This chapter also includes details regarding the UHPFRC precast jackets, such as the mix design used, ways of casting, and flexure testing results. The dimensions, casting method, and mix design for the plain unreinforced concrete rectangular columns are described in this chapter. All the above led to the section that is related to the final column specimen assembly as well as the monotonic and cyclic testing performed on the retrofitted rectangular column specimens.

5.2 Optimization of the Connection Device Geometry for the Precast Jacket

5.2.1 Finite Element Analysis for the Connection Device Geometry

The rectangular concrete columns, made from normal unreinforced concrete, studied in this research are to be retrofitted with precast jackets made with UHPFRC. These columns have a rectangular cross-section of 150 mm by 150 mm with a height of 300 mm. The precast jackets needed to be connected to each other with a particular connector device. From this section onwards, the connector device is referred to as a *key*. The rectangular columns when tested with an axial load (process to be described later in this chapter below) will dilate and therefore produce passive transverse tension in the precast jackets. Therefore, one of the main mechanical properties of the key is tensile strength, so the tensile stress that may develop in the connected precast jacket components may attain the tensile capacity and localization strain of the UHPFRC material used in the jackets. Hence, a special key had to be created as a pre-requisite for the feasibility of the precast solution that could be installed on-site.

The precast jackets encasing the concrete columns were to be thin elements, weighing no more than 13 kg each for ease of handling by the technicians who would assemble the jackets in the field. To improve the assembly process of the retrofitted columns, the precast jackets were divided into horizontal strips. For the problem in hand, where the height of the column was 300 mm, this was developed into two sections: top and bottom. Figures 5.1 (a) and (b) show a sketch of the retrofitted column with a preliminary geometry for the key connecting the precast jackets. The key to be placed must be able to support the tension force described in Eq 5.1., where T is the tension force in Newton, H in mm is the height of the precast jacket, t is the thickness in mm of the precast jacket and $f'_{t,U}$ the tensile strength of the jacket in MPa.

$$T = H \cdot t \cdot f'_{t,U} \tag{5.1}$$

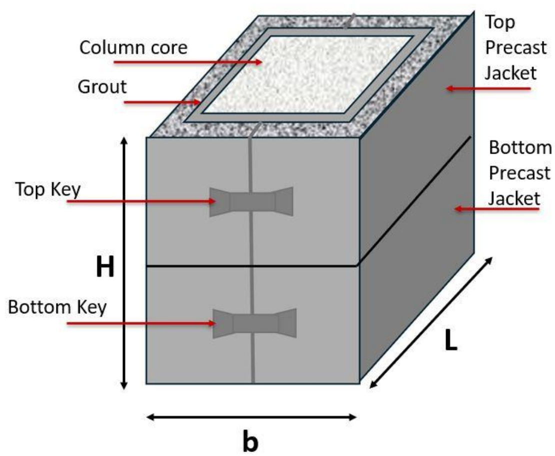

(a)

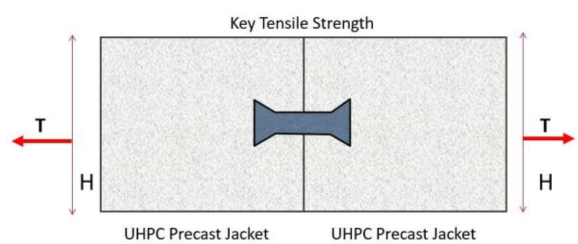

(b)

Figure 5.1. Initial sketches for (a) the retrofitted unreinforced concrete column jacketed with independent horizontal strips, and (b) the geometry of the key.

Finite element analyses were developed in SAP2000 to study different possible geometries for the key before casting them in the laboratory along with the precast jackets. Three different geometries shown in Figure 5.2 (a), (b), and (c) were studied in this research, having a *Y* geometry, a *T* geometry, and a *dogbone* geometry respectively. Figure 5.2 shows only half of the key due to symmetrical conditions. As a result, joints at the right side of the model were restricted from movement in the *x* direction, and the joints at the lower edge of the models were restricted in the *y* direction, according to the *x* and *y* axis. Three different sets of material properties were input in these models: one set to represent the encased normal strength concrete properties, one to represent the layer of adhesion between the column and the precast jacket, and one for the UHPFRC jacket properties. The different material properties are shown in Figure 5.3. The initial stages of the analytical models for the different possible key geometries involved a precast jacket made out of a UHPFRC mix with a volumetric fiber ratio of 2%, while the keys were made out of a UHPFRC mix with a 3% volumetric fiber ratio. As a starting reference point, the stress-strain curve for the UHPFRC is shown in Figure 5.4. The values from Fig 5.4 were used as a reference point in order to start the finite element analysis for the research, since the experimental program (i.e. the characterization tests) had to be postponed due to maintenance that was done in the lab facilities.

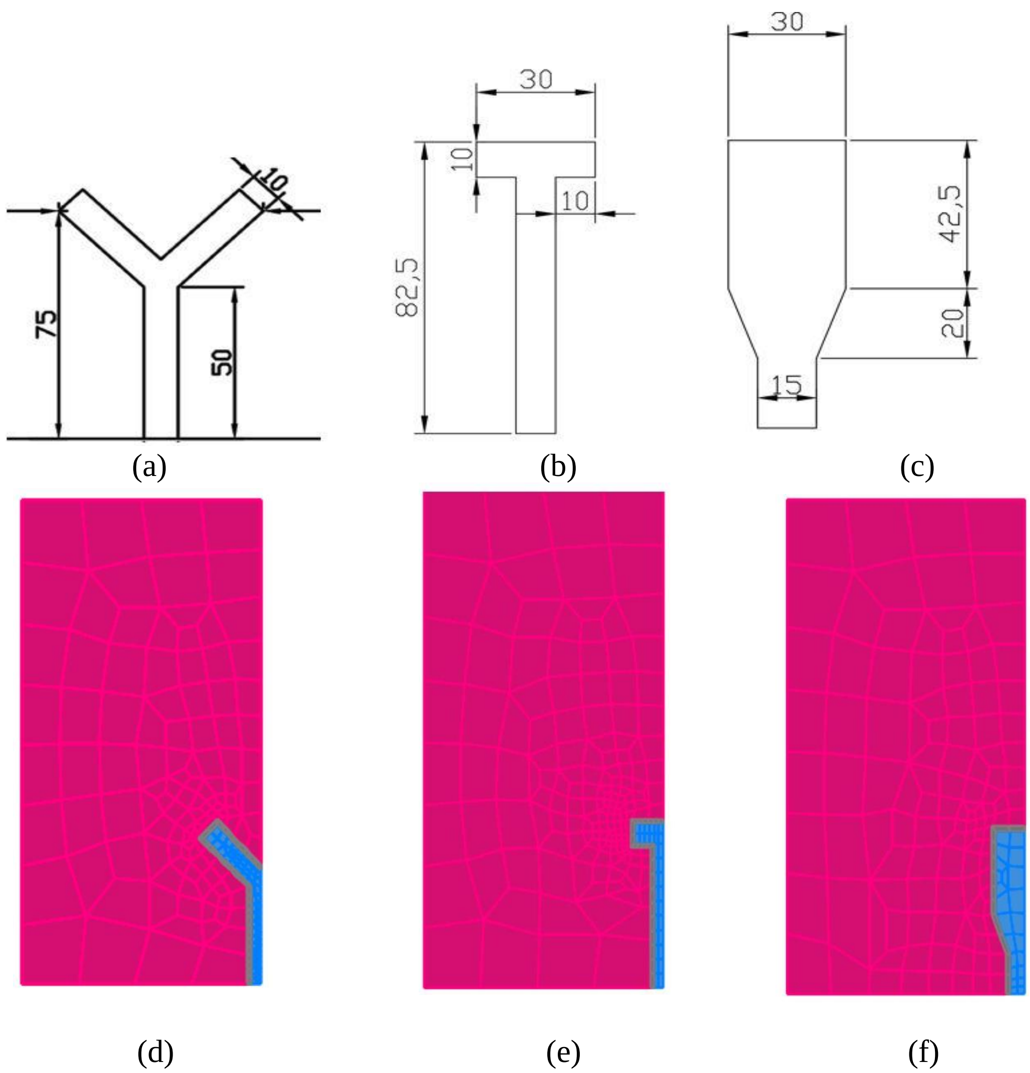

Figure 5.2. Finite element analysis for the (a) & (d) *Y* geometry, (b) & (e) *T* geometry, and (c) & (f) *dogbone* geometry in SAP2000. All dimensions in mm.

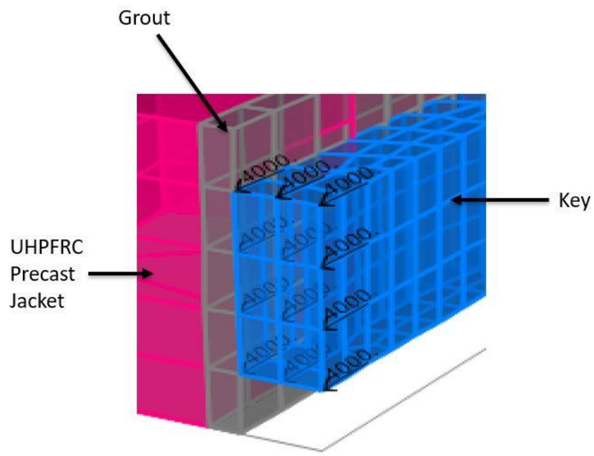

Figure 5.3. Different material properties were applied to the three geometry models.

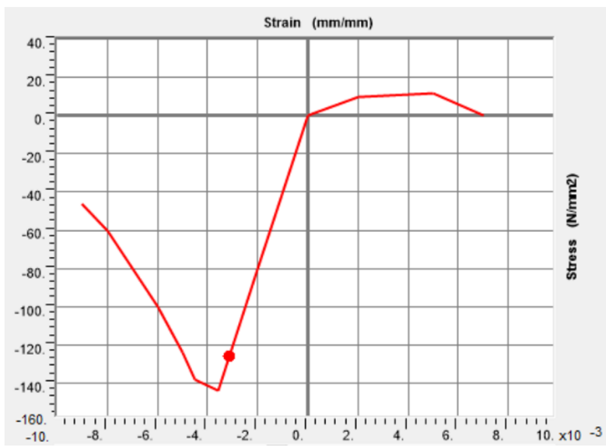

Figure 5.4. Stress-Strain curve for the UHPFRC used in SAP2000 for the key models.

The UHPFRC was expected to have a tensile strength of around 10 MPa, a compression strength of 144 MPa, a modulus of elasticity close to 49.45 GPa, and a Poisson's ratio of 0.20; these were properties of UHPFRC materials obtained in the lab for premixes that had been used in other UHPFRC experiments (Tsiotsias 2023). The concrete used in all models had a compression strength of 30 MPa, a modulus of Elasticity equal to 26.7 GPa, Poisson's ratio of 0.20, and the tensile strength of normal concrete was neglected.

Non-linear static analyses were performed on the finite element models. Different amounts of load were applied only at the joints at the lower edge of the key model (which is along the plane of symmetry of the key), as shown in Figure 5.3. The main results of the analysis are shown in Table 5.1 below. After analyzing the data obtained from Table 5.1, the *dogbone* key was selected due to its tensile capacity and its uniform stress distribution along its perimeter. The first *dogbone* key had the dimensions shown in Figure 5.6 (a), with a 15 mm thickness. This was the first key to be created in the experimental process, along with the UHPFRC plates simulating the UHPFRC precast jacket, in order to move to the next stage in the experimental program which was the proof of concept with direct tension testing. Moreover, an alternative mild steel key was created once the *dogbone* geometry was selected. This mild steel key was a smaller scale key with a 25 mm thickness, and it was also tested in direct tension with UHPFRC thin plates. The mild steel key is shown in Figure 5.6 (b).

Table 5.1. Shell stresses for the different key geometries for given applied lateral force.

Model	**F= 4 kN**	**F= 5 kN**	**F= 7 kN**	**F= 8 kN**	**F=15 kN**	**F= 18.5 kN**
Y	10 MPa	11 MPa	16 MPa	-	-	-
T	10 MPa	10 MPa	11 MPa	12 MPa	13 MPa	14 MPa
Dogbone	2 MPa	4 MPa	5 MPa	5 MPa	10 MPa	11.6MPa

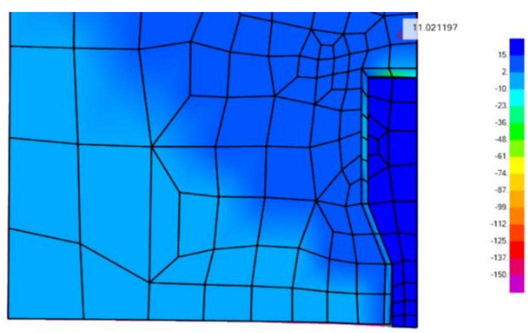

Figure 5.5. Stress distribution along the *dogbone* geometry perimeter.

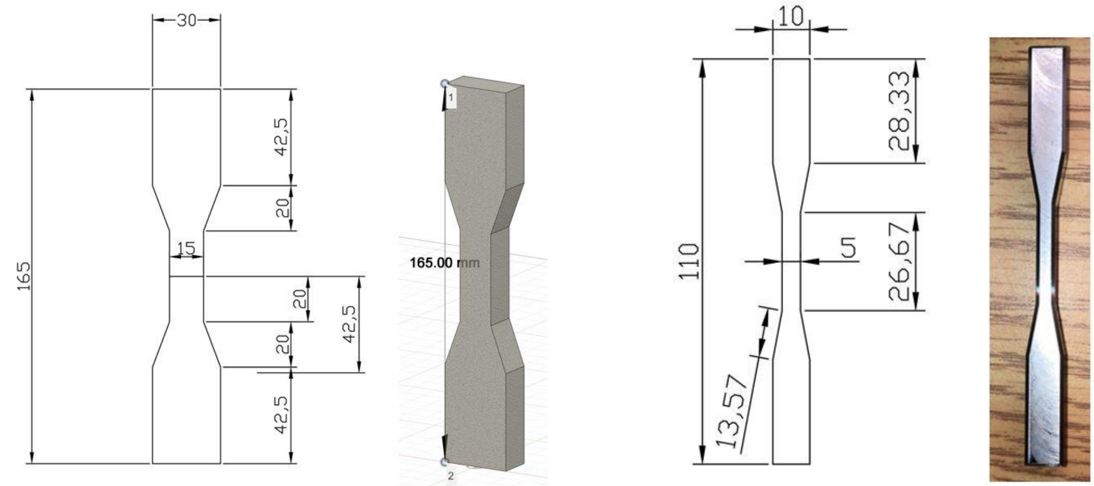

(a) (b)

Figure 5.6. Initial *dogbone* key dimensions for the (a) UHPFRC key and (b) mild steel key. All dimensions in mm with a 15 mm thickness.

5.2.2 Preliminary Key Specimens

The mix proportions for all the key specimens are listed in Table 4.1. The steel fibers were introduced in the mix with a volumetric ratio of 2%; Table 4.1 shows that for 2% steel fibers, the weight of fibers for 1 L of the mix is 156 g (therefore 156 kg /m^3 of cementitious material). All the precast UHPFRC jacket shells had a 2% volume fraction. However, the keys had a volume fraction of 3%, corresponding to 156 g and 234 g per 1L of mix, respectively. The preliminary stage of the experimental program involved several trials for the keys, each time improving and optimizing the final product of the key. These trials were performed using a small in-house laboratory mixer, with a capacity of 2 L. All the keys in this research were created on rectangular steel molds. Three keys were created with steel molds, and a total of three molds were used. The dimensions of the compartments in the steel molds were 30 mm in width by 180 mm in length with a 40 mm thickness. The molds were coated with oil using a brush before pouring the UHPFRC. In order to create 15 mm thick keys with the geometry shown in Figure 5.6, a 3D printer was used to generate all the different inserts and special sections of the mold. The 3D printer used in this research is *Anycubic Megazero 2.0®* using a commercial PLA filament.

(a) (b) (c) (d) (e)

Figure 5.7. Preliminary stage of the key preparation involving (a) an in-house 2 L mixer, (b) steel molds for the keys, (c) the first keys created, (d) the first UHPFRC precast jacket shell, and (e) the first key assembly.

The first UHPFRC keys were prepared using a 3% volumetric fibers, along with the first precast UHPFRC 2% jacket shells, and they are shown in Figure 5.7 (c) and (d), correspondingly. The precast UHPFRC jacket shell had 25 mm in width, 125 mm in length with a 25 mm thickness. In the first trial for the precast UHPFRC jacket shells, once assembled they were not perfectly aligned, and that may cause eccentric response under direct tension applied in the jacket. Initially, as shown in Figure 5.7 (e), the key was not fitting properly due to zero tolerances. This situation was addressed immediately and on the second trial more 3D printed pieces were created to improve the alignment; surface pieces along with bigger inserts to generate a 1 mm tolerance in the precast UHPFRC shell were the keys would be placed. Once alignment was achieved, the key was fixed in position using the same adhesive as when gluing the shims on the direct tension specimens (*Sikadur-31 Hi-Mod Gel A+B Epoxy* ®, at a volumetric ratio of 1:1). The UHPFRC mix used in this research used a black superplasticizer (containing carbon nanofiber additives) that generates a dark gray color on the final samples, therefore, before testing in tension the first set of specimens they were all coated with White Kilz primer to facilitate observations of the cracking pattern.

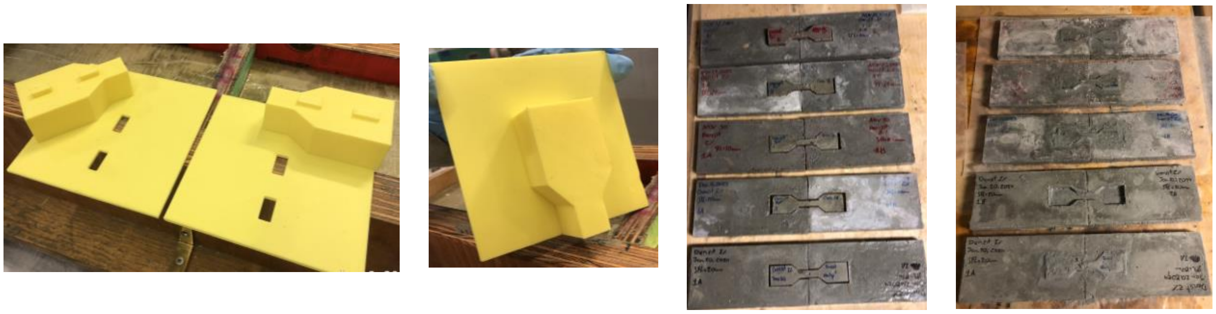

(a) (b) (c) (d)

Figure 5.8. Improving the alignment to the first UHPFRC key and UHPFRC jacket shells by (a) & (b) adding 3D inserts, (c) placing the keys, and (d) securing the keys with *Sikadur* ® epoxy.

The six specimens shown in Figure 5.8 (d) comprising an assembly of two precast layers connected with a centrally placed key, were tested in direct tension and they were conducted in a displacement-controlled, close-loop universal testing machine MTS. This was the same MTS machine used for testing the CEK2 mix used for material characterization. These first six specimens were tested using a test rate of 0.15 mm/min and they provided on average a peak tension load of 2.78 kN. When applying Eq 5.1, the value of H equals 125 mm and t equal to 25 mm, solving for $f'_{t,U}$ the obtained value for the tensile strength is 1.48 MPa. The mode of failure was governed by the weakest link, in this case the key itself. Since the main objective was to create a key that can transfer the tensile stresses from the key to the precast jacket, this type of key setup needed improvement to achieve higher tensile capacity.

(a) (b) (c)

Figure 5.9. The first set of UHPFRC keys (a) before testing, (b) & (c) after peak.

Therefore, the third set of UHPFRC keys underwent three modifications: the length of the key was reduced to 130 mm, the thickness was increased to 25 mm and it was cast along with a 125 m length embedded threaded rod, $^{1}/_{4}$ inches in diameter (6.35 mm), with a top and bottom ($^{1}/_{4}$ -20) nuts, while maintaining the same geometry. No alterations were performed to the precast UHPFRC jacket shell. The threaded rod was placed at the mid-height of the key. Due to the dense matrix of the UHPFRC mix, the threaded rod could be held in place. The mix was poured up to mid-height, and then the threaded rod was placed, following what was remaining to complete the 25 mm thickness of the key. The third set of keys to be tested in direct tension is shown in Figure 5.10 below. The average developed force by this set of UHPFRC keys was 12.12 kN when dividing with the cross-sectional area of the jacket, the obtained value for the tensile stress developed by the jacket is: 12120/(125x25) = 3.87 MPa. The stress developed in the key is 12120/(15x25) = 32 MPa, which is the average stress considering the key is now reinforced with the threaded rod.

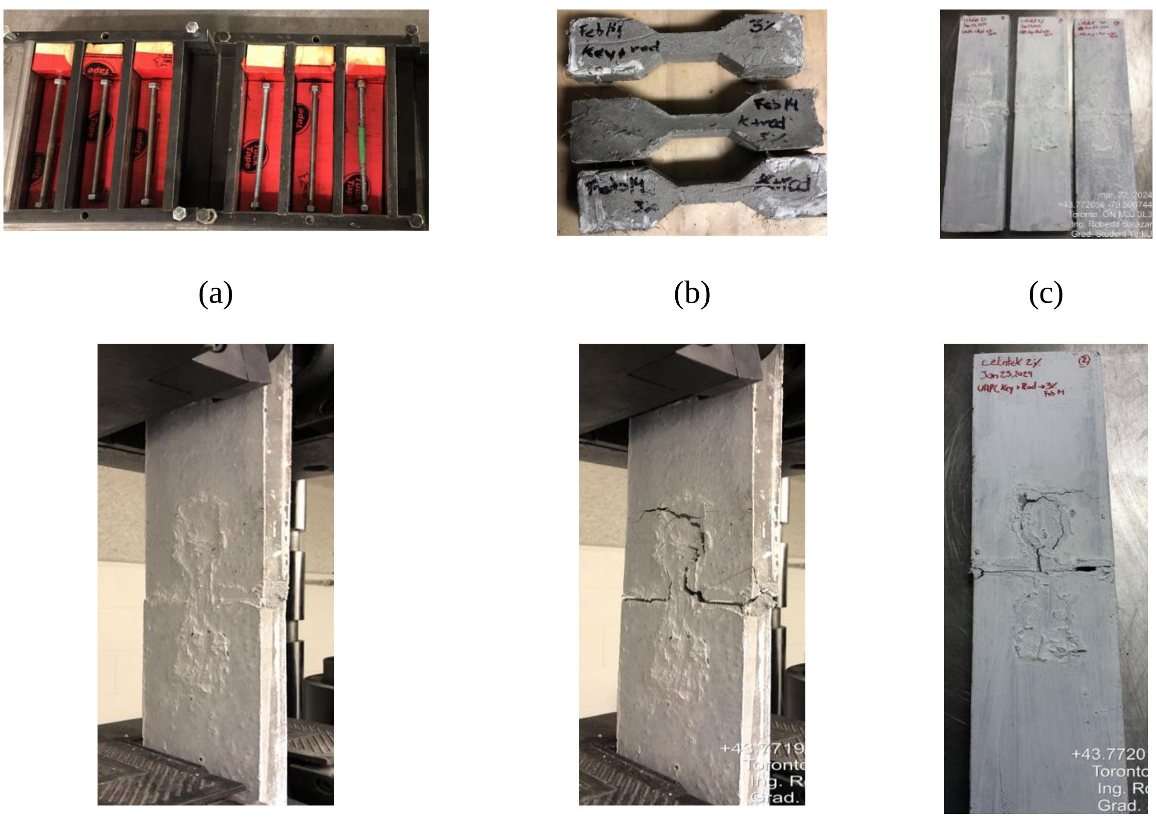

(a) (b) (c)

(d) (e) (f)

Figure 5.10. A third set of UHPFRC keys (a) incorporating a 125 mm threaded, (b) ready to place on the UHPFRC jacket shell and (c) & (d) specimens ready for direct tension testing, (e) & (f) after peak load.

The mode of failure shown in Figure 5.10 (e), and (f) was different than the prior set of UHPFRC keys (Figure 5.9 (b) and (c)). First of all, a higher tension was achieved, however, it still needed improvement. Additionally, the tensile stresses were transferred to the precast UHPFRC jacket shell while the key remained uncracked. The stresses followed the bonding agent *Sikadur-31* surface, deboning the key from the jacket shell until they reached the 90° angle at the top edge of the key. The key did not suffer any damage, meaning that the threaded embedded rod possibly yielded, and the forces were transmitted to the UHPFRC shell, cracking the shell transverse to the direction of the load. These results led to the fourth generation of UHPFRC keys, which required two modifications both on the key and on the precast UHPFRC shell. The first modification was in the geometry of the key itself, where both sides of the key were curved while keeping a 15 mm width at the mid-section. The second modification was to replace the threaded rod with a 130 mm in length 10M rebar. The new curved inserts used as the sides for the fourth set of keys were made with the 3D printer.

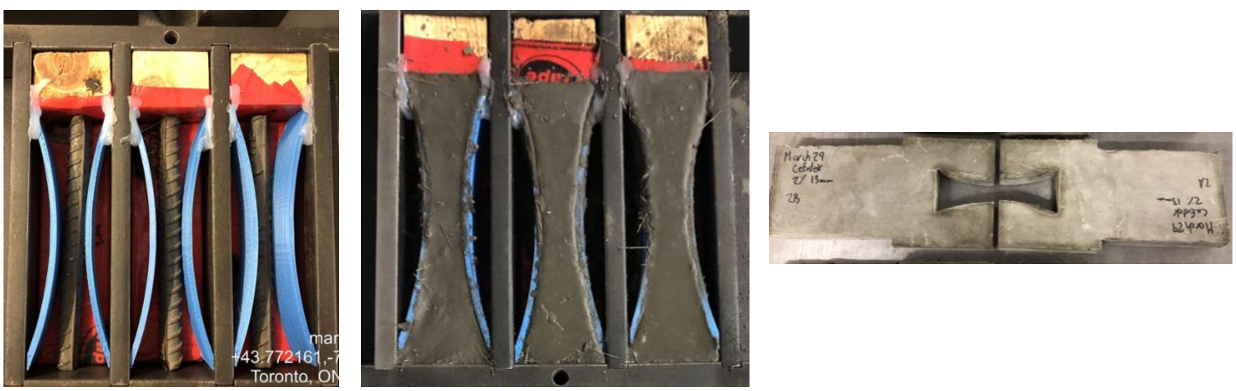

(a) (b) (c)

Figure 5.11. Fourth set of (a) curved UHPFRC keys with 10 M rebar, (b) fourth set of precast UHPFRC jacket shell.

The test setup for the fourth set of specimens had to be different than the prior ones to avoid slippage. A similar approach to the one described in Section 4.3.4 in Chapter 4 was performed. Similar to the material characterization direct tension tests, before the tests were performed, aluminum shims were glued to the original level surfaces of the specimen. Four aluminum shims were used per side for each specimen, using a total of eight shims per specimen. These aluminum shims had the same dimensions as the ones described in Section 4.3.4. The thicker side of the shim was glued flush to the edge of the specimen. The shims were glued with the same epoxy and it followed the same 24-hour drying time per side before testing, as recommended by the supplier. The setup of the specimen was done, 24 hours after gluing the last shim, on a level stainless steel table. The setup again can be divided into two phases: top and bottom. Starting with the top phase, as a first step, two new steel transfer loading plates were placed on the specimen and then joined with four steel threaded bolts and nuts. The second step was to secure each bolt with a torque wrench and a socket wrench at 40 N.m. As a third and last step for phase I, was to torque and secure the first four bolts on one end of the specimen. Phase II was initiated by flipping the specimen carefully and repeating the same steps to secure the transfer loading plates. Figure 5.12. shows the two steel loading jigs (top and bottom) that were used to hold the prismatic specimen in place, while the jigs were being connected to the MTS grips using ¾ in diameter steel rods. These jigs were different than the ones used for the material characterization direct tension tests. The MTS machine was gripping the steel rod, not the specimen itself. Once the specimen was assembled as described in phase I and II, the specimen was placed inside the available space between the top and bottom jigs in the MTS.

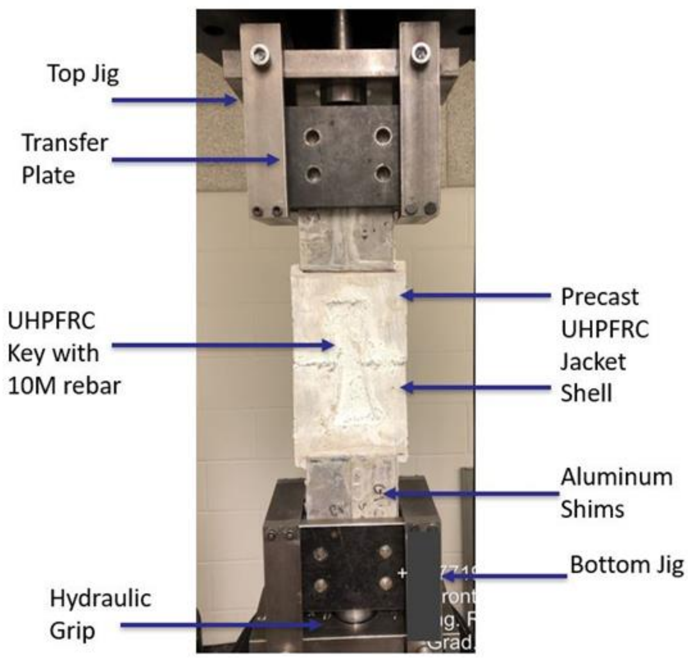

Figure 5.12. Direct tension specimen setup for the fourth and Lap Splice specimens for testing in the MTS.

(a) (b) (c)

Figure 5.13. Fourth set of UHPFRC keys (a) specimens ready for direct tension testing (b) & (c) mode of failure.

The mild steel metal key sample was tested along with the fourth set of UHPRC key specimens. The mild steel key specimen had the same dimensions as the second precast UHPFRC jacket shell. Figure 5.6 (b) and Figure 5.14 (a & b) show the geometry of the mild steel key and the precast UHPFRC jacket shell, correspondingly. This specimen was tested in direct tension in the MTS machine, and the results obtained were similar to the fourth set of UHPFRC keys. This alternative achieved development of a maximum load of 10.97 kN, meaning a tensile strength of 3.51 MPa. The tensile stresses were successfully transferred to the UHPFRC jacket, the key itself yielded and no visible cracks were found. However, due to the complexity of creating these mild steel keys, the material costs, and the amount of steel being used as a key to be used in tension, this key alternative was discarded and the research focused on testing precast UHPFRC elements.

(a) (b)

Figure 5.14. Mild steel key specimen tested under direct tension in MTS machine.

5.2.3 Precast curved UHPFRC key with 10M rebar

The average value for this fourth set of UHPFRC keys was 10.95 kN. By applying Eq. 5.1, the obtained value for the tensile strength is 3.51 MPa, with a similar mode of failure when compared to the last set of specimens. After these results, a fifth and final modification was performed of the UHPFRC key. The keys still had a 130 mm in length 10M rebar embedded. Since the cracking pattern followed the top edge of the key, the modification was a new top and bottom edges to have a round head geometry so as to minimize stress concentrations and eliminate the occurrence of cracking at the tip corners of the previous key. The fifth set of keys are shown in Figure 5.15.

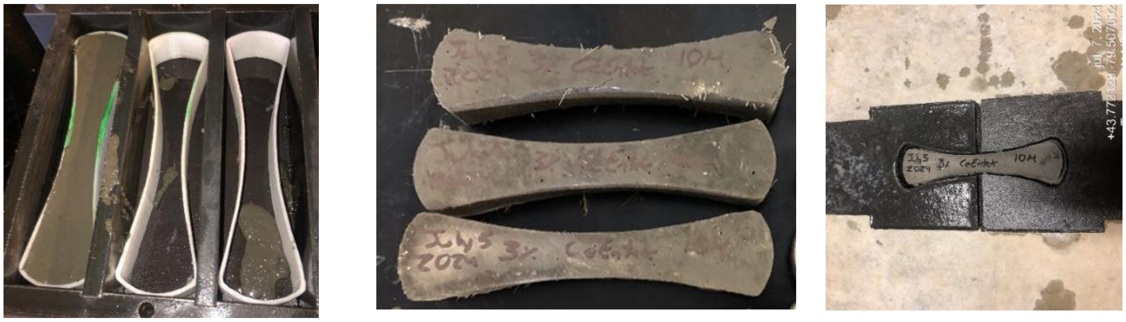

(a) (b) (c)

Figure 5.15. Fifth set of (a) & (b) round head curved UHPFRC keys with 10 M rebar, (c) fifth set of precast UHPFRC jacket shell specimen.

These were the final set of key specimens to be tested with precast UHPFRC connected layers under direct tension. The test setup for these specimens is similar to the one described above for the fourth set of keys, by also adding proper instrumentation. To capture displacement values, two linear variable differential transformers (LVDTs) were used on each specimen. Like the process described in Section 4.3.4, the readings were taken by connecting the instruments to a data acquisition system (DAQ), which was then plugged into the computer. Both instruments were placed by implementing a top and bottom instrumentation aluminum frame attached on the specimens. Levels and different metal angles were used in these frames, and by using magnets the instruments were secured to the frame. The gauge length for these specimens was 140 mm. A total of three specimens were tested for this fifth curved key specimens, named *CKS1*, *CKS2*, and *CKS3* (curved key specimen one). The data obtained from uniaxial tensile testing is shown in Figure 5.17 and summarized in Table 5.2.

Figure 5.17 shows the ductility of the precast curved UHPFRC selected; at this point, and considering the available time frame it was decided to move on with the experimental program. Even though the tensile capacity could still be improved by modifying and implementing a new geometry of the key, a desired mode of failure was obtained. The UHPFRC 3% key remained uncracked, and the precast UHPFRC 2% jacket shell cracked. The weakest link in this setup is the bonding agent, *Sikadur-31*. Specimen CKS3 is marked with a star (*) since the result is an outlier, although the same mode of failure was obtained. The data for CKS3 was not considered to calculate the average data for this setup in Table 5.2.

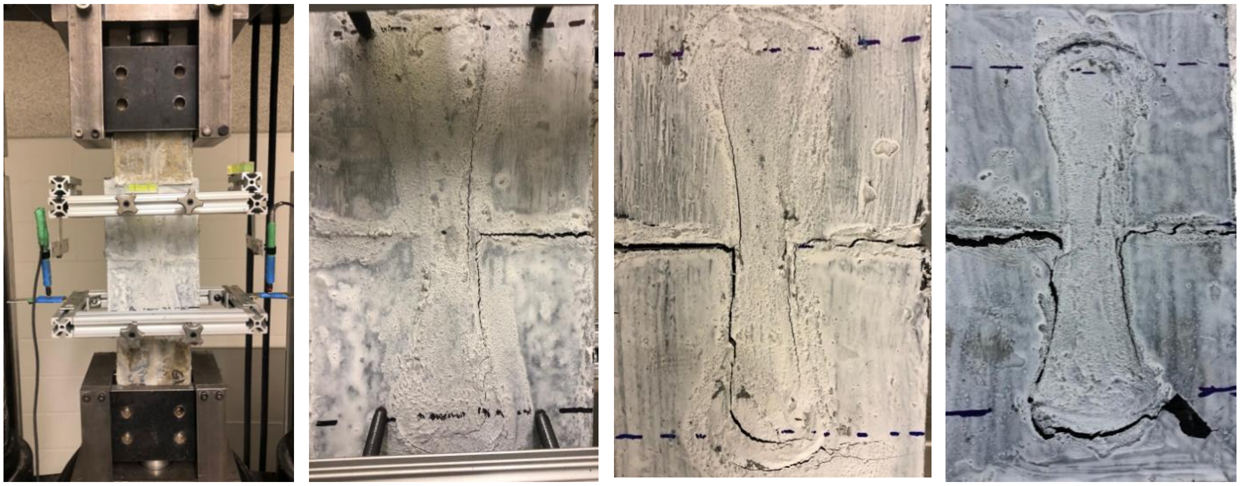

(a) (b) (c) (d)

Figure 5.16. Fifth curved UHPFCR key specimen (a) ready for testing, (b) & (c) & (d) mode of failure after testing for CKT1, CKT2, and CKT3 respectively.

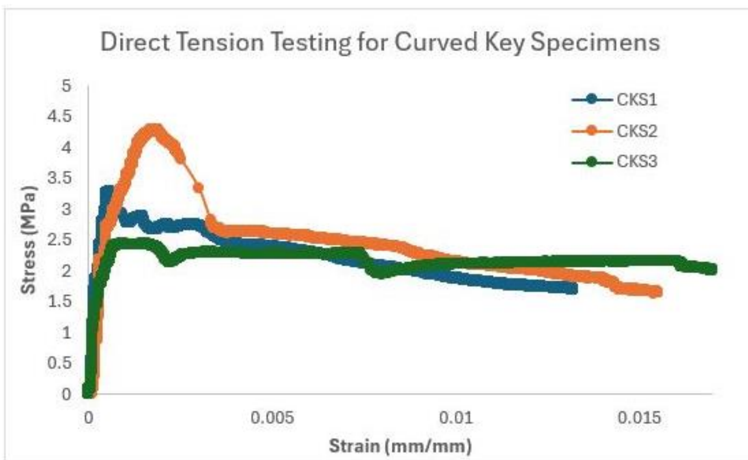

Figure 5.17. Direct tension testing for curved UHPFRC key with 10M rebar specimens.

Table 5.2. Direct tension data for the curved UHPFRC keys with 10M rebars.

ID	Peak Load (kN)	Peak stress (MPa)	Peak Strain (mm/mm)	Yielding stress (MPa)	Yielding Displacement (mm)	Ultimate stress (MPa)	Ultimate Displacement (mm)	Ductility μ (mm/mm)
CKS1	10.33	3.30	0.00058	2.31	0.05	2.81	0.22	4.4
CKS2	13.42	4.29	0.00188	2.35	0.06	3.65	0.42	7.0
CKS3*	7.64	2.45	0.00147	1.77	0.05	2.08	2.26	45.2
Average	11.87	3.80	0.00123	2.33	0.055	3.23	0.32	5.5

Figure 5.17 shows the ductility of the precast curved UHPFRC selected; at this point, and considering the available time frame it was decided to move on with the experimental program. Even though the tensile capacity could still be improved by modifying and implementing a new geometry of the key, a desired mode of failure was obtained. The UHPFRC 3% key remained uncracked, and the precast UHPFRC 2% jacket shell cracked. The weakest link in this setup is the bonding agent, *Sikadur-31*. Specimen CKS3 is marked with a star (*) since the result is an outlier, although the same mode of failure was obtained. The data for CKS3 was not considered to calculate the average data for this setup in Table 5.2.

5.2.4 Cast-in Place Lap Splice Key

As part of the experimental program, additional jacket connecting alternatives other than the curved UHPFRC key were considered. When creating and testing the precast UHPFRC key specimens, the mild steel key specimen idea was discarded due to the results obtained. The results obtained from the UHPFRC curved key left more improvements or alternatives to be desired. Therefore, a new possible solution for connectivity was studied: a splice connection involving 2 pairs of 10M rebars lapped in the connection region over a length of 8Db = 80 mm , 160 mm in total length each. The initial sketch of this alternative is shown in Figure 5.18 below. The precast UHPFRC jacket shell mix proportions are shown in Table 4.1, and just like the UHPFRC curved keys, the light blue region was made using the same proportions but with a 3% fiber volume fraction. The UHPFRC 3% connection was cast-in place.

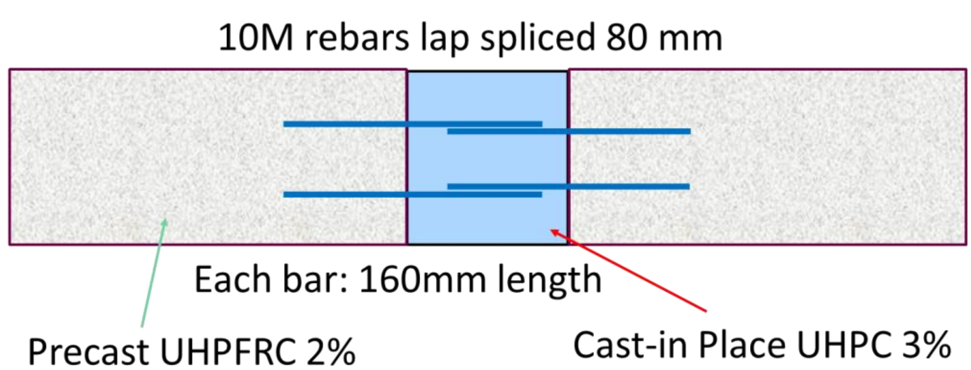

Figure 5.18. Lap Splice key specimen sketch.

(a) (b) (c) (d)

Figure 5.19. Lap Splice Specimens (a), (b) & (c) lab production and (d) final specimens.

Wooden molds were used to fabricate the lap splice specimens, where the precast UHPFRC 2% jacket shells had a cross-sectional area of 125 mm by 25mm, and a length of 250 mm. The UHPFRC 3% connection had a cross-section of 125 mm by 25 mm with 80 mm = $8D_b$ in length. Since a higher volume of mix was needed, a 10 L capacity in-house laboratory mixer was used. As shown in Figure 5.19 (a), several 3D inserts were printed and coated before pouring. Some of the wooden molds and inserts were covered with commercial plastic adhesive tape to facilitate the demolding process. This turned out to be beneficial since plastic adhesive tape also generated a smooth and clear surface; similar results can be found when using plexiglass molds in the fabrication process. The lap splice connections were poured 48 hours after the precast UHPFRC jacket shells were cast. Just like the previous curved key specimens, the lap splices were also coated with White Kilz primer to facilitate observations after testing. Similar to the fifth set of UHPFRC curved keys described above, the lap splice specimens shared the testing setup described in Figure 5.12. Lap slice specimens used the same instrumentation setup as the curved UHFRC key specimens.

(a) (b) (c) (d)

Figure 5.20. Lap splice specimens (a) ready for testing and (b), (c) & (d) after testing. The gauge length of the specimens was 140 mm (70 mm from its center) and its marked with the dash lines in (a), (b) and (c).

Table 5.3. Direct tension data for the lap splice specimens.

ID	Peak Load (kN)	Peak stress (MPa)	Peak Strain (mm/mm)	Yielding stress (MPa)	Yielding Displacement (mm)	Ultimate stress (MPa)	Ultimate Displacement (mm)	Ductility μ (mm/mm)
DTLS1	25.28	8.09	0.0107	7.55	0.140	6.88	0.392	2.80
DTLS2	20.12	6.43	0.0026	-	-	-	-	-
DTLS3	19.03	6.09	0.0040	4.43	0.086	5.18	0.294	3.38
Average	21.48	6.88	0.0057	5.99	0.113	6.02	0.343	3.09

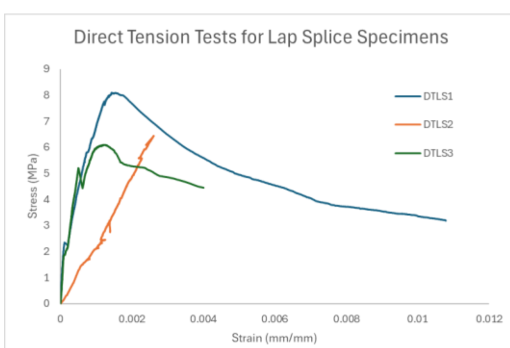

Figure 5.21. Direct tension testing for curved UHPFRC key with 10M rebar specimens.

The specimens were named DTLS1 which corresponded to direct tension lap splice #1 specimen tested. DTLS2 and DTLP3 were the second and third specimens tested correspondingly. Figure 5.21 shows the stress-strain response curves for the three lap splice specimens tested. All the specimens had the instrumentation frame at a 70 mm distance measured from their center, corresponding to a total 140 mm gauge length. DTLP2 had no post-peak data since it cracked at the top 70 mm where the instrumentation frame was placed, causing false displacement readings. Representative strains are shown in Figure 5.21. Moreover, specimen DTLP2 showed a constant slope until reaching the peak, therefore no visible yielding point was obtained. DTLP1 and DTLP3 had similar behavior but they reached different peak loads. The average peak stress sustained by the jackets in these specimens was 6.88 MPa, which is close to the tensile strength of 7.37 MPa reported in Chapter 4. After analyzing the data, the average ductility of the DTLP specimens was found to be 3.09.

5.3 Casting the Unreinforced Rectangular Concrete Column Specimens

In this research, the encased part of the retrofitted columns were to be rectangular and unreinforced, as shown in Figure 5.1. The columns had a cross-section of 150 mm by 150 mm with a height of 300 mm due to the space available in the compression machine used for testing. A total of thirteen columns were created using various steel and wooden molds. The inside of the molds was coated with oil and any elements used as breakers between columns were covered with plastic. Along with the columns, concrete cylinders were cast to test the compressive strength at 28 days of age and on the day of testing the final retrofitted columns. The concrete mix for the columns was performed with general-use Portland limestone cement, fine aggregate, 19 mm maximum coarse aggregate, and w/c ratio=0.57. The concrete batch for the columns was mixed in a pan-type drum mixer, and was vibrated during placement with a concrete vibrator. The compressive strength for the columns was aimed to be 25 MPa, representing normal strength concrete (NCS) for an existing/old concrete column. Table 5.4 shows the mix design for NSC where the total volume was 0.11 m^3 considering the columns, concrete cylinders, and waste. The concrete cylinders were poured into standard plastic molds, having a diameter of 100 mm with a height of 200 mm. The cylindrical molds were also coated with oil before casting. These specimens were covered with wet burlap and surrounding plastic after casting. After demolding, the columns and concrete cylinders were placed in a curing tank for 28 days. At 28 days of age, the cylindrical specimens were tested in a load-controlled compression machine (*Controls),* where the average compressive strength for the concrete column mix was found to be 32.4 MPa after testing three concrete cylinders.

Table 5.4. Mix design proportions for column concrete mix.

Column Concrete Mix	Volume (L)	Portland cement (kg)	Coarse Aggregate (kg)	Fine Aggregate (kg)	Water (kg)
Proportions by weight	110	64.41	68.59	83.37	36.75

(a) (b) (c) (d)

Figure 5.22. (a) Column molds before casting, (b) columns after casting, (c) columns in the curing tank, and (d) concrete cylinder tested at 28 days of age.

Once the columns were demolded, the next step in the research was to set the final testing scheme before proceeding with the preparation and casting of the precast UHPFRC jackets and keys. To expand the UHPFRC jacket alternatives, a cast-in place solution was also going to be tested once the final retrofits were assembled. As part of the parametric testing program, two different thicknesses were tested for each jacket alternative. Therefore, the entire experimental involved three UHPFRC jacket possibilities: the first one being a cast-in-place solution, the second one corresponding to a precast UHPFRC jacket using a precast UHPFRC curved key with a 10M embedded rebar, and the third alternative a precast UHPFRC jacket with a lap splice solution incorporating 160 mm long 10M rebars. All jackets had a 2% fiber volume content while the curved key and the lap splice section had a 3% fiber volume content. The jacket thicknesses to be tested were 25mm (1 in) and 37.5 mm (1.5 in). From the thirteen columns, five were assigned to the cast-in-place solution, four to the precast UHPFRC jacket with the precast UHPFRC curved key, and the four columns were used to study the option of the precast UHPFRC jacket with the lap splice connection. Some of these columns were tested with monotonic loading and some were tested with cyclic loading. Table 5.5 summarizes the column testing scheme.

Table 5.5. Testing scheme for the retrofitted columns.

Set	Description	Jacket Thickness	Specimen
1	Cylinders for compression	NA	3 at 28 days and 3 at the period of testing
2	UHPFRC Cast-in-Place	25 mm	1 Monotonic 2 Cyclic
3	UHPFRC + Curved key	25 mm	2 Monotonic
4	UHPFRC + Lap Splice	25 mm	1 Monotonic 1 Cyclic
2’	UHPFRC Cast-in-Place	37.5 mm	1 Monotonic 1 Cyclic
3’	UHPFRC + Curved key	37.5 mm	1 Monotonic 1 Cyclic
4’	UHPFRC + Lap Splice	37.5 mm	1 Monotonic 1 Cyclic
		Total Number of Specimens	13

5.4 Precast UHPFRC Jacket Fabrication

Figure 5.1 shows the retrofitted column having a top and bottom strip of precast UHPFRC jacket, with a grout layer between the column and the precast jackets. The columns tested with the cast-in-place solution did not have this layer of grout since the UHPFRC was directly poured on the columns. In all grouted columns the grout type used was *Sika ® Grout-212 Versatile Non-Shrink Grout*. For all the columns that involved precast UHPFRC jackets, a grout layer thickness of 20 mm was considered and taken into consideration to calculate the final dimensions of the jackets. Each precast UHPFRC jacket was considered a C-shaped specimen. Therefore, for the columns that had a precast UHPFRC jacket as a solution, a total of four C-shaped elements were needed, two for the top and two for the bottom strips. All of the C-shaped elements casting followed the mix design described in Section 4.2 in Table 4.1 in Chapter 4, using a 2% steel fibers volume fraction. All of the C-shaped specimens were made on the steel molds used for the column casting. Each mold was coated with oil prior to casting. All of the wooden separators and the C-shaped wooden specimens required to shape the precast jackets were covered with the same commercial plastic adhesive tape to facilitate the demolding process used for the key fabrication.

The precast UHPFRC jackets were made by pouring the UHPFRC mix into steel molds . To create C-shaped precast elements, special formwork was made prior and placed inside the steel mold before pouring. This special formwork had C-shaped geometry made with 18 mm plywood pieces, two used as vertical supports and one as a horizontal base used to connect the supports from the top. The formwork used for the 25 mm thick C-shapes was slightly different than the ones used for the 37.5 mm in thickness, due to the final length of the horizontal piece used for holding the two vertical supports. To enhance the bond between the grout and the precast UHPFRC jacket, a layer of plastic large-size commercial bubble wrap (*Large bubble cushion (5/16) in)* was placed on top of the wooden insert of the C-shaped formwork. The bubble wrap generated a rough and uneven surface on the inside face of the jacket components after demolding by just removing it from the precast UHPFRC jacket as shown in Figure 5.23.

(a) (b)

Figure 5.23. C-shaped inserts used to create the precast C-shaped UPHFRC jackets (a) without and (b) with a layer of large 5/16 in bubble wrap. These inserts with the bubble wrap were placed inside the steel molds in order to formulate the precast jacket components as depicted in Fig. 5.24.

All of the precast C-shaped UHPFRC jackets were poured from the top, allowing the UHPFRC to flow to both sides simultaneously. This method of casting also helped with the fiber distribution, ensuring the steel fibers were equally distributed in the precast C-shaped UHPFRC jacket. A batch of 10 L of UHPFRC 2% was prepared to cast a total of 8 C-shaped elements, to then be poured from the top. These specimens were covered with wet burlap and surrounding plastic after casting, demolded 48 hours after pouring, to then be placed inside the curing tank for 28 days. For each UHPFRC and grout prepared, a set of three 50 mm by 50 mm by 50 mm cubes were made to check the compressive strength of both materials for quality control. The details mentioned above were applied when preparing both sets of specimens: Lap Splice and Curved Key C-shaped precast Jackets.

5.4.1 Precast C-Shaped UHPFRC Jackets for Lap Splice Connection

A unique set of 3D printed pieces were made to ensure that the 10M rebars remained in place for this precast UHPFRC jacket solution. The lap splice connection had a cross-section of 80 mm by 150 mm, where the thickness of this connection was either 25 mm or 37.5 mm. The total length of each 10M rebar, including the lap splice region, was 160 mm. Per precast UHPFRC Jacket, a total of eight 160 mm long 10M rebars were cut and placed inside the steel molds, along with the C-shaped formwork before pouring.

(a)

(b)

(c) (d)

Figure 5.24. Precast C-Shaped UHPFRC Jackets for Lap Splice Solution (a) & (b) preparation, (c) & (d) after demolding.

5.4.2 Precast C-Shaped UHPFRC Jackets for Precast Curved Key

Similar to the case above, a particular set of 3D printed pieces were made to ensure that the hollow section where the curved key was placed had the proper geometry. The hollow space was made by placing an insert having the geometry mentioned in section 5.2.3 for the curved key specimen. Two types of specimens were printed, one was 25 mm, and the other one was 37.5 mm. Per precast UHPFRC Jacket, a total of two inserts were placed and secured with hot glue, along with the C-shaped formwork before pouring.

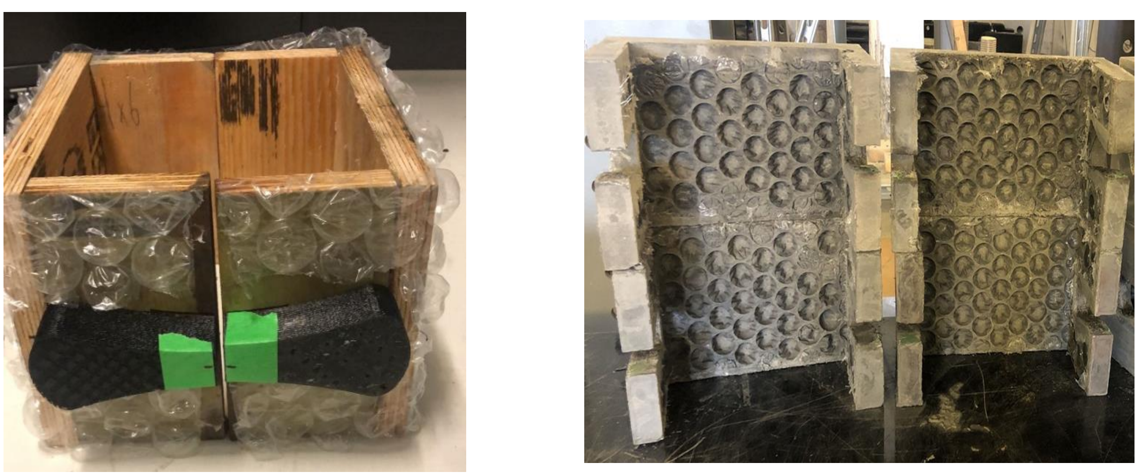

(a) (b)

(c)

(d)

Figure 5.25. Precast C-Shaped UHPFRC Jackets for Precast Curved Key (a) & (b) preparation, (c) & (d) after demolding.

5.4.1 Precast C-Shaped UHPFRC Jackets for Flexure Testing

An extra set of precast C-shaped UHPFRC jackets was prepared in order to test their flexural capacity against out of plane bending. A total of 3 specimens were tested in the displacement-controlled, close-loop universal testing machine MTS. The C-Shapes rested on a 25 mm diameter bronze roller at the bottom that moved upward applying axial load, while a 12.5 mm diameter roller was placed at the top. These three precast C-shaped UHPFRC jackets were tested with a test rate of 0.15mm/min. The instrumentation to capture the vertical and horizontal displacement of the specimens was supported on aluminum frames as shown in Figure 5.26 (a) below. One LVDT was placed at the left side of the C-shaped specimen in the vertical direction to capture longitudinal displacement, while another LVDT was placed horizontally at mid-height to measure outwards deflection due to bending. Two out of three specimens cracked at the mid-height, with the cracks going across the cross-section from one side to the other, while the remaining specimen cracked at the top, near the vertical support. These precast C-shaped UHPFRC jackets were fabricated following the same method as in the case of the precast jacket components, however without the addition of large bubble wrap or 3d printed inserts since they were made just for testing the bear jackets' flexural capacity. The UHPFRC was poured from the top, allowing the steel fibers to be equally distributed to both vertical supports. Figure 5.26 and Table 5.6 show the main results for these specimens. The specimens were named as *PCSJ1*, meaning *Precast C-Shaped Jacket* with its corresponding number.

(a) (b) (c) (d)

Figure 5.26. C-Shaped UHPFRC Jackets (a) setup and (b), (c) & (d) after flexure testing.

Table 5.6. Flexural capacity of the precast C-Shaped UHPFRC jacket specimens.

ID	Vertical LVDT (mm)	Horizontal LVDT (mm)	Vertical Strain (mm/mm)	Horizontal Strain (mm/mm)	Peak Load (kN)	Area (mm2)	Peak stress (MPa)	Flexural Strength (kN.m)
PCSJ1	0.568	0.764	0.003	0.006	9.46	3961.5	2.41	1.06
PCSJ2	0.163	0.281	0.001	0.002	5.58	4042.5	1.38	0.63
PCSJ3	0.281	2.525	0.001	0.022	6.14	3865.5	1.59	0.69
Average	0.337	1.190	0.001	0.010	7.062	3946.5	1.792	0.795

5.5 Assembly of Retrofitted Columns

Once all of the precast C-shaped UHPFRC jackets were 28 days of age, the assembly process started. A total of thirteen columns were cast to perform the testing scheme presented in Table 5.4. Of those thirteen columns, five were used to test a cast-in-place solution with two different thicknesses, 25 mm and 37.5 mm. The remaining eight columns were employed to test the retrofit technique involving precast C-shaped UHPFRC jackets with two different jacket thicknesses, 25 mm, and 37.5 mm. As shown in Figure 5.1 (a), the Retrofitted Column with precast C-shaped UHPFRC jackets involved a top and a bottom strip of jackets with one of two alternative connection methods: either a precast UHPFRC key or a lap splice connection. Both cases had a 20 mm gap between the column and precast C-shaped UHPFRC jackets that were filled with *Sika ® Grout-212 Versatile Non-Shrink Grout.* This is a premixed material with an estimated compressive strength of 56 MPa. To validate this value, 50 mm grout cubes were cast and tested at 28 days of age. However, the cubes were tested at 60 days of age and the value obtained was 87.33 MPa under unixial compression . All the UHPFRC jacket solutions had a 2% fiber content, following the mix design presented in Table 4.1. When testing the Retrofitted Columns, the load was meant to be applied only on the column cross-sectional area by using a 12.5 mm thick steel plate. Therefore, after all the precast C-shaped UHPFRC jackets had been placed in position around the columns and after the grout was poured, the final step in the assembly process was to generate an even-level surface on top of the columns to guarantee that the stress applied by the compression machine is equally distributed on a 12.5 mm thick steel plate. The level surface was achieved with *Hydro-Stone ® Gypsum Cement.* Moreover, the surfaces of the Retrofitted Columns were coated with White Kilz primer to facilitate observations of the cracking pattern followed by spraying black color to form a distinct speckle pattern for digital image correlation (DIC) readings. This technique is highly valuable for tests where local deformations and strain readings are difficult to measure during the experiment. In order to perform DIC-Analysis, a high-resolution digital camera was placed on a stand in front of each specimen during testing, recording high-resolution photographs every 10 s. DIC-Analysis was not performed in this research.

Figure 5.27. White Kilz primer used for coating the specimen's surfaces and Rust-Oleum black spray used for speckles.

5.5.1 Retrofitted Column with Cast-in-Place Jacket

From the thirteen columns available, five of them were selected randomly in order to place the proper formwork around them so as to create the cast-in-place UHPFRC jacket. The formwork consisted of four pieces of 18 mm thick plywood sheets with different dimensions to generate the specified jacket thickness. Three column specimens had a 25 mm jacket thickness, and two column specimens had a 37.5 mm jacket thickness. All cast-in-place solutions were made on the same day.

Prior to locking the formwork in place, the columns were placed on top of an acrylic smooth plate (*plexiglass*) to generate an even-level surface. The pieces of plywood were coated with oil before pouring the UHPFRC, and these pieces were secured by using hot glue and heavy-duty construction clamps. The UHPFRC mix was poured from the top by collecting mix from the mixer bowl with a scoop, pouring the material around the jacket thickness in the counterclockwise direction until reaching the top edge of the column. This was performed to ensure that all four sides of the jacket had proper fiber distribution. Additionally, this casting methodology helped the fiber orientation to be as close to horizontal as possible in the final arrangement (when compared to the axial loading when testing).

(a) (b) (c)

Figure 5.28. Final Retrofitted Columns with Cast-in-Place UHPFRC Jacket (a) fabrication and (b) & (c) specimens prior to painting.

5.5.2 Retrofitted Columns with Precast UHPFRC Jacket with Curved Key

Eight columns were used to complete the assembly of the Retrofitted Columns. Two setups were explored, where the first set prepared was the one involving the precast C-shaped UHPFRC Jackets with Curved Keys. Following the design from Figure 5.1, two UHPFCR jackets were placed at the top and two at the bottom. For every two jackets used, one precast UHPFRC curved key with an embedded 10M rebar was used as a connection method at each point of contact. This setup had a 20 mm gap between the precast UHPFRC jackets and the column. The precast UHPFRC curved key was glued into the hollow sections of the precast UHPFRC jacket with *Sika Sikadur-31 Hi-Mod Gel A+B Epoxy* ®, using a volumetric ratio of 1:1. The epoxy gel hardened after 24 hours of preparation, and then the gap was poured. The gap was filled with *Sika ® Grout-212 Versatile*

Non-Shrink Grout. This is a premix cementitious material that only needs a specific amount of water. The mix proportions for this non-shrink grout are given by the manufacturer *SIKA*, and they are specified with reference to the desired mix flowability by ensuring at least 56 MPa compressive strength. A total of 10.77 kg of premix mixed with 1.33 L of water was mixed in a 30 L in-house lab mixer for a period of 3 minutes, as recommended by the manufacturer. To be certain that the grout was filling the gap in its totality, the first layer of precast UHPFRC jackets were placed (the bottom jackets) and then the non-shrink grout was poured. A tamping rod was used to guarantee no voids as the grout was poured since this was a non-shrink material. Once the grout reached the top edge of the precast jacket, the next set of jackets were placed (the top jackets). The gap was again filled with the non-shrink by pouring directly from the top. Once the gap was filled, the Retrofitted Columns were covered with wet burlap for 28 days in a controlled environment.

(a) (b) (c)

Figure 5.29. Retrofitted Columns with Precast UHPFRC Jackets and Curved Key (a) & (b) when pouring the non-shrink grout and (c) the specimens prior to painting.

5.5.3 Retrofitted Columns with Precast UHPFRC Jacket and Lap Splice Connection

Four columns were used for the last setup studied, namely, the precast C-shaped UHPFRC Jackets with Lap-Spliced connections. As shown in Figure 5.1, two C-shaped UHPFCR jackets were placed at the top and two at the bottom. For every two jackets used, an 80 mm gap needed to be cast in place using UHPFRC 3% mix in the connection region. The rebars for the lap splice were embedded in the precast UHPFRC jackets, therefore they were in the way when casting the two thicknesses. The 37.5 mm jacket thickness was more practical to pour with since a UHPFRC with a 3% generated a very dense paste, and it flowed better in the gap since the connection was thicker.

This setup had a 20 mm gap between the precast UHPFRC jackets and the column. The gap was filled with *Sika ® Grout-212 Versatile Non-Shrink Grout.* To assemble the Retrofitted Columns, the following procedure was performed: A total of 10.77 kg of premix mixed with 1.33 L of water was mixed in a 30 L in-house lab mixer for a period of 3 minutes, as recommended by the manufacturer. To be certain that the grout was filling the gap in its totality, the first layer of precast UHPFRC jackets were placed (the bottom jackets) and then the non-shrink grout was poured. A tamping rod was used to guarantee no voids as the grout was poured since this was a non-shrink material. Once the grout reached the top edge of the precast jacket, the next set of jackets were placed (the top jackets). The gap was again filled with the non-shrink by pouring directly from the top. Once the gap was filled, the Retrofitted Columns were covered with wet burlap for 28 days in a controlled environment. To cast the lap-splice region, two pieces of the plywood were installed on the inside and outside face of the UHPFRC Jacket with a small quantity of commercial hot glue. This was done prior pouring the grout, and hot glue was used so that these pieces of plywood would be esay to remove before proceeding.

(a) (b) (c) (d)

Figure 5.30. Retrofitted Columns with Precast UHPFRC Jackets and Lap Splice Connection (a) prior to pouring the UHPFRC 3%, (b) & (c) prior to pouring the non-shrink grout, and (c) the final specimens before painting.

5.6 Testing the Retrofitted Columns with the UHPFRC Precast Jackets

The next and final step in the experimental program was testing the Retrofitted Columns. All tests were performed in the displacement-controlled compression-testing machine (*Controls Pilot)* shown in Figure 4.5. The testing protocol is presented in Table 5.4. However, the Retrofitted Columns were tested with different testing rates. For all the tests performed, the compression machine (Controls Pilot) applied a preload of 4.9 kN as part of its default values and the safety procedure. When the compression machine reached this value of preload, the load was paused and held on the specimen for an estimated time of 45 seconds. This was enough time to corroborate all the instruments were reading. After this, the test was started by clicking the *start test* option on the machine. As mentioned above, a thin layer made out of *Hydro-Stone ® Gypsum Cement* was poured on top of the columns to generate a level surface before placing the loading steel plates. The top and bottom plates had a rectangular cross-section of 50 mm by 50 mm with a 12.5mm thickness as shown in Figure 5.30. All the columns had instrumentation placed at the front and at the back to measure vertical and out-of-plane displacements. Due to the limited space inside the compression machine, no instrumentation frame was used. Instead, a set of rectangular magnets, steel shims, and on/off magnetic bases with holders were used to place the different devices. A combination of linear variable differential transformers (LVDTs), differential transformers (DTs), and linear potentiometers (LPs) were used to test the Retrofitted Columns. All the devices were properly connected to a data acquisition (DAQ) to measure displacements with an individual laptop, while the *Controls Pilot* was recording load. The testing of the Retrofitted Columns started with the monotonic loading tests on the seven specimens selected, followed by the cyclic loading tests. Sections 5.6.1 and 5.62 above explain the testing performed on all the Retrofitted Columns. While these were developed, the 50 mm cubes prepared for quality control testing of the UHPFRC precast elements, grout, and the concrete cylinders for the concrete columns were tested, to validate their strengths during the stage of final testing (see Table 5.7).

Figure 5.31. Steel loading plates used on top and bottom of the Retrofitted Columns.

Table 5.7. Compressive strength results of material cube or cylinder samples during monotonic and cyclic loading.

Material & specimen Form	Age (days)	Peak Load (kN)	Area (mm2)	Compressive Strength (MPa)	Average (MPa)
UHPFRC 2% (cubes)	90	420.85	2636.38	159.45	170.83
	90	453.38	2605.51	174.01	
	90	461.13	2575.56	179.04	
UHPFRC 3% (cubes)	60	461.06	2623.38	175.75	173.85
	60	476.19	2655.26	179.34	
	60	435.18	2614.19	166.47	
Non-Shrink Grout (cubes)	60	227.63	2619.83	86.89	87.33
	60	232.68	2624.49	86.46	
	60	225.75	2611.08	88.66	
NSC (cylinders)	210	322.28	7991.23	40.33	41.59
	210	335.08	7970.65	42.04	
	210	337.49	7957.99	42.41	

5.6.1 Retrofitted Columns - Monotonic Tests

A total of seven Retrofitted Columns were tested under monotonic loading at a test rate of 0.12 mm/min. Table 5.8 presents the columns in the order in which they were tested.

Table 5.8. Summary of Retrofitted Columns under Monotonic Tests.

Set	Column No	Description	Jacket Thickness (mm)
2	C4	Cast-in Place	25
3	C6	Precast Jacket + Curved Key	25
3	C13	Precast Jacket + Curved Key	25
4	C12	Precast Jacket + Lap Splice	25
2’	C8	Cast-in Place	37.5
3’	C11	Precast Jacket + Curved Key	37.5
4’	C1	Precast Jacket + Lap Splice	37.5

All the tests are first described in this section individually. Following their description, the column responses are plotted in Figure 5.42, to then be compared with the NSC stress-strain response on Figure 5.43. A summary is presented in Table 5.9.

5.6.1.1 Monotonic Testing for Cast-in Place Column C4

Monotonic testing started with specimen C4. This specimen was one of the few for which the space available inside the compression machine was enough to place all six instrumentation devices. However, C4 had to be rotated 45° with respect to its edge in order to fit both linear potentiometers due to their length (front and back). For proper DIC, the camera lens has to be placed at 90° with respect to its front surface. Since this was the first specimen tests, it was decided to test it in this orientation and to then correlate the results. Thus, the high-resolution photographs for DIC were compromised since only one camera was available. Figure 5.31 shows the setup for C4.

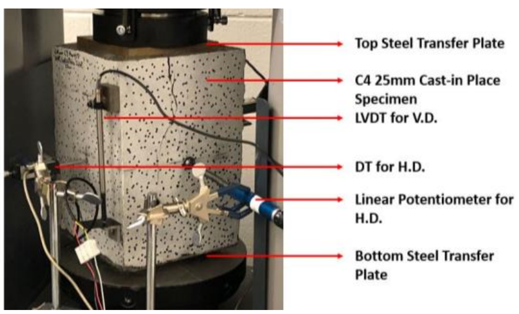

(a)

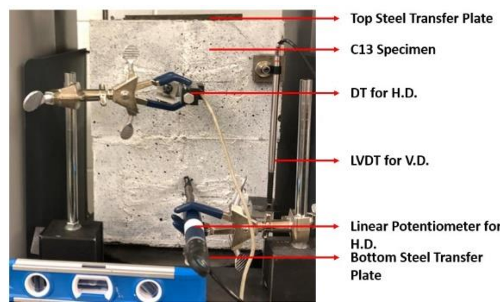

(b)

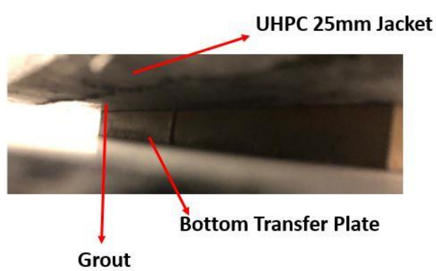

(c)

Figure 5.32. Set up for monotonic testing when testing (a) C4 specimen with all instrumentation, (b) C13 specimen with the instrumentation, and (c) bottom steel plate placed below column.

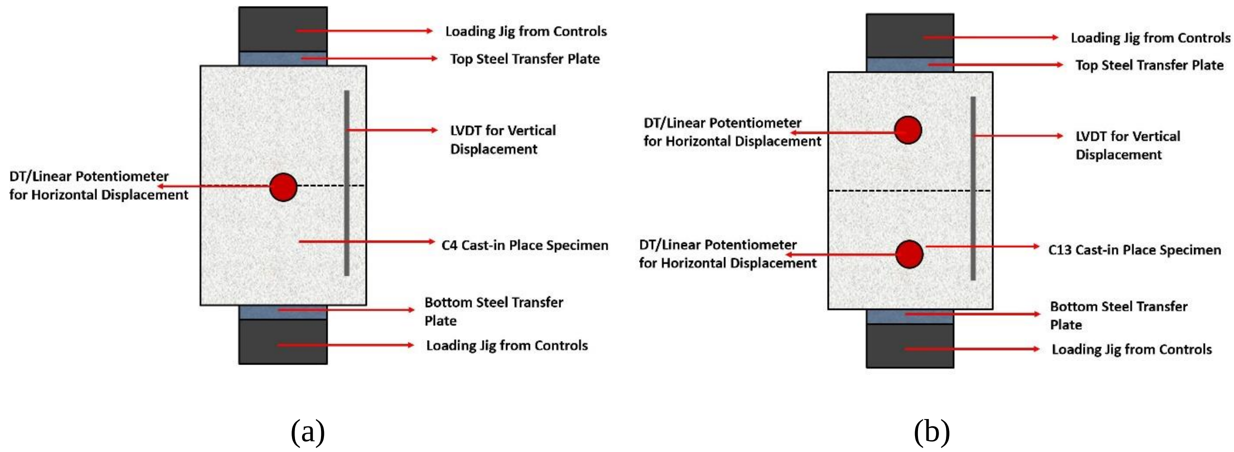

Figure 5.33. Scheme showing the position of the instruments relative to the top and bottom plate of the Controls ® when (a) testing the Cast-in Place Retrofitted Columns and (b) the remaining Retrofitted Columns.

As shown in Section 5.3, the average compression strength of the concrete column core at 28 days f_c' was 32 MPa. The final results were compared to f_c' equal to 41.56 MPa, which was the compressive strength at the day of testing. The columns had a cross-sectional area of 22,500 mm^2. The cast-in-place solution for this setup was expected to provide an estimated increment in the compression strength of 12 % due to the confinement effect. After the monotonic testing, the peak load achieved was 1012 kN, resulting in 46.68 MPa meaning an increment of 12.3 %. However, the most relevant gain is the strain gain once the column is retrofitted. The NSC cylinder data is shown in Figure 5.43 and all the specimens are compared in Figure 5.44. While the NSC cylinders reached a strain of 0.0031 mm/mm at peak stress, column C4 reached 0.0105 mm/mm at peak stress. This corresponds to a 339 % increment given by the UHPFRC Jacket. This particular specimen started to crack on one side, corresponding to its front as seen in Figure 5.31 (a). This crack was visible before reaching peak load, and when the test was in the descending branch the crack was highly visible and was gradually extending downwards, opening the cast-in-place jacket. It was also observed that the LVDTs placed in the vertical direction were not recording relevant changes in displacement. This meant that while the column was being compressed, the UHPFRC jacket was displacing outward and not vertically. Basically, the UHPFRC jackets kept their position in the vertical direction as the column was the one element being under compression. When the specimen was removed from the machine, it was noticed that the opposite side was also cracked, although the UHPFRC jacket did not open as much as in the front side. Basically, the

UHPFRC jacket was holding the load that was being transferred to it until the confining pressure reached the maximum capacity of the UHPFRC. Once the UHPFRC was cracked from one side, all the resistance decayed. The cracking pattern in the post-peak behavior seeks for the weakest link, which for UHPFRC means the areas where a lesser number of horizontally oriented fibers were gathered. Specimen C4 reached a high ductile behavior due to the bridging capacity provided by the steel fibers, which is a characteristic of UHPFRC materials. Once the specimen reached the descending branch it was still capable of achieving high levels of damage. It was only after testing that cracks were noticed at three of the four corners of the top cross-sectional area. This led to the conclusion that the confining pressure in a rectangular UHPFRC jacket is higher at the sides than at the corners when it is a cast-in-place solution. The maximum displacement value set in the compression machine for this specimen was 5 mm, although it was observed that C4 could take more damage. This value was changed for other specimens to a maximum limit displacement of 8 mm. For analyzing the data for all columns (i.e. monotonic and cyclic) the value for the ultimate load was taken as a 15% drop in the descending branch, therefore its ultimate displacement and ultimate strain were automatically defined.

Figure 5.34. Specimen C4, cast-in place UHPFRC Jacket, after testing.

5.6.1.2 Monotonic Testing for Precast Jacket with Curved Key Column C6

Due to the larger sectional dimensions owing to the grout layer, specimen C6 did not have enough space to place instrumentation around its total perimeter. The six instrumentation devices were placed differently. The column was loaded at angle of 90° with respect to the lens of the high-resolution camera placed in front of it. For C6, the instrumentation was placed at the front and at the back of the column. One *LVDT* was placed on each front and back surface, in the vertical direction and on opposite corners to measure the vertical displacement on the outside face of the UHPFRC Precast Jacket. One *DT* was placed exactly at mid-height of the top precast UHPFRC curved key, and one *LP* was placed exactly at mid-height of the bottom precast UHPFRC curved key horizontally, to measure out of plane dilation. The peak load achieved was 944 kN, resulting in 41.95 MPa meaning a strength increase only by 0.96 %. This strength increment is not as relevant as the strain increment. Just like specimen C4, the strain at peak for specimen C6 obtained was 0.006 mm/mm, corresponding to an increment of 194 %. The jacket connection in this particular specimen behaved similarly to the observed direct tension specimens from Section 5.2.3. The tensile stresses were successfully transferred to the UHPFRC jacket but no visible cracks were found on the precast UHPFRC key which remained uncracked, whereas cracking was observed on the precast UHPFRC 2% jacket. The weakest link in this setup is again the bonding agent, the *Sikadur-31*. Once the specimen was removed from the compression machine, cracks were found on the four corners of the cross-sectional area. During testing, after cracking in the jacket around the roundhead edge of the curved key, the jacket was displaced outwards until both top jackets separated. The largest localized crack happened in the jackets below the roundhead edge of the curved key.

Figure 5.35. Specimen C6, precast UHPFRC Jacket with Curved Key, after testing.

5.6.1.3 Monotonic Testing for Precast Jacket with Curved Key Column C13

A similar setup was used here as in specimen C6. The LVDTs, DTs, and LPs were placed in the same positions as C6. The peak load obtained was 1044 kN, resulting in an average compressive strength of 46.4 MPa achieving an increment of 11.6 % over the unconfined value. For this specimen, the first cracking happened near 436 kN in the ascending branch, at 19.37 MPa. This specimen behaved similarly to C6. Nonetheless, when comparing the strain at peak for specimen C13 to the NSC the increment was again 198 %, since the strain at peak for C13 recorded was 0.006 mm/mm. The tensile stresses were successfully transferred to the UHPFRC jacket, no visible cracks were found on the precast UHPFRC key, and the LPs did not record relevant displacement changes. A pattern was discovered for this type of setup. Once the specimen was removed from the compression machine, cracks were found on the four corners of the cross-sectional area, the precast jacket was displaced outwards until both top jackets separated. The biggest crack happened in the jackets below the roundhead edge of the curved key similar to C6.

Figure 5.36. Specimen C13, precast UHPFRC Jacket with Curved Key, after testing.

5.6.1.4 Monotonic Testing for Precast Jacket with Lap Splice Connection Column C12

Specimen C12 was tested using the same setup as in C13, with the same positions of the LVDTs, DTs, and LPs . The peak load obtained was 932 kN, leading to 41.4 MPa where technically there was no increment in the strength capacity. This was the first lap splice connection specimen to be tested. The first cracking happened near 555 kN in the ascending branch, at 25 MPa. The recorded strain t peak was 0.0088 mm/mm, corresponding to an increment of 258 %. When reaching the peak, the specimen cracked at the cold joint between the precast jacket and the connection zone, which was also seen when testing the direct tension specimens. The tensile stresses were again successfully transferred to the UHPFRC jacket. The largest cracks were found on one corner of the cross-sectional area before removing the specimen from the testing frame. The precast jacket behaved in the transverse direction of the column, similarly to the flexural test mentioned in Section 5.4.1. For this type of setup, the method of casting and fiber orientation controlled the mode of failure.

Figure 5.37. Specimen C12, precast jacket with Lap Splice Connection, after testing.

5.6.1.5 Monotonic Testing for Cast-in Place Jacket Column C8

Specimen C8 was the first 37.5 mm thick specimen to be tested where the LVDTs and DTs were placed at the mid-height of the specimen.. The instruments were placed as shown in the Figure

5.32 (a) due to space limitations, since the Retrofitted Columns having 37.5 mm thick UHFRC Jackets had bigger dimensions.

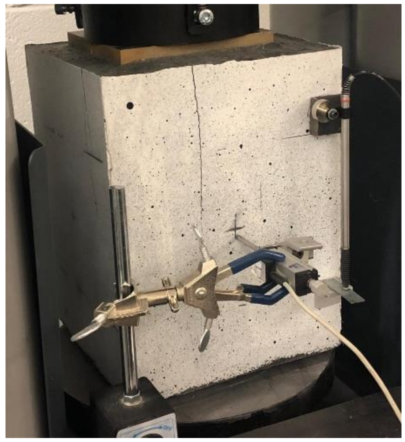

Figure 5.38. Rotation of specimen C8 due to dimensions and space limitations. Only DTs were place on the front and back face of the Retrofitted Column, the LVDTs remain in position.

The peak load obtained was 999 kN, corresponding to an average compressive stress of 44.38 MPa, a 6.78 % increase in strength. The observed strain at peak for C8 was 0.0095 mm/mm, leading to an increment of 306%. The first cracking was noticed close to 650 kN in, at 28.8 MPa average compressive stress. This specimen was a cast-in-place solution, and the same cracking pattern was observed in column C4, where the specimen started to crack on one side. The confining pressure again reached its maximum capacity, UHPFRC then cracked from one side, the resistance decayed as all the pressure was released and then the crack found the weakest path. Specimen C8 showed segregation of steel fibers, and this could have been due to the method of casting which was performed by filling the void space while using a scoop. When collecting UHPFRC 2% from the mixing bowl, steel fibers segregate, which could lead to this behavior. To improve the mode of failure, the UHPFRC mix could be poured directly from the bowl (i.e. without scooping) or by using UHPFRC 3% volume fraction.

Figure 5.39. Specimen C8, cast-in place jacket, after testing.

5.6.1.6 Monotonic Testing for Precast Jacket with Curved Key Column C11

Specimen C11 had a similar setup to C8, and the specimen was placed at 90̊. The peak load obtained was 918 kN, corresponding to an average compressive strength of 40.8 MPa, which when compared to the average compressive strength on the day of testing there was no increment. However, just like the previous specimens, the strain at peak was significantly increased. The recorded strain at peak for C11 was 0.007 mm/mm, leading to a 226 % increment. The first cracking was noticed around 465 kN, at 20.7 MPa. This specimen had the precast UHPFRC 3% curved key, and the same cracking pattern was observed in column C6, where the specimen started to crack at the corner, and also the weakest link was the bonding agent. The confining pressure again reached its maximum capacity by splitting the precast jacket, meaning that the precast curved key had the capacity to transfer the tensile stresses in the jacket successfully without failing. The key then cracked at one end near the roundhead region, at which point the precast jacket components started to separate away from each other. When testing specimen C11, the LP placed at the back got detached near 400 kN in the descending branch.

Figure 5.40. Specimen C11, precast jacket with curved key, after testing.

5.6.1.7 Monotonic Testing for Precast Jacket with Lap Splice Connection Column C1

Specimen C1 did not have enough space to place instrumentation, so, a similar setup was used as in specimen C12 including the instrumentation. The peak load obtained was 1069 kN, leading to 47.5 MPa and a strength increase of 14.3 %. Specimen C1, along with C4, were the two specimens with the higher strain at peak gain when compared to the concrete core from the NSC cylinder tests. The starin at peak for C1 was 0.011 mm/mm, which leds to a gain in deformation of 3355 %. This was the second lap-splice connection specimen tested. First cracking was observed near 750 kN in the ascending branch, at a compressive stress in the encased core equal to 33 MPa. A visible crack was noticed at one corner at 850 kN, 37.7 MPa. When reaching the peak, the specimen again cracked at the cold joint between the precast jacket and the connection region, showing in the transverse direction the same failure mechanism as the direct tension specimens for the lap-splice connection. The tensile stresses were successfully transferred to the UHPFRC jacket. The biggest crack developed on the corner that was noticed at 850 kN, and it continued to open its way across the specimen until reaching the bottom. Only one of their four sides of the precast jackets cracked, the rest remained less damaged.

Figure 5.41. Specimen C1, precast jacket with lap splice connection, after testing.

5.6.8. Monotonic Testing Summary

The seven Retrofitted Columns data for the monotonic tests are summarized in Table 5.9. To define the yield point, first the 60% of the peak stress was identified in the specimen envelope. Then, a tangent was drawn based on the 60% peak stress value. At the same time, a horizontal line at peak was drawn on the envelope. The intersection between the tangent and the horizontal line is known as the yield point. The ultimate values are calculated as the 85% of peak stress in the descending branch of the envelope. The ductility shown in Table 5.9 refers to the ultimate deformation divided by the NSC cylinder deformation at the same ultimate deformation. The results for the uniaxial cylinder test (stress-strain curves) are showed in Figure 5.40. While the strength gain for the Retrofitted Columns when tested under monotonic loading was less than 14.5 %, the deformation capacity of the column was significantly increased by the precast UHPFRC Jackets. The deformation capacity increased in the range of [1988 – 355] %.

Table 5.9. Summary for all the monotonic loading tests performed on seven Retrofitted Columns.

Technique	Column	*t*	Yield stress	Yield Strain	Peak stress	Peak Strain	Ultimate stress	Ultimate Axial Strain	Ductility
		(mm)	(MPa)	(mm/mm)	(MPa)	(mm/mm)	(MPa)	(mm/mm)	(μ)
Cast-in Place	C4	25	40.31	0.0053	46.69	0.0066	29.68	0.0086	1.62
	C8	37.5	32.87	0.0066	44.39	0.0112	37.73	0.0141	2.14
Curved Key	C6	25	37.93	0.0078	41.95	0.0087	35.66	0.0111	1.42
	C13	25	36.93	0.0053	46.41	0.0077	39.45	0.0091	1.72
	C11	37.5	33.23	0.0065	40.80	0.0088	34.68	0.1010	1.55
Lap Splice	C12	25	32.89	0.0072	41.45	0.0101	35.23	0.0134	1.86
	C1	37.5	42.14	0.0097	47.52	0.0121	40.39	0.0157	1.62

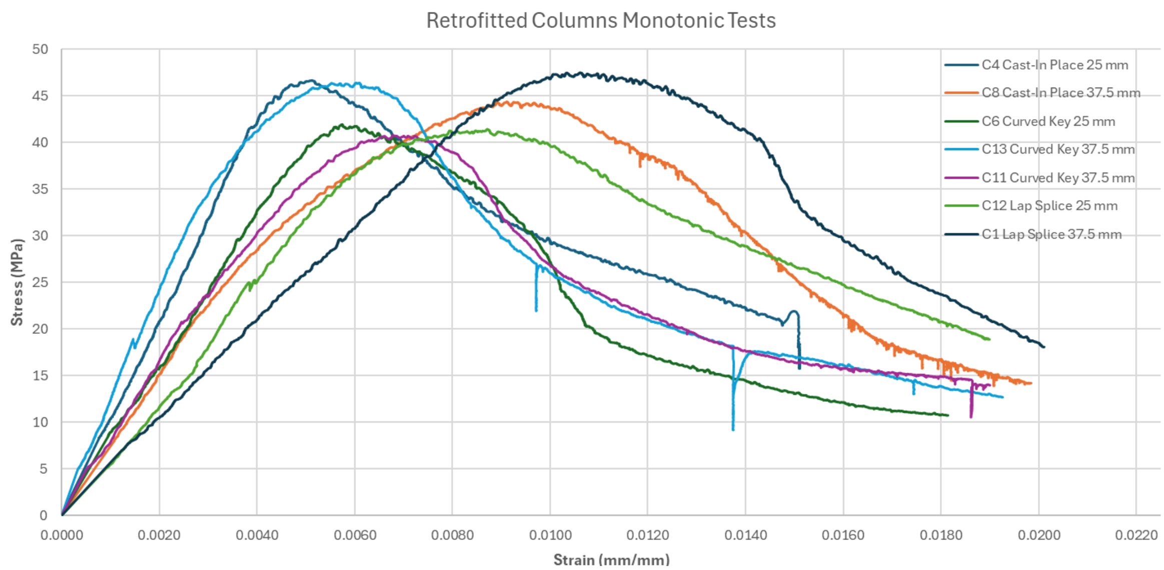

Figure 5.42. Stress-strain curves for the seven Retrofitted Columns under monotonic loading tests.

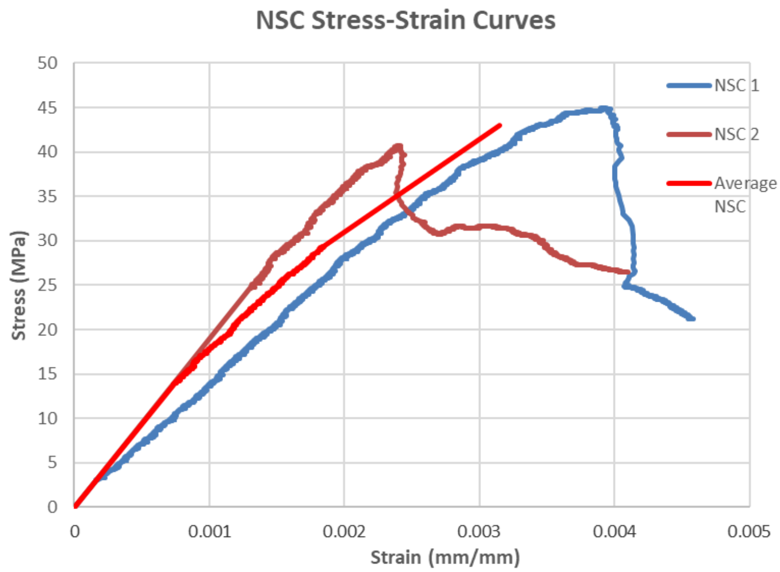

Figure 5.43. Stress-strain curves for the uniaxial compression for NSC1 and NSC2.

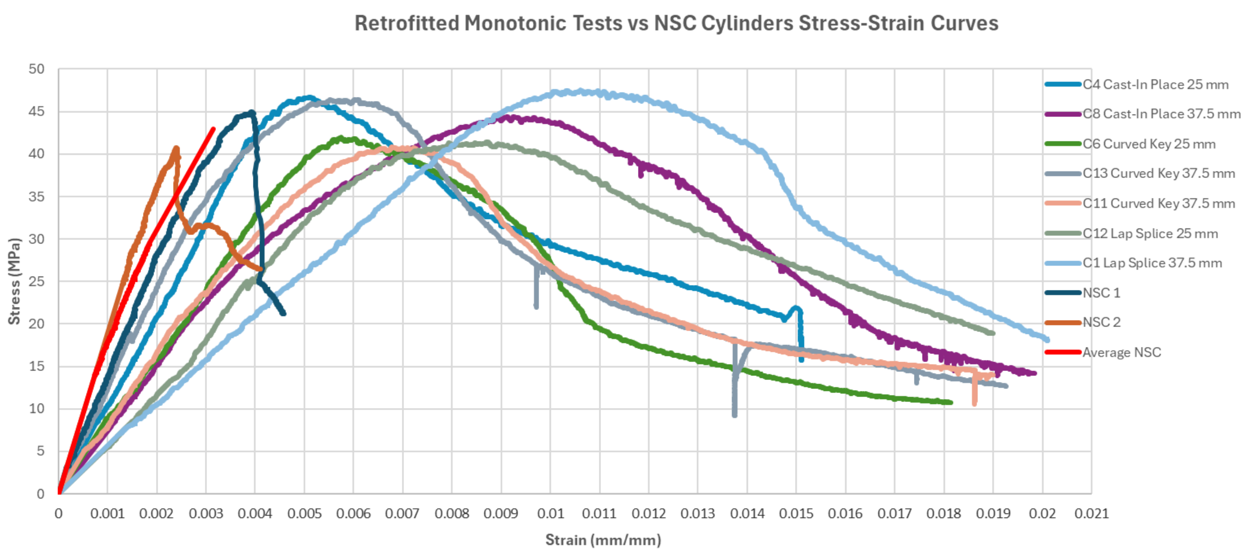

Figure 5.44. Stress-Strain of all monotonic test compared to the NCS results.

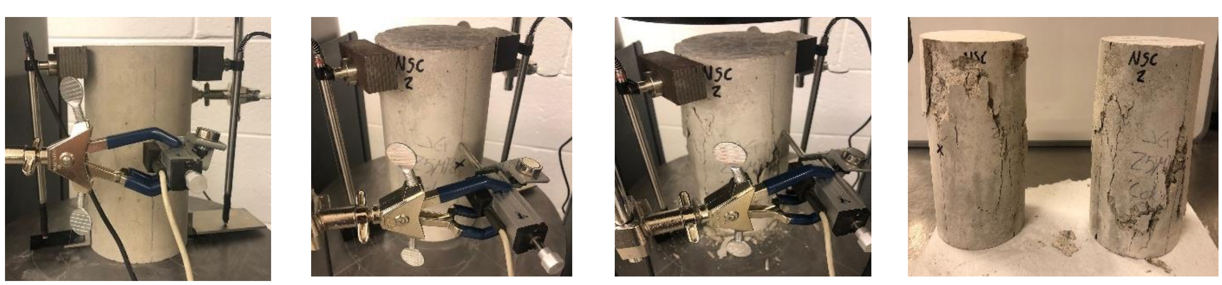

Figure 5.45. NSC1 and NSC2 concrete cylinders after being tested in uniaxial compression to obtain the compression strength value of the unreinforced concrete column.

5.6.2 Retrofitted Columns - Cyclic Tests

From the thirteen Retrofitted Columns, the remaining six were tested under cyclic loading. The others were for the monotonic tests presented in the previous section. Table 5.10 organizes the order of testing for the specimens under cyclic loading. The cyclic loading was conducted in cycles of load/unload repeatedly applying and removing axial load on the specimen at a specifically defined rate. The previous rate for the monotonic tests was 0.12 mm/min. This process helps to simulate conditions occurring under seismic loads where materials (i.e. a concrete column in this research) experience fluctuating loads over time.

Table 5.10. Summary of Retrofitted Columns under Cyclic Tests.

Set	Column N^{o}	Description	Jacket Thickness (mm)
2	C7	Cast-in Place	25
2	C5	Cast-in Place	25
4	C3	Precast Jacket + Lap Splice	25
2’	C10	Cast-in Place	37.5
3’	C9	Precast Jacket + Curved Key	37.5
4’	C2	Precast Jacket + Lap Splice	37.5

The loading regime was programmed to produce two loading/unloading cycles at increments of 0.5 mm (see Table 5.11). In each cycle, the test algorithm applied displacement-controlled load until the target actuator displacement was reached (i.e., 2.0 mm, 2.5 mm, 3.0 mm, etc.) at a test rate of 0.12mm/min. Upon unloading, the algorithm switched to load control and the load direction was reversed until the applied actuator load would reach a residual compressive load of 200 kN at an unloading test rate of 7 kN/s; this value of the load was chosen to avoid disconnecting the loading platens from the specimen surface. All the cyclic tests are described in this section individually. Following their description, the column responses are plotted in Figure 5.52 and then compared with the NCS cylinders on Figure 5.53. A summary is presented in Table 5.12.

Table 5.11. Cyclic loading regime programmed on *Controls Pilot*.

Step	Feedback	Speed	Target	Cycle
1	Ch 5	0.12 mm/min	2 mm	1
2	Load	7,000 N/s	200 kN	
3	Ch 5	0.12 mm/min	2 mm	
4	Load	7,000 N/s	200 kN	
5	Ch 5	0.12 mm/min	2.5 mm	1 & 2
6	Load	7,000 N/s	200 kN	2
7	Ch 5	0.12 mm/min	2.5 mm	
8	Load	7,000 N/s	200 kN	
9	Ch 5	0.12 mm/min	3 mm	2 & 3
10	Load	7,000 N/s	200 kN	3
11	Ch 5	0.12 mm/min	3 mm	
12	Load	7,000 N/s	200 kN	
13	Ch 5	0.12 mm/min	3.5 mm	3 & 4
14	Load	7,000 N/s	200 kN	4
15	Ch 5	0.12 mm/min	3.5 mm	
16	Load	7,000 N/s	200 kN	
17	Ch 5	0.12 mm/min	4 mm	4 & 5
18	Load	7,000 N/s	200 kN	5
19	Ch 5	0.12 mm/min	4 mm	
20	Load	7,000 N/s	200 kN	
21	Ch 5	0.12 mm/min	4.5 mm	5 & 6
22	Load	7,000 N/s	200 kN	6
23	Ch 5	0.12 mm/min	4.5 mm	
24	Load	7,000 N/s	200 kN	
25	Ch 5	0.12 mm/min	5 mm	6 & 7
26	Load	7,000 N/s	200 kN	7
27	Ch 5	0.12 mm/min	5 mm	
28	Load	7,000 N/s	200 kN	
29	Ch 5	0.12 mm/min	5.5 mm	7 & End

5.6.2.1 Cyclic Testing for Cast-in Place Jacket Column C7

Specimen C7 was the first cyclic test performed under the regime described in Table 5.9 above. The behavior of this cast-in-place solution was similar to those tested under monotonic loading. The instrumentation devices were placed following the pattern of specimen C8, where only the front and back faces of the column were instrumented. It was placed at 90° with respect to the lens of the high-resolution camera placed in front of the test frame, like shown in Figure 5.32 (a) and Figure 5.33. The peak load achieved was 950 kN, resulting in 42.23 MPa corresponding to a compressive strength increase of 1.61 %. This particular specimen behaved similarly to the monotonic tests, where once the jacket cracked and opened on one side, then the pressure is released, and the confining pressure decays. However, the strain at peak was significantly increased, just like the specimens tested under monotonic loading. The strain at peak recorded for

C7 was 0.0095 mm/mm, which means a 306 % increment in the deformation capacity of the retrofitted column. The biggest crack happened at the front face of the jacket, and once the jacket opened the crack followed its path until reaching the bottom. After removing the specimen from the testing frame, minor cracks were noticed at two opposite corners.

Figure 5.46. Specimen C7, cast-in place jacket, after testing.

5.6.2.2 Cyclic Testing for Cast-in Place Jacket Column C5

Specimen C5 is set up and behaves similarly to specimen C7. However, even though the testing regime was set and checked before testing, the test was discontinued after the peak load was attained, and then suddenly captured the descending branch. The peak load achieved was 1060 kN, resulting in 47.12 MPa, i.e., a strength increase of 13.6 %. Before reaching peak load, cracks were found visible at one corner of the UHPFRC jacket. These were the biggest cracks happening in the jackets when testing the cast-in-place alternative. The corner cracked, extending completely across from top to bottom.

Figure 5.47. Specimen C5, cast-in place jacket, after testing.

5.6.2.3 Cyclic Testing for Precast Jacket with Lap Splice Connection Column C3

For C3, the instrumentation was placed at the front and at the back of the column, see Figure 5.31 (a) and Figure 5.32. The peak load attained was 1060 kN, resulting in 47.12 MPa which corresponds to a strength increase of 13.4 %. The tensile stresses were successfully transferred to the UHPFRC jacket, the connection itself did not show any visible cracks besides at the cold joints, and the precast UHPFRC 2% jacket cracked only at one corner. The strain at peak for this specimen was 0.0062 mm/mm. Compared to the NSC core, an increment of 200 % in the deformation capacity was achieved. Once the specimen was removed from the compression machine, minor cracks were found on the remaining three corners of the cross-sectional area. However, the biggest crack happening follows again a splitting path that extends completely from top to bottom.

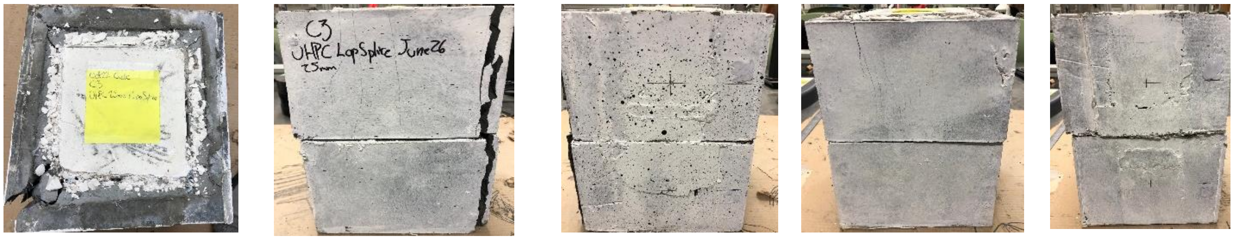

Figure 5.48. Specimen C3, precast jacket with Lap Splice connection, after testing.

5.6.2.4 Cyclic Testing for Cast-in Place Jacket Column C10

Specimen C10 was the last cyclical and last test performed on the cast-in-place specimens, so by then, a pattern had already emerged: once the jacket cracked and opened on one side, then the pressure was released, and the confining pressure decayed. The peak load achieved was 1023 kN, resulting in 45.29 MPa, i.e., a strength increment by 8.98 %. Once the specimen was removed from the compression machine, cracks were found on the four corners of the cross-sectional area. The strain obtained at peak for this specimen was 0.0068 mm/mm, providing an increment of 222 %. As predicted, once the jacket cracks the confining pressure given by the jacket is lost and then the crack follows a path that extends from top to bottom.

Figure 5.49. Specimen C10, cast-in place jacket, after testing.

5.6.2.5 Cyclic Testing for Precast Jacket with Curved Key Column C9

When testing specimen C9 the Controls Pilot machine did not operate correctly in the middle of the second cycle. Therefore, in the final plot presented below this section, the curve for C9 is incomplete after a 3 mm displacement. Nonetheless, the behavior of this precast UHPFRC curved key solution was similar to those tested under monotonic loading, and therefore the jacket performed in the transverse direction as in the direct tension tests. The specimen started to crack at the corner and also the weakest link was the bonding agent. The confining pressure again reached its maximum capacity by splitting the precast jacket. Therefore, the precast curved key had the capacity to develop the tensile stress demands of the jacket successfully without failing. The key then cracked at one end near the roundhead region. Beyond that point, the precast jacket components started to separate away from each other. The peak load achieved was 1040 kN, resulting in 46.24 MPa, which corresponds to a compressive strength increase by 11.3 %. By taken this value as the peak value, the strain for this specimen would be 0.0052 mm/mm. This led to an increase in the deformation capacity of at least 167 %. The starin at peak and the peak stress for this specimen could have been greater if the malfunction of the *Controls* ® would not had happened, but even so its shown that the precast UHPFRC Jacket provides a significant increase in the deformation capacity of the concrete column.

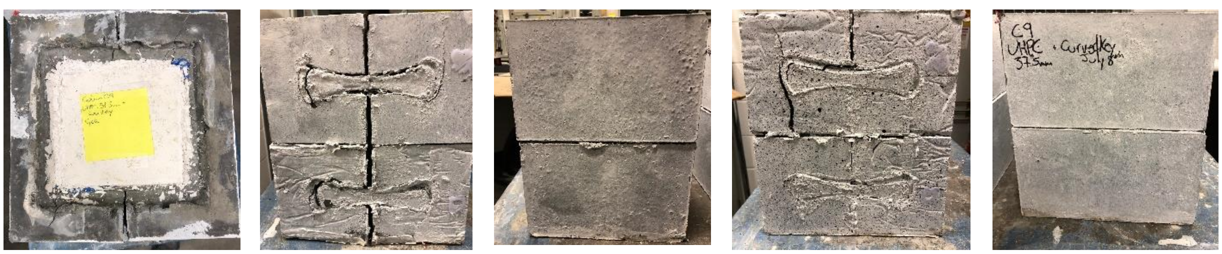

Figure 5.50. Specimen C9, precast jacket with curved key, after testing.

5.6.2.6 Cyclic Testing for Precast Jacket with Lap Splice Connection Column C2

Specimen C2 did not allow enough space to place instrumentation, and therefore, a similar setup was used as in specimen C1, see Figure 5.31 (a) and Figure 5.32. As this was the last specimen to be tested, based on the observations from the previous test it was possible to anticipate the mode of failure. The peak load attained was 1060 kN, resulting in 47.12 MPa. This is equivalent to a compression strength increase by 13.4 %. The observed strain at peak for C2 is 0.0075 mm/mm, which was the second highest value for the retrofitted columns under cyclic testing. This corresponds to an increment in the deformation capacity of 242 %.. The tensile stresses were successfully transferred to the UHPFRC jacket, the connection remained practically uncracked besides the cold joints, and the precast jacket cracked only at one corner. Once the specimen was removed from the compression machine, minor cracks were found on the remaining only at two corners of the cross-sectional area.

Figure 5.51. Specimen C2, precast jacket with Lap Splice Connection, after testing.

5.6.8. Cyclic Testing Summary

The Data from the six Retrofitted Columns tested under cyclic loading is shown in Table 5.12 below. Just like the monotonic cases, when performing cyclic testing on the Retrofitted Columns the strength increment is less than 14.5 %. However, when analyzing the deformation capacity obtained from strain and when comparing the stain at peak of the specimens with the strain at peak of the NSC cylinders, the increment in the deformation capacity is the range of [200 – 306] %. This range corresponds to all cyclic tests with the exception of specimen C9, which in Table 5.12 is marked as *C9***.

Table 5.12. Summary for all the cyclic loading tests performed on six Retrofitted Columns.

Technique	Column	*t*	Yield Stress	Yield Strain	Peak Stress	Peak Strain	Ultimate Stress	Ultimate Strain	Ductility
		(mm)	(MPa)	(mm/mm)	(MPa)	(mm/mm)	(MPa)	(mm/mm)	(μ)
Cast-in Place	C7	25	38.73	0.0075	42.21	0.0091	35.88	0.0116	1.55
	C5*	25	39.41	0.0048	46.11	0.0061	39.19	0.0063	1.31
Lap Splice	C3	25	39.73	0.0069	47.12	0.0084	40.05	0.0109	1.58
	C2	37.5	39.68	0.0070	46.32	0.0100	39.37	0.0117	1.67
CurvedKey	C9**	37.5	39.42	0.0066	46.24	0.0084	39.31	0.0086	1.30
Cast-in Place	C10	37.5	38.43	0.0054	45.49	0.0084	38.67	0.0101	1.87

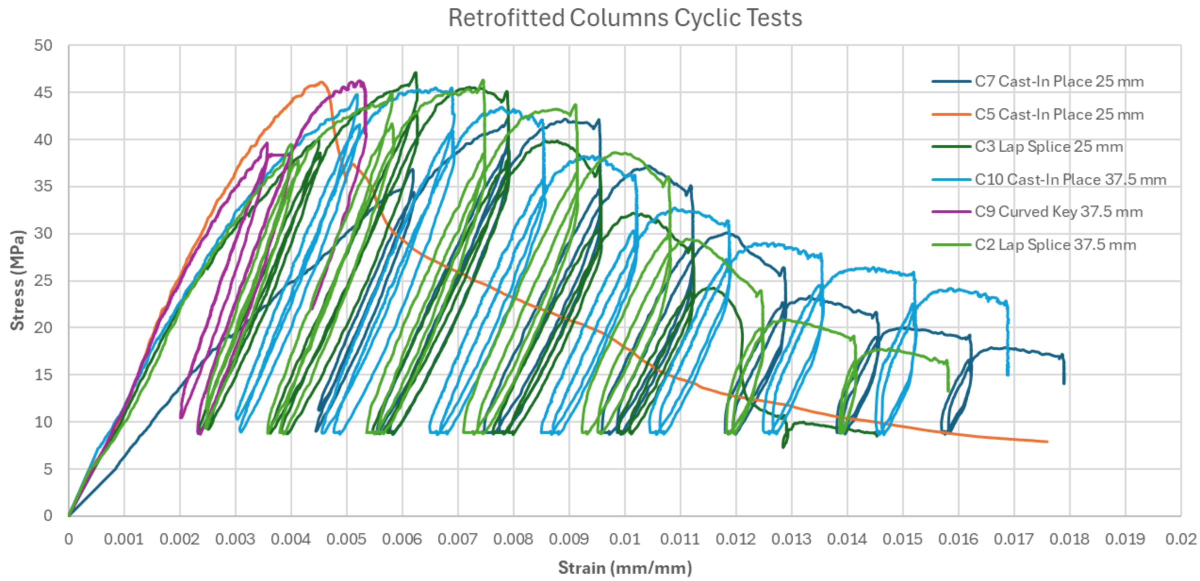

Figure 5.52. Stress-strain curves for the six Retrofitted Columns under cyclic loading tests.

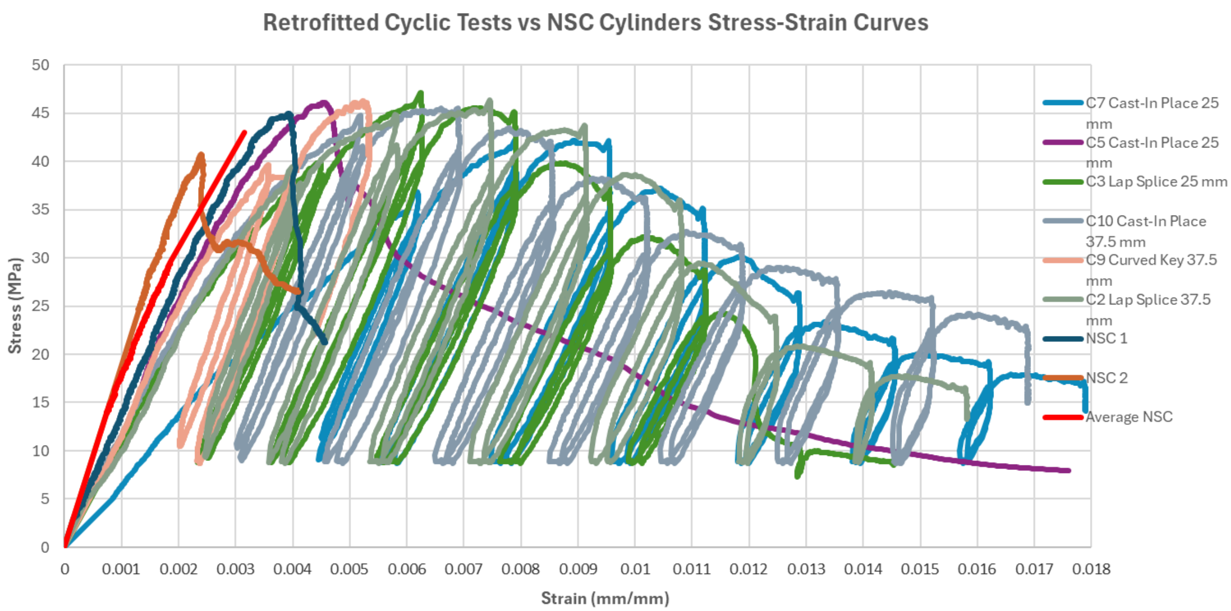

Figure 5.53. Stress-strain curves of all cyclic tests compared to the NSC results.

5.7 Mechanical Interaction on Retrofitted Columns

Mechanical interaction between concrete surfaces is a complex phenomenon influenced by several physical and material factors. It primarily involves the transfer of forces and relative movement at the interface between two concrete surfaces that are in contact. This interaction is crucial in applications such as construction joints, repairs, or where new concrete is bonded to old concrete. This phenomenon was studied in this research by creating three concrete specimens simulating the interlocking action that occurs between the precast UHPFRC jacket and the non-shrink grout used and described in the section above. This mechanical behavior mostly depends on the surface texture and the roughness of the inside of the precast UHPFRC jacket which was formed with the help of the commercial bubble wrap (i.e. large bubble cushion $^{5}/_{16}$ in). The objective was to generate better mechanical interlock due to the penetration formed from the grout into the jacket once the bubble wrap was removed, enhancing the bond strength and resisting the shear forces.

5.7.1 Sandwich Specimen for Interlocking Testing

To test the mechanical interaction between the precast UHPFRC jacket and the non-shrink grout, three specimens were fabricated, and they were referred to as *Sandwich Specimens*. These specimens were made by casting two pieces of UHPFRC with the same mix proportions used for the Retrofitted Columns with the addition of the large bubble wrap plastic. Just like precast C-Shapes, a rough surface was formed by the ($^{5}/_{16}$ in) bubble size cushion once the plastic bubble wrap was removed. The UHPFRC pieces had a cross-section of 100 mm by 150 mm with a thickness of 25 mm, and they were prepared by placing a rectangular layer of plastic bubble wrap of 100 mm by 150 mm at the base of the steel molds used for the preparation of the precast UHPFRC C-Shapes. Afterward, the UHPFRC mix was poured from the top. The samples were demolded 24 hours after pouring and the bubble wrap was easily removed. Once the pieces were demolded, they whey placed vertically on top of an acrylic smooth plate (*plexiglass*) to generate an even level surface; the pieces were resting on the 25 mm by 100 mm cross-sectional area. The two pieces were fixed on the plexiglass with hot glue and clamps. The gap between the UHPFRC to be filled with non-shrink grout from the top was 25 mm. However, in these *Sandwich Specimens*, the non-shrink grout was not aligned with the edges of the UHPFRC pieces intentionally, since they were meant to be tested by applying axial load only on the 100 mm by 25 mm cross-sectional area of the non-shrink grout. The three *Sandwich Specimens* were placed in the curing tank 24 hours after casting the non-shrink grout. Figure 5.54 shows the Sandwich specimens before testing.

(a) (b) (c)

Figure 5.54. Sandwich Specimens for interlocking testing.

The specimens shown in Fig. 5.54 where tested in the same displacement-controlled machine MTs used for Direct Tension for he characterization tests, explained in Chapter 4. The specimens from Fig 5.54 were tested with compression test setup with a test rate of 0.12 mm/min. The specimens had an interlocking cross-sectional area of 105 mm by 120 mm, equal to 12,600 mm^2. The interlocking shear stress developed in the face between the UHPFRC bubble surface, and the non-shrink grout was in the range of [1.15 – 1.60] MPa with a maximum strain in the range of [0.0038 – 0.006] mm/mm. The strain for these specimens was calculated by dividing the vertical displacement (given by the MTS machine) by the total height of the specimen (i.e. 105 mm). Fig. 5.55 shows the results of the three sandwich specimens and Fig. 5.56 shows the specimens after testing.

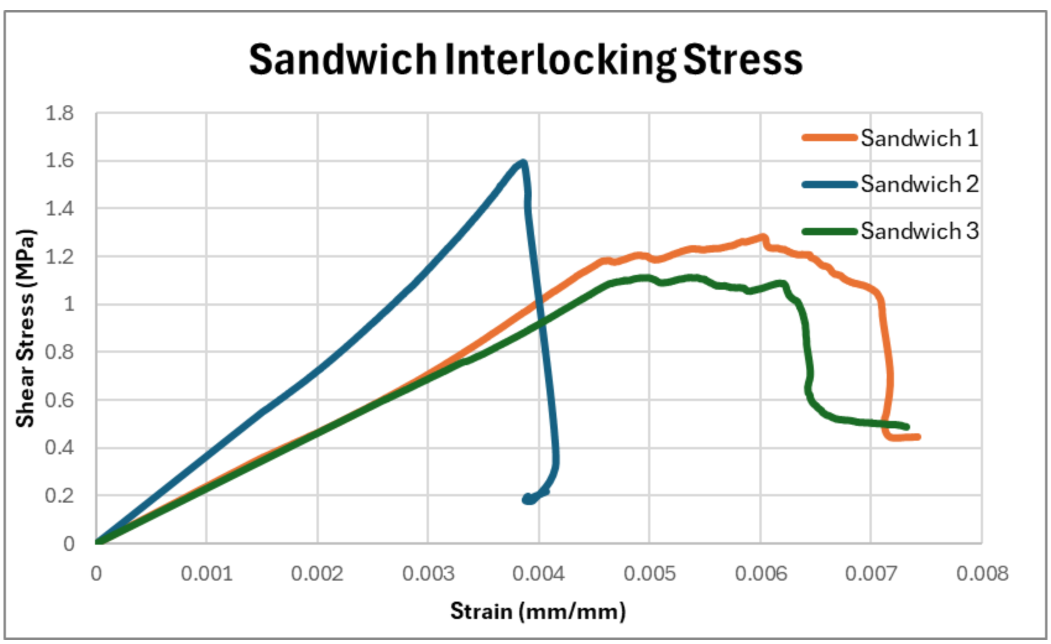

Figure 5.55. Results for the Sandwich Specimens for interlocking testing.

Figure 5.56. Sandwich Specimens after testing under axil load at the top surface of the non-shrink grout.

Chapter 6: Finite Element Modelling of Columns with Precast UHPFRC Jackets

This chapter presents simulation of the tests in the three dimensional nonlinear Finite Element software suite GiD-ATENA (Červenka Consulting, 2007). The primary objective of this effort is to understand better the confinement effectiveness provided by the Precast UHPFRC C-Shaped Jackets. The main objective of the finite element analysis was to obtain the relationship between axial strain of the encased component, and lateral pressure exerted by the confining jacket. The modeling was performed using GiD (graphical user interface program) whereas the finite element analysis and post-processing were performed using ATENA studio. Three alternative modeling approaches were used to model the interaction between the normal strength concrete core and the precast UHPFRC jacket. The first model represented the cast-in place solution, while the second and third models were used to study the precast UHPFRC Jacket with the precast curved key and the precast UHPFRC with the lap splice connection respectively. The finite element analysis responses obtained through the above methods were compared with the experimental behavior so as to verify the models through comparison with the experimental observations.

6.1 3-D Column Model

The models were constructed using three-dimensional solid elements only. In these models, both the UHPFRC and column core prisms were modeled using tetrahedral and hexahedral solid elements.

6.1.1 Model Geometry and Boundary Conditions

By taking advantage of symmetry, only part of the column setups were modelled. For instance, $^{1}/_{8}$ of the actual Final Retrofitted Column was modelled for the precast UHPFRC jackets having the precast UHPFRC curved key and the cast-in place solution, while a $^{1}/_{4}$ model was constructed to study the precast UHPFRC jackets with the lap splice connection. Geometry details corresponding to all models were developed in a computer-aided design software application (CAD) to obtain a precise coordinate system. Symmetrical models ease computational time in the analysis and favor better convergence in the results. Figure 6.1 (a), (b) and (c) shows the geometry details of the modeled members. Dimensions of the three dimensional models are shown in Table 6.1.

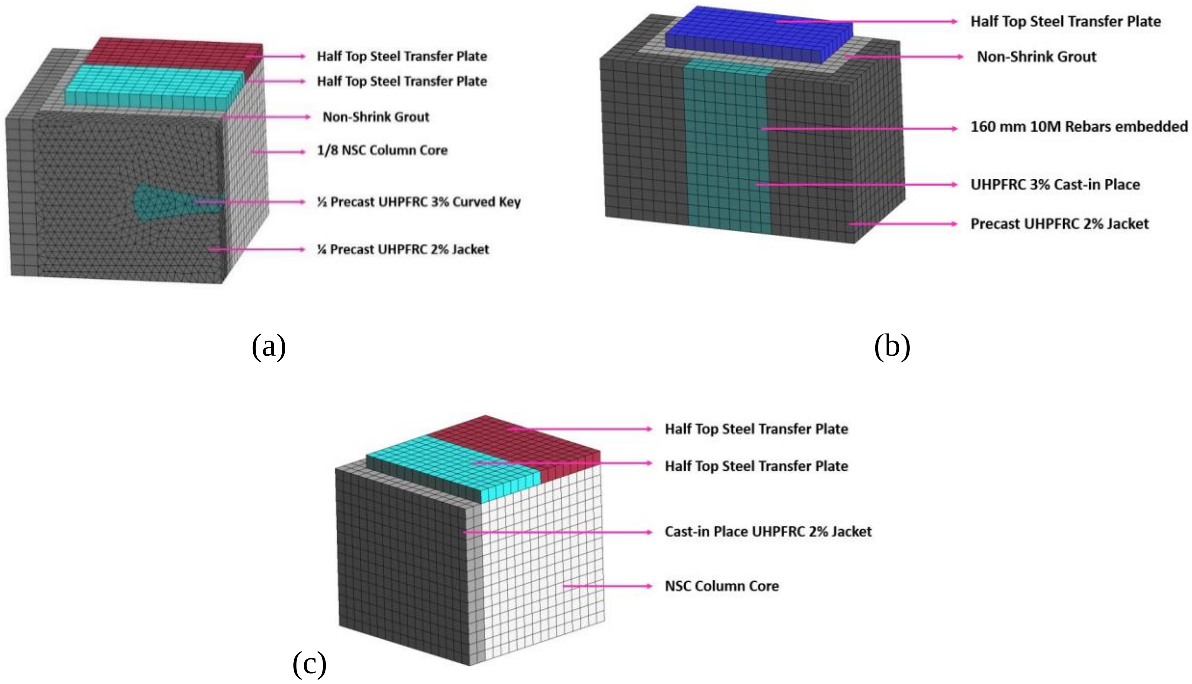

Figure 6.1. Outline of 3-D model and layer details of the Final Retrofitted Column Model (a) with the precast UHPFRC curved key, (b) with the lap splice connection and (c) cast-in place alternative.

Table 6.1. Model geometry details for 3-D ATENA GiD ® models.

Element	Shape	Dimensions
Transfer Plate	Rectangular	a=75 mm, b=75 mm, t=12.5 mm
NSC Column Core	Rectangular	a=75 mm, b=75 mm, h=150 mm
Non-Shrink Grout	L-Shape 1	b_1=100 mm, t_1=25 mm, h_1=150mm
	L-Shape 2	b_2=100 mm, t_2=25 mm, h_2=150mm
UHPFRC 2% Jacket	L-Shape 1	b_1=100 mm, t_1=25 mm, h_1=150mm
	L-Shape 2	b_2=100 mm, t_2=25 mm, h_2=150mm
Curved Key	Curved	L=80 mm, t=25 mm, w=[15-40] mm
Embedded rebar (10M)	Linear	L= 75 mm, R= 5.65 mm
Transfer Plate	Rectangular	a=75 mm, b=150 mm, t=12.5 mm
NSC Column Core	Rectangular	a=75 mm, b=150 mm, h=150 mm
Non-Shrink Grout	C-Shape	b_1=b_2=100 mm, w_1=150 mm, h_1=150mm
UHPFRC 2% Jacket	C-Shape	b_1=b_2=125 mm, w_1=200 mm, h_1=150mm
UHPFRC 3% Connection	Rectangular	a=80 mm, t=25 mm, h=150 mm
Embedded rebars (10M)	Linear	L= 155 mm, R= 5.65 mm
Transfer Plate	Rectangular	a=75 mm, b=75 mm, t=12.5 mm
NSC Column Core	Rectangular	a=75 mm, b=75 mm, h=150 mm
UHPFRC 2%	C-Shape	b_1=100 mm, w_1=75 mm, h_1=150mm

Table 6.1 shows the main dimensions of each 3-D Model in ATENA GiD ®. For the curved key model and the cast-in place model, the transfer loading plate has a rectangular cross-section of 75 mm by 75 mm with a thickness of 12.5 mm. The lap splice model also has a rectangular cross-section but with different dimensions since this model is not symmetrical in the *y* plane. The dimensions are 75 mm by 150 mm with a 12.5 mm thickness. Each model was drawn by defining rectangular surfaces that were then extruded to obtain the proper height of the specimen. Since each surface was a rectangle, their sides are defined in Table 6.1 as *a* and *b*. The subindex assigned to each *a* and *b* corresponds to the specific surface for each model. The same criteria applies for the thickness *t* and/or the width *w* of the surface defined. For the embedded rebars for the lap splice model, L is the length of the 10M rebar and R represents the radius.

6.2 Material Properties for 3-D Column Models

Even though three different 3-D column models were created, they use the same material properties when needed. Various parameters were considered in this finite element analysis, among them the most important being the thickness of the UHPFRC precast jacket, cross-sectional area of the NSC column core, the thickness of the non-shrink grout, and the mechanical properties of the lap-spliced bars. All models drawing sequence started by defining a unique coordinate system for a set of points sharing the z axis, these set to z=0. This was done intentionally, to later extrude the desired surfaces into volumes with a specific height and/or thickness. By leveraging the advantage of symmetry, specific boundary conditions had to be assigned to the models. The nodes that lie on surfaces had to be fixed in the (*x*,*z*) axes at the lateral face of the model in contact with the loading plate region. The other surface nodes of the back face of the model that share the loading plate region where restricted from movement in the (*y*,*z*) axes. Each layer of the materials (i.e. NSC columns core, steel loading plate, non-shrink grout, UHPFRC 2%, UHPFRC 3% and/or UHPFRC 3% curved key) had the specific thickness that corresponded to the actual test arrangements and were endowed with surfaces. To account for the interaction between the contacting surfaces at the boundaries of different material layers, the corresponding surfaces had to be connected using the fixed contact for surface *Master-Slave* condition. In between the transfer steel plates and the concrete column, the transfer plates were the *master* and column was the *slave*. For all the remaining surfaces, going in the out-of-plane direction, the *Master-Slave* condition was always applied from the inside to the outside of the member. For example, in the Cast-in Place model, the surfaces of the concrete column were the *master*, and the surfaces of the UHPFRC

Jacket were the *slave*. When two surfaces are in contact with the bigger mesh should be the *master* surface; in other applications the *master* surface is the surface whose displacements are controlled externally (for example in the case of the loading plate that is in contact with the concrete column, the *master* is the steel plate, the *slave* is the concrete column, whereas the contact occurs only in the z-axis). Therefore, this option had to be assigned before meshing the model. The cast-in place model showed in Figure 6.1 (c) was the only model that did not use the non-shrink material properties; consequently, it only consists of three materials (i.e. steel, concrete and UHPFRC). The connection method showed for the models in Figure 6.1. (a) & (b) was always defined prior to defining the surrounding UHPFRC jacket, which was allocated always as the final modeling step. It is also noted that nodes in the surface with z=0, are only restrained against displacement in the z-axis, only if they belong to the encased column; jacket nodes are not restrained in the z-direction in that level.

The NSC column core and the non-shrink grout were assigned a material option named *SOLIDConcrete,* by using the predefined prototype “CC3DNonLinCementitious2”. The UHPFRC material was modelled by using a similar predefined prototype named “CC3DNonLinCementitious2SHCC”. The properties were modified for each material to represent the individual mixes used in the experimental program. The mechanical properties of the NSC, UHPFRC 2%, UHPFRC 3% and non-shrink grout, were described in Section 4.3 and Section 5.6. These material properties were assigned to the extruded volumes individually. The reinforcement used for the embedded 10M rebar in the UHPFRC 3% curved key and of the lap splice connection were modelled with the material model “1D Reinforcement”, applied for the rebars drawn as line elements. These rebars were totally embedded in both the UHPFRC Jacket and in the UHPFRC Connection Region. The steel loading plates were assigned the material named Steel VonMises3D by using the material prototype “CC3DBilinearSteelVonMises” available in the *SOLIDSteel* menu. A displacement step was applied on the steel loading plates top surface with the option Displacement for Surface–in the global coordinate system with a value of -0.5 mm. Reaction monitor points were placed at the steel loading plate surface in order to record the load acting on the model, and several displacement monitors points were placed on the models. The objective of the 3D models was to capture outwards deflections happening on the UHPFRC jackets when the NSC core was under axial loading. The mesh was discretized at 10 mm elements. This size was recommended by the GiD interface matched for optimum value in accuracy and computational load. Meshing of the reinforcement elements was performed automatically by the program. An overview of the mesh is shown in Figure 6.1 (a), (b) and (c).

Table 6.2. Main mechanical properties used for the *SOLIDConcrete* materials for models.

Property	Value	Unit
CC3DNonLinCementitious2 for NSC		
Young Modulus	29020	MPa
Poisson's Ratio	0.2	
Tensile Cracking Strength	3.869	MPa
Compression Strength	41.6	MPa
Material Density (default)	2350	kg/m^3
CC3DNonLinCementitious2 for Non-Shrink Grout		
Young Modulus	29020	MPa
Poisson's Ratio	0.2	
Tensile Cracking Strength	2.3	MPa
Compression Strength	87.33	MPa
Material Density (default)	2350	kg/m^3
CC3DNonLinCementitious2SHCC		
Young Modulus	46950	MPa
Poisson's Ratio	0.21	
Tensile Cracking Strength	7.37	MPa
Compression Strength	174	MPa
Fiber Volume Fraction UHPFRC Jacket	2	%
Fiber Volume Fraction Curved Key and Lap Splice Connection	3	%
Fiber Modulus	200	GPa
Fiber Diameter	0.2	mm
Fiber Shear Modulus	75	GPa
Material Density (default)	2300	kg/m^3

6.3 Results from the 3D Column Models

All the models were analyzed using the ATENA Studio post-processor by using static analysis under displacement control, using Newton-Raphson stepping algorithm, by using an interval multiplier of 15 over a total of 50 load steps. The main results for the load and deflections from the monitor points were taken from the software. The first step was to organize the extracted data as texts files (i.e. having *.txt* extension) to then be plotted in a spreadsheet. The data was taken by organizing the monitor points for displacements as follows:

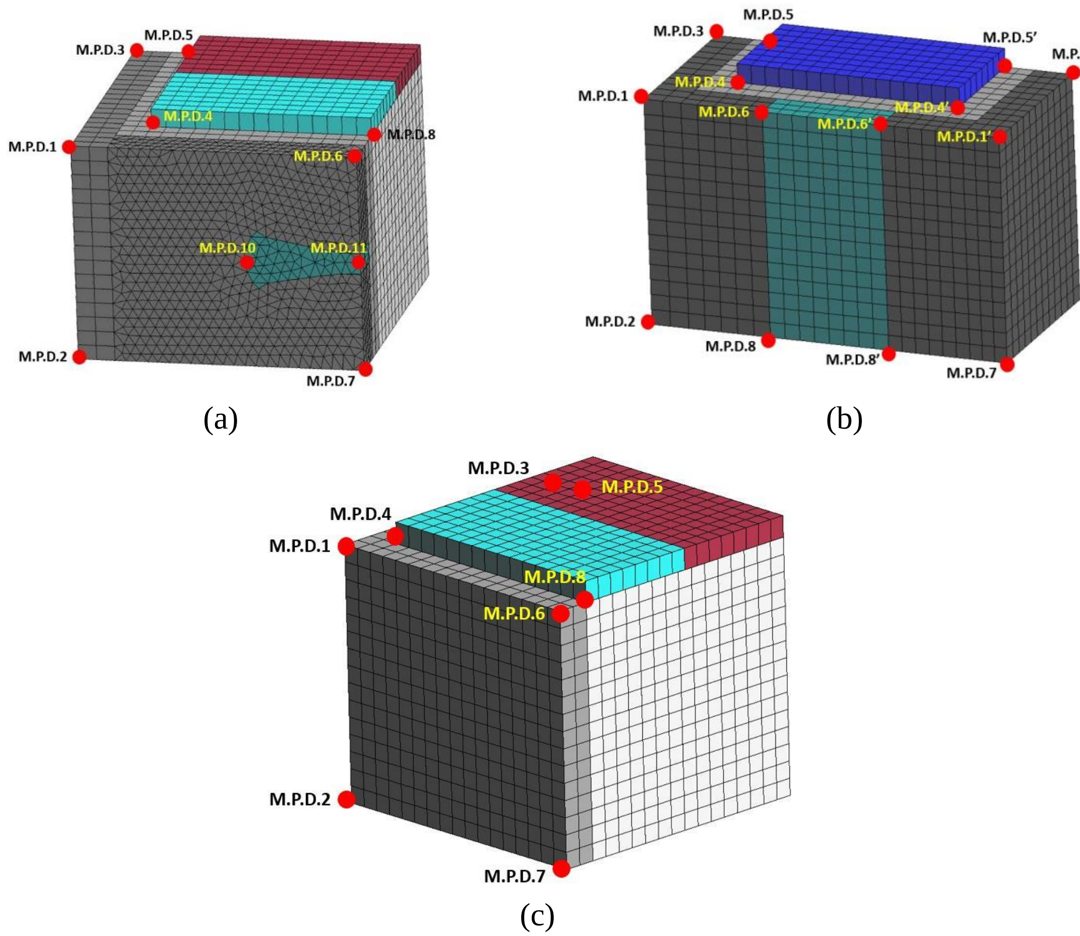

Figure 6.2. Location of monitor points on the 3-D models to capture displacements for (a) the precast UHPFRC curved key, (b) the lap splice connection and (c) cast-in place alternative.

Table 6.3. Monitor points used for recording displacements data.

Location	Direction
Curved Key 3D Model	
UHPFRC Top Corner	x, y, z
UHPFRC Bottom Corner	x, y
UHPFRC Mid Top	x, y, z
Column Core Top 1	z
Column Core Mid Top 1	z
UHPFRC Mid Length Top	x, y, z
UHPFRC Mid Length Bottom	x, y
Column Core Mid Top 2	z
Curved Key Head	x, y, z
Curved Key Neck	x, y, z
Lap Splice 3D Model	
UHPFRC Top Corner	x, y, z
UHPFRC Bottom Corner	x, y
UHPFRC Mid Top	x, y, z
Column Core Top 1	z
Column Core Top 2	z
Column Core Mid Top 1	z
Column Core Mid Top 2	z
UHPFRC Connection Top 1	x, y, z
UHPFRC Connection Top 2	x, y, z
UHPFRC Mid Length Bottom	x, y
UHPFRC Connection Bottom 1	x, y, z
UHPFRC Connection Bottom 2	x, y, z
Cast-in Place 3D Model	
UHPFRC Top Corner	x, y, z
UHPFRC Bottom Corner	x, y
UHPFRC Mid Top	x, y, z
Column Core Top 1	z
Column Core Mid Top 1	z
UHPFRC Mid Length Top	x, y, z
UHPFRC Mid Length Bottom	x, y
Column Core Top 2	z
***Note**: M.P.D.3* & M.P.D.5* correspond to nodes for UHPFRC and column; the steel loading plates mesh is covering those nodes in Figure 6.2.*	

6.4. Cast-in Place Results

The Cast-in Place results are summarized in Table 6.4 below, showing the stresses in the out-of-plane direction. A comparison is done when the UHPFRC Jackets are fixed and not fixed in the Z direction, by using the same Master/Slave condition described in Section 6.2 above. When the UHPFRC Jacket is not fixed in the Z direction, the stresses in the out-of-place direction stay within the range of [0.05 – 0.67] MPa. This model was developed for proper validation of the results for the finite element model. On the other hand, when the UHPFRC Jacket is fixed in the Z direction, the stresses on the face of the model are in the range of [4.90 – 6.41] MPa. This provides a good estimate of the lateral stress on the UHPFRC Jacket since the maximum tensile capacity was set to a value of 7.37 MPa.

Table 6.4. Stresses in the YY direction of the Cast-in Place Model.

Z (mm)	Cast-in Place Jacket not fixed in Z	Cast-in Place Jacket fixed in Z
Axes & Scales	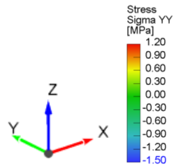	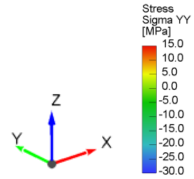
0	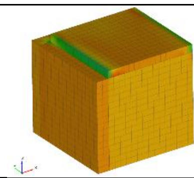	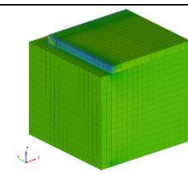
0.25	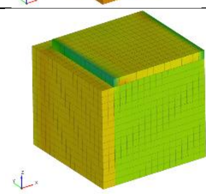	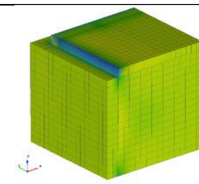
0.50	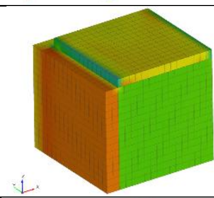	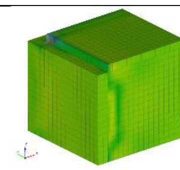
0.75	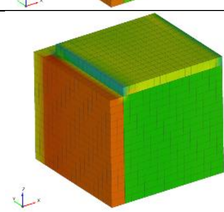	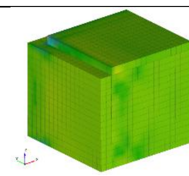
1.00	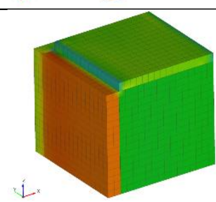	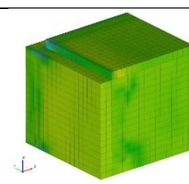
1.25	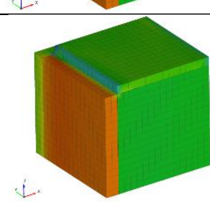	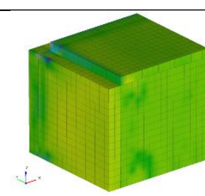
1.50	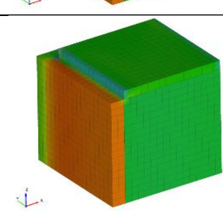	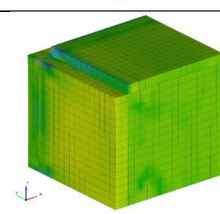

Chapter 7: Summary and Conclusions

This thesis explored the design, installation and behavior of Ultra-High-Performance Fiber Reinforced Concrete (UHPFRC) Jackets for retrofitting of concrete columns. These jackets were highly ductile and can withstand significant deformations under tension. The study comprised an analytical and an experimental component. In the analytical part of the investigation a database of the published experiments conducted on columns retrofitted by thin UHPFRC jackets and tested under lateral load reversals to simulate earthquake effects was assembled. The database was used to explore the mechanics of the jacketing retrofits and their effects on the lateral load resistance of columns. A simple confinement model was defined whereby the strength and deformation increase of encased concrete were linked to the confining pressure and confinement effectiveness provided by the jackets. It was observed that contrary to conventional confining devices – such as FRPs, the thin UHPFRC jackets possess flexural stiffness against lateral dilation of the core which further enhances the deformation capacity of the encased material. Through analysis of jacketed cross sections to combined flexure and axial load, an expression was derived for the flexural strength increase provided by the jacket. It was found that the strength increase is mild, owing primarliy to the increase in the lever arm of the compression resultant as the UHPFRC jacket participates in sectional equilibrium. The methodology for calculation of the column strength enhancement due to retrofit with UHPFRC jacketing includes also expressions for the shear strength increase and the enhancement of the longitudinal reinforcements' lap-splice strain development capacity above the footing. Considering the mechanical response of the jacketing materials the study formulates performance limits for seismic design of this type of retrofits.

The experimental part of the thesis focusses into the development of a new type of precast UHPFRC jackets that would be installed rather than being cast on site in field applications. It also characterized the mechanical properties of the UHPFRC mix used, the bond between the normal strength concrete (NSC) column core and the UHPFRC matrix, the effectiveness of the rectangular precast jacket in providing confinement, and the impact of various design variables (i.e. jacket thickness and volumetric fiber content). The research aimed to assess the performance of precast UHPFRC jackets in retrofitting conventional concrete columns. Experimental investigations included mainly small-scale tests on UHPFRC conventional concrete cores under monotonic and cyclic axial loading, and direct tension tests on UHPFRC specimens and precast jacket assemblies. The study verified the effectiveness of UHPFRC jackets as a retrofitting technique, quantifying the tensile strength of UHPFRC reinforced with 2% steel fibers, and illustrated the contribution of the UHPFRC jacket to the deformation capacity of the encased concrete columns. The research also characterized the tensile behavior of the UHPFRC material using the AASHTO guidelines for specimen size and testing, which is crucial for retrofitting applications. The steel fibers distributed (2% and 3% by volume) in the UHPFRC matrix enabled the development of large deformation capacity. A finite element model was used as a starting point to obtain the proper shape of connector device before initializing the experimental program, but also to analyze the confining effectiveness of UHPFRC jackets.

7.1 Mechanical Properties

7.1.1 Cylinder Compression Strength Tests

The cylinder specimens tested to obtain compressive strength of the UHPFRC mix provided results greater than 120 MPa when using 2% volume fraction steel fibers. In the ascending branch of the stress-strain curve for the compression tests, when first cracking was visible on the specimens, the compression strength kept increasing due to the bridging effect of the steel fibers. For UHPC mixes having no fibers, the compression strength would achieve lower values due to the fact that there are no fibers retaining cracking expansion. In addition, in the descending branch peak load the cylinders held their integrity due to the bridging effect provided by the fibers. Moreover, compressive strength increased from 158 MPa to 174 MPa tested after 28-day and 270-day curing periods, respectively. The fiber distribution and orientation were successfully achieved when pouring and testing the cylindrical specimens. The CEK2 batch had a flowability of 230 mm for UHPFRC mixes with 2% and 3% fiber content, that for cylinder preparation provided no issues.

7.1.2 Direct Tension Testing for CEK2

A unique, challenging and effective procedure was performed to obtain the uniaxial tensile strength of the UHPFRC mix used in this research, denominated CEK2. The setup conditions, specimen dimensions assisted in acquiring cracking patterns captured inside the gauge length. Tensile strength attained was 7.37 MPa, whereas the material demonstrated a strong tension hardening behavior. The one-way casting method helped with fiber distribution and orientation. However, further research is required to study and determine the proper fiber orientation occurring inside the specimen since this is one of the crucial factors in UHPFRC results.

7.1.3 Direct Tension Testing for Connection Devices

The proper shape of the key started with finite element analysis for three different geometries, and the shape that showed better results was the denominated *dogbone* shape. This geometry was optimized until a precast UHPFRC 3% roundhead curved key with a 10M embedded rebar was developed and selected as the key device between precast UHPFRC Jackets. This connection method once assembled on precast UHPFRC shells simulating the jacket provided satisfactory results. The curved key had the capacity to transfer the tensile stress from direct tension testing to the precast UHPFRC shell without cracking. The curved key specimen had an average peak tensile strength of 3.80 MPa with an average peak strain of 0.001 mm/mm, owing to failure in the epoxy used as the bonding agent. The cracking path followed the perimeter of the key until the roundhead of the precast UHPFRC shell. At this region the stresses were successfully transferred to the precast shell.

The other mechanism of connection successfully tested was the lap splice connection, which again had the capacity of transferring the stresses from direct tension testing to the precast UHPFRC shell. This mechanism provided better results than the precast UHPFRC curved key. The failure mode for this connection was focused at the cold joint between the precast shell and the UHPFRC 3% zone, then cracking the precast shells. These specimens reached an average peak tensile strength of 6.88 MPa with an average peak strain of 0.0057 mm/mm, illustrating that the lap splice connection had the capacity of resisting higher levels of damage. The fiber distribution for all six specimens may be improved by furthering studying and enhancing the flowability of this particular UHPFRC mix by modifying the admixtures given by the provider. It was noticed that the flowability of the mix was increasing for higher mixing volumes. In addition, by adding steel fibers the flowability also increased. The reason for this behavior could be related to the geometry of the steel fibers, since they might act as blades opening a path along the UHPFCR matrix. Even though the flowability was good enough to allow self-consolidation, the issue was that the fibers tended to group and to segregate due to their self-weight – it is believed that better results could be obtained with a relatively smaller flowability.

7.1.4 Flexural Testing for Precast C-Shapes

Three precast C-Shapes made with UHPFRC 2% steel volume fraction were tested to capture their flexural capacity. This test was performed with a compression setup by generating two-point outwards bending of the C-Shape. The average peak flexural strength of the C-Shapes was 1.79

MPa with an average outward bending peak strain of 0.01 mm/mm. The C-Shapes cracked within the gauge length and due to their rectangular shape, the cracking happened at their mid height and not at the inside 90° angle. These specimens were cast along with the characterization batch, with had a total volume of 101 L. They were poured using the one-way casting method, by casting from the top, allowing the mix to flow equally to both sides. Even though the C-Shapes behaved as expected, the flowability and fiber distribution could be an issue because these specimens were the last to be prepared from the 101 L batch. Once the UHPFRC 2% was taken out from the mixing pan into individual buckets, the steel fibers were segregating. After these tests were performed, once conclusion that helped the next step in the experimental program was to prepare UHPFRC 2% batches with the premix material and admixtures in no larger than 10 L batches to avoind increased flowability which was observed when scaling up the batch volume. Further studies should be made on the proportions of this UHPFRC mix design for different mixing volumes to prevent steel fibers from segregation.

7.2 Database of UHPFRC Jackets & Modelling of the Jacket Contribution

In this research, evidence of reinforced concrete columns retrofitted with UHPFRC jackets was critically reviewed and further used to establish design provisions, performance limit states and safety factors. Subsequently, simple expressions for the confining pressure, enhanced strength and deformation capacity of the encased concrete were derived. Finally, a performance based framework of design provisions for bridge pier retrofitting with UHPC jackets was proposed. The proposed framework included performance limit states and safety factors, the model for the encased concrete core, and mechanistic models for the enhancement of flexural and shear strength imparted by the UHPFRC jacket. It was found that in large size cross sections such as those encountered in the field of bridge engineering, the confining pressures exerted by UHPFRC jackets with usual thickness of about 1/10 of the section size have negligible contribution to the compressive strength of the encased core. However, the confinement effect significantly enhances the members' deformation capacity, and it also contributes to the mitigation of premature failures owing to poor detailing (such as insufficient lap splice lengths of longitudinal reinforcement at the base of the pier, and inadequate transverse reinforcement for shear strength). Where direct bearing of the jacket shell on the footing was eliminated by the creation of a discontinuity gap, the flexural strength increase was negligible over the original cross section; but the confining pressures are sufficient to enable lap-splices to enable a significant increase in the bar's inelastic strain development capacity. The gap provides the benefit of distributed strain in the tension reinforcement in the critical section. Flexural strength increase was in the range of 30% - 35% for jackets where direct bearing of the jacket on the footing was possible (in cases of cold joint or extension of the jacket into the footing). Apart from the contributions mentioned in the preceding, this retrofit arrangement should be combined with bond breakers or a comprehensive control of the lateral drift ratio in order to avoid strain localization in the bars and a second order compressive strain increase due to kinematic interaction between pullout slip on the tension side and the increase in jacket compressive strain. Simple expressions for the confining pressure and strength enhancement were derived whereas the experimental data regarding the deformation capacity of the encased member was organized through correlation with an effective jacket index that accounts for the critical parameters that control the sensitivities of lateral drift capacity (aspect ratio, axial load ratio, transverse, and longitudinal reinforcement ratios). Overall, UHPFRC represented an effective form in jacketing applications, as it eliminates brittle failures, enhances deformation capacity, and increases mildly the strength and stiffness without increasing the amount of longitudinal reinforcement; owing to this mild influence in stiffness and strength, this form of jacketing may be considered a local intervention with little effect on global lateral strength and stiffness.

7.3 Precast UHPFRC Jackets for Retrofitting Concrete Columns

A practical approach for the design, installation and testing of precast UHPFRC jackets for retrofitting NSC column cores was presented in this research. By using 3D printed inserts, non-shrink grout, structural epoxy adhesive paste, plastic bubble wrap and other details, the precast UHPFRC jackets were successfully assembled on the NSC specimens to then be tested under monotonic and cyclic axial loading. The final retrofitted NSC specimens showed moderate increments in compressive strength and significant enhancements of axial strain capacity in compression. The contributions in terms of strength and ductility were similar for the three arrangements and for both jacket thicknesses, 25 mm and 37.5 mm respectively. For both monotonic and cyclic loading, it was observed that the overall increment in the compressive strength for the final retrofitted columns was no higher than 12%. Moreover, the deformation capacity of the final retrofitted columns showed an average increase by more than 400 %. Despite the small contribution in compressive strength, the precast UHPFRC jackets enhanced enormously the deformation capacity of the NSC column core. Therefore, the research developed showed that significant improvements can be achieved by applying precast UHPFRC jackets for retrofitting concrete columns. This retrofit alternative can become relevant for seismic performance and rehabilitation projects, as well as new structures without compromising the original cross-sectional area of the column.

7.4 Finite Element Models

Non-linear finite element analysis was performed using the ATENA-GiD software. The GiD interface has a predefined model for UHPFRC materials, which was utilized with user-defined constitutive stress-strain laws in compression and tension. However, it does not consider any fiber orientation nor fiber distribution along its matrix – the effects of these properties need be specified by the user in properly defining the material input variables. Reinforcement was modeled with a simple geometry as a 1-D rebar model while the UHPFRC components were 3D extruded volume models. The Cast-in Place provided reasonable results, while the other models stil need further study. The lateral stresses on the UHPFRC Jackets when fixed in the Z direction, are in the range of [4.90 – 6.41] MPa, since the maximum tensile capacity was set to a value of 7.37 MPa.

7.5 Recommendations and Future Work

The research developed involved a series of challenges at both experimental and analytical stages. Some recommendations for future work in this matter are listed below.

- The Retrofitted Columns with Precast UHPFRC Jackets in this research consisted of rectangular cross sections only. A similar approach can be performed to design and install circular precast elements on circular concrete specimens (reinforced and/or unreinforced) to study all the above variables mentioned. Some important differences may be captured due to the change in the stiffness from a rectangular element when compared to a circular element. Moreover, this research may be extended to test full scale specimens.
- This research focused on one type of retrofit in the form of jacketing, which was explained in Chapter 3. Parameters for jacket thickness, volumetric fiber content and original column cross sections need to be studied further, with an emphasis on flowability of the UHPFRC material in the fresh state and the effect it may have in the actual response.
- The most challenging stage was developing direct tension testing for the prismatic specimens with adequate results. There is a need for provisions for standardizing the test method with the relevant Canadian standard, Annex U of CSA A23.1 or Annex 8.1 of CSA

S6. AASHTO standard for the tensile behavior of UHPC (AASHTO T 397, 2022) may be used as a reference for this matter.

- Further experimental and analytical research is needed to fully understand and improve the bond occurring in the interface of precast UHPFRC Jackets with the NSC column core. For this research, the material selected was a commercial non-shrink grout where the internal surfaces were roughened by using plastic bubble wrap when preparing the precast jackets, which was removed after demolding. For instance, different bubble wrap sizes can be used or different materials may be used to fill the gap between column and jacket, such as expansive cementitious material, conventional concrete, self-consolidating concrete, UHPFRC, among others.
- The high-resolution images taken for Digital Image Correlation were not analyzed for the Final Retrofitted Columns. They could be further studied to compare the deflections from the captured images against the real deflections obtained from the experimental phase. This involves both monotonic and cyclic loading tests. It’s also recommended to either relocate the displacement-controlled compression machine in a wider area or to use at least two high-resolution cameras for capturing opposite surfaces of the Retrofitted Columns Specimens.
- Experimental stress-strain behavior for new and novel UHPFRC materials is continuously growing as this material is gaining popularity in structural and architectural applications. Databases should still be assembled to collect information regarding tensile behaviors, strain capacities, ductility measurements and flexural responses.
- Further studies need to be performed to obtain the stress-strain response of UHPFRC, especially its post-peak behavior. A series of cylinders were tested by attaching strain gages. However, the mode of failure that comes naturally when testing UHPFRC materials causes a sudden change in the load reading that the displacement-controlled compression machine was not capable of recording. This may be due to insufficient stiffness in the test setup.
- Finite element modelling for UHPFRC materials including fiber distribution and flowability of the UHPFRC matrix is an encouraging tool to provide insights regarding the intricate details of the confining interaction between the jacket and the encased core. The absence of transverse fibers and the method of casting may influence the results regardless

of the main parameters of the jacket, such as thickness and mechanical properties. Additionally, it is recommended to investigate the effect of combined bending and axial load to obtain the UHPFRC Jacket performance on a finite element modelling.

References

AASHTO T 397-22 (2022). Standard Method of Test for Uniaxial Tensile Response of Ultra-High Performance Concrete. American Association of State Highway and Transportation Officials.

ACI 222R-19. (2019). Guide to Protection of Reinforcing Steel in Concrete Against Corrosion. American Concrete Institute (ACI) Committee 222, 1–65.

ACI 544.8R-16. (2016). Report on Indirect Method to Obtain Stress-Strain Response of Fiber-Reinforced Concrete (FRC). American Concrete Institute (ACI) Committee 544.

AFGC-SETRA. (2002). (Association Francaise de Genie Civil-Service d'etudes Techniques des Routes et Autoroutes) Ultra-High-Performance Fibre-Reinforced Concretes, Recommendations provisoires-interim recommendations.

AFNOR NF EN 13670/CN. (2013). Exécution des Structures en Béton-Complément National à la Norme NF EN 1367.

AFNOR NF P18-470. (2016). French Standard: Concrete — Ultra-high performance fibre-reinforced concrete — Specifications, performance, production and conformity.

AFNOR NF P18-710. (2016). French Standard: National addition to Eurocode 2 — Design of concrete structures: specific rules for Ultra-High Performance Fibre-Reinforced Concrete (UHPFRC).

Ahmad, S., Rasul, M., Adekunle, S. K., Al-Dulaijan, S. U., Maslehuddin, M., & Ali, S. I. (2019). Mechanical properties of steel fiber-reinforced UHPC mixtures exposed to elevated temperature: Effects of exposure duration and fiber content. Composites Part B: Engineering, 168, 291–301. https://doi.org/10.1016/J.COMPOSITESB.2018.12.083

Amran, M., Huang, S. S., Onaizi, A. M., Makul, N., Abdelgader, H. S., & Ozbakkaloglu, T. (2022). Recent trends in ultra-high performance concrete (UHPC): Current status, challenges, and future prospects. In Construction and Building Materials (Vol. 352). Elsevier Ltd. https://doi.org/10.1016/j.conbuildmat.2022.129029

Ángel López Martínez Director, J., Serna Ros, P., & Navarro-Gregori, J. (2017). Characterisation of the tensile behaviour of uhpfrc by means of four-point bending tests.

ASTM C1609/C1609M-19. (2019). Standard Test Method for Flexural Performance of Fiber-Reinforced Concrete (Using Beam With Third-Point Loading). American Society for Testing and Materials.

ASTM C1856/C1856M-17. (2017). Fabricating and Testing Specimens of Ultra-High-Performance Concrete. American Society for Testing and Materials.

ASTM C469/C469M-14. (2014). Standard Test Method for Static Modulus of Elasticity and Poisson's Ratio of Concrete in Compression. ASTM International, West Conshohocken, PA. https://doi.org/https://doi.org/10.1520/C0469_C0469M-14

ATENA Program Documentation, (2021). Part 1: Theory; by Červenka, V., Jendele, L., & Červenka, J. Prague, Czech Republic, 1–360.

ATENA Program Documentation, (2010). Part 3-1: Example Manual, ATENA Engineering; by Kabele, P., Červenka, V., & Červenka, J. Prague, Czech Republic, 1–90.

ATENA Program Documentation, (2021). Part 8: User's Manual for ATENA-GiD interface; by Červenka, V., Červenka, J., Janda, Z. & Pryl, D. Prague, Czech Republic, 1–153.

ATENA Program Documentation, (2020). Part 11: Troubleshooting Manual; by Pryl, D. & Červenka, J. Prague, Czech Republic, 1–69.

ATENA Program Documentation, (2021). Part 12: User's Manual for ATENA Studio; by Beneš, S., Mikolášková, J. & Altman, T. Prague, Czech Republic, 1–83.

Azmee, N. M., & Shafiq, N. (2018). Ultra-high performance concrete: From fundamental to applications. Case Studies in Construction Materials, 9. https://doi.org/10.1016/j.cscm.2018.e00197

Billah, A. H. M. M., Alam, M. S., & Bhuiyan, M. A. R. (2013). Fragility Analysis of Retrofitted Multicolumn Bridge Bent Subjected to Near-Fault and Far-Field Ground Motion. Journal of Bridge Engineering, 18(10), 992–1004. https://doi.org/10.1061/(ASCE)BE.1943-5592.0000452

Blais, P. Y., & Couture, M. (1999). Precast, prestressed pedestrian bridge - world's first Reactive Powder Concrete structure. *PCI Journal*, *44*(5), 60–71. https://doi.org/10.15554/pcij.09011999.60.71

Blais, P. Y., Senior, P. E., Le Groupe, P., Sherbrooke, T., Canada, Q., Couture, M., Operations Manager, P. E., Bolduc, B., & Beauce, Ste.-M. (n.d.). Precast, Prestressed Pedestrian Bridge World's First Reactive Powder Concrete Structure.

Červenka Consulting. (2007). ATENA Program. *https://www.cervenka.cz/products/atena/* Prague, Czech Republic.

CSA A23.1:19, Annex U. (2019). 'Ultra-High-Performance Concrete, Annex-U'. Canadian Standards Association.

CSA S6:19, Annex 8.1. (2019). Standard: Canadian Highway Bridge Design Code. In Canadian Standards Association.

Dagenais, M.-A., Massicotte, B., & Boucher-Proulx, G. (2018). Seismic Retrofitting of Rectangular Bridge Piers with Deficient Lap Splices Using Ultrahigh-Performance Fiber-Reinforced Concrete. Journal of Bridge Engineering, 23(2), 04017129. https://doi.org/10.1061/(ASCE)BE.1943-5592.0001173

Del Zoppo, M., Menna, C., Di Ludovico, M., Asprone, D., & Prota, A. (2021). Opportunities of light jacketing with Fibre Reinforced Cementitious Composites for seismic retrofitting of existing RC columns. Composite Structures, 263. https://doi.org/10.1016/j.compstruct.2021.113717

Deng, M., Zhang, Y., & Li, Q. (2018). Shear strengthening of RC short columns with ECC jacket: Cyclic behavior tests. Engineering Structures, 160, 535–545. https://doi.org/10.1016/j.engstruct.2018.01.061

El-Joukhadar, N., Dameh, F., & Pantazopoulou, S. (2023). Seismic Modelling of Corroded Reinforced Concrete Columns. Engineering Structures, 275. https://doi.org/10.1016/j.engstruct.2022.115251

El-Joukhadar, N., & Pantazopoulou, S. J. (2021). Effectiveness of UHPFRC cover in delaying bar corrosion. Construction and Building Materials, 269. https://doi.org/10.1016/j.conbuildmat.2020.121288

Farzad, M., Asce, S. M., Shafieifar, M., & Azizinamini, A. (2019). Retrofitting of Bridge Columns Using UHPC. https://doi.org/10.1061/(ASCE)BE.1943

Flexural. (n.d.). 2/2 Sikadur®-31 Hi-Mod Gel CA CSC Master Format TM 03 64 23 EPOXY INJECTION GROUTING. www.sika.ca

Graybeal, B. A. (2005). Characterization Of The Behavior Of Ultra-High Performance Concrete. PhD Dissertation, Univ. of Maryland, College Park.

Graybeal, B. A. (2006). Material Property Characterization of Ultra-High Performance Concrete. FHWA-HRT-06-103, U.S. Department of TransportationU.S. Department of Transportation, August.

Graybeal, B. A., & Baby, F. (2013). Development of direct tension test method for ultra-high-performance fiber-reinforced concrete. ACI Materials Journal, 110(2), 177–186. https://doi.org/10.14359/51685532

Graybeal, B. A., & Baby, F. (2019). Tension Testing of Ultra-High Performance Concrete FWHA-HRT-17-053. FHWA, U.S. Department of Transportation United States. Federal Highway Administration. Office of Infrastructure Research and Development., (No. FHWA-(February), 210.

Graybeal, B., & Hartmann, J. l. (2003). Strength and Durability of Ultra-High Performance Concrete Materials and Structures. 2003 Concrete Bridge Conference, December, 1–20.

Guan, D., Chen, Z., Liu, J., Lin, Z., & Guo, Z. (2021). Seismic performance of precast concrete columns with prefabricated UHPC jackets in plastic hinge zone. Engineering Structures, 245. https://doi.org/10.1016/j.engstruct.2021.112776

Guan, D., Xu, R., Yang, S., Chen, Z., & Guo, Z. (2022). Development and seismic behavior of a novel UHPC-shell strengthened prefabricated concrete column. Journal of Building Engineering, 46. https://doi.org/10.1016/j.jobe.2021.103672

Habib El-Joukhadar, N., Nicolas, ©, & El-Joukhadar, H. (2022). Seismic Assessment, Repair and Retrofit of Existing Corroded Structures Using UHPC Jacketing.

Hung, C. C., Kuo, C. W., & Shao, Y. (2021). Cast-in-place and prefabricated UHPC jackets for retrofitting shear-deficient RC columns with different axial load levels. Journal of Building Engineering, 44. https://doi.org/10.1016/j.jobe.2021.103305

Hung, C. C., Lin, C. C., & Do, T. D. D. (2024a). Seismic rehabilitation of RC frames with innovative precast U-shaped UHPC jackets: Experimental evaluation and computational simulation. Engineering Structures, 318. https://doi.org/10.1016/j.engstruct.2024.118746

Hung, C. C., Lin, C. C., & Do, T. D. D. (2024b). Seismic rehabilitation of RC frames with innovative precast U-shaped UHPC jackets: Experimental evaluation and computational simulation. Engineering Structures, 318. https://doi.org/10.1016/j.engstruct.2024.118746

Husain, S. A. B. (2021). Characterization of UHPFRC Materials for Bridge Construction: An Opportunity to Eliminate the Need for Prestressing in Bridges.

Kennedy-Kuiper, R. C. S., Wakjira, T. G., & Alam, M. S. (2022). Repair and Retrofit of RC Bridge Piers with Steel-Reinforced Grout Jackets: An Experimental Investigation. Journal of Bridge Engineering, 27(8). https://doi.org/10.1061/(ASCE)BE.1943-5592.0001903

Lavorato, D., Azeredo, J., Bergami, A. V., Salvador Filho, J. A. A., Nuti, C., Santini, S., & Briseghella, B. (2019). RC column repaired with hpfrcc and confined with cfrp: numerical analyses to evaluate the column section capacity. Lecture Notes in Civil Engineering, 9, 17–29. https://doi.org/10.1007/978-981-10-8016-6_2

Li, X., Chen, K., Hu, P., He, W., Xiao, L., & Zhang, R. (2020). Effect of ECC jackets for enhancing the lateral cyclic behavior of RC bridge columns. Engineering Structures, 219. https://doi.org/10.1016/j.engstruct.2020.110714

Li, X., Wang, J., Bao, Y., & Chen, G. (2017). Cyclic behavior of damaged reinforced concrete columns repaired with high-performance fiber-reinforced cementitious composite. Engineering Structures, 136, 26–35. https://doi.org/10.1016/j.engstruct.2017.01.015

Mohammed, I. (2023). Stress-Strain Models for UHPFRC and Application in Seismic Design and Retrofit of Bridges.

Mohammed, I., Tsiotsias, K., & Pantazopoulou, S. J. (n.d.-b). Design of Bridge Pier Seismic Retrofit Using THFRC.

Naaman, A. E., & Reinhardt, H. W. (2006). Proposed classification of HPFRC composites based on their tensile response. Materials and Structures/Materiaux et Constructions, 39(5), 547–555. https://doi.org/10.1617/s11527-006-9103-2

Naeimi, N., & Moustafa, M. A. (2021). Analytical Stress–Strain model for steel spirals-confined UHPC. Composites Part C: Open Access, 5. https://doi.org/10.1016/j.jcomc.2021.100130

Priestley, M. J. N., Seible, F., & Calvi, G. M. (1996). Seismic Design and Retrofit of Bridges. Seismic Design and Retrofit of Bridges. https://doi.org/10.1002/9780470172858

Priestley, M. J. N., Seible, F., Xiao, Y., & Verma, R. (1994). Steel Jacket Retrofitting of Reinforced Concrete Bridge Columns for Enhanced Shear Strength-Part 1: Theoretical Considerations and Test Design. Aci Structural Journal, 91(4), 394–405. https://doi.org/10.14359/9885

Priestley, M. J. N., Verma, R., & Xiao, Y. (1994). Seismic Shear Strength of Reinforced Concrete Columns. Journal of Structural Engineering-Asce, 120(8), 2310–2329. https://doi.org/10.1061/(ASCE)0733-9445(1994)120:8(2310)

Ralli, Z. G., Salazar Gonzalez, R., & Pantazopoulou, S. J. (2024). Effectiveness of UHPC Jackets in Pier Retrofitting for Lateral Load Resistance.

Ralli, Z. G., Salazar Gonzalez, R., Tsiotsias, K., & Pantazopoulou, S. J. (2023). Seismic retrofitting of bridge piers using ultra-high performance concrete.

Reggia, A., Morbi, A., & Plizzari, G. A. (2020). Experimental study of a reinforced concrete bridge pier strengthened with HPFRC jacketing. Engineering Structures, 210. https://doi.org/10.1016/j.engstruct.2020.110355

Russell, H. G. (n.d.-a). Ultra-High Performance Concrete: A State-of-the-Art Report for the Bridge Community.

Saikali, R. (2019). Bond behaviour of steel reinforcing bars embedded in ultra-high-performance steel fiber reinforced concrete.

Salazar Gonzalez, R., Wakjira, T. G., Pantazopoulou, S. J., & Alam, S. (2023). *Seismic Retrofitting of RC Bridge Piers using Ultra-High-Performance Concrete Jacketing: State-of-the-art Review*.

Schmidt, Michael., Fehling, Ekkehard., & Geisenhanslüke, Carsten. (2004). Ultra High Performance Concrete (UHPC) : Ein Forschungsbericht. Kassel University Press GmbH.

Shao, Y., Kuo, C. W., & Hung, C. C. (2021). Seismic performance of full-scale UHPC-jacket-strengthened RC columns under high axial loads. Engineering Structures, 243. https://doi.org/10.1016/j.engstruct.2021.112657

Standard Method of Test for Uniaxial Tensile Response of Ultra-High Performance Concrete. (2022).

Standard Test Method for Static Modulus of Elasticity and Poisson's Ratio of Concrete in Compression 1. (n.d.-a). www.astm.org,

Standard Test Method for Static Modulus of Elasticity and Poisson's Ratio of Concrete in Compression 1. (n.d.-b). https://doi.org/10.1520/C0469_C0469M-1

Tastani, S. P., Pantazopoulou, ; S J, Asce, M., Zdoumba, ; D, Plakantaras, ; V, & Akritidis, E. (2006). Limitations of FRP Jacketing in Confining Old-Type Reinforced Concrete Members in Axial Compression. Journal of Composites for Construction, 10(1), 13–25. https://doi.org/10.1061/(ASCE)1090-0268(2006)10:1(13)

Tian, H., Zhou, Z., Wei, Y., & Zhang, L. (2021). Experimental and numerical investigation on the seismic performance of concrete-filled UHPC tubular columns. Journal of Building Engineering, 43. https://doi.org/10.1016/j.jobe.2021.103118

Tong, T., Yuan, S., Zhuo, W., He, Z., & Liu, Z. (2019). Seismic retrofitting of rectangular bridge piers using ultra-high performance fiber reinforced concrete jackets. Composite Structures, 228. https://doi.org/10.1016/j.compstruct.2019.111367

Tsiotsias, K.; Pantazopoulou, S. J. (2022). Cyclic Testing of Concrete Cores Under Confinement with UHPFRC Jackets. 12th Ntnl. Conf. on Earthquake Engineering (12NCEE), Salt Lake City, Utah.

Tsiotsias, K. (2023). Cyclic Performance of RC Columns Retrofitted with UHPFRC. PhD Dissertation, York Univ.

Wang, P., Huang, J., Tao, Y., Shi, Q., & Rong, C. (2022). Seismic performance of reinforced concrete columns with an assembled UHPC stay-in-place formwork. Engineering Structures, 272. https://doi.org/10.1016/j.engstruct.2022.115003

Wang, Y. Z., Wang, Y. B., Zhao, Y. Z., Li, G. Q., Lyu, Y. F., & Li, H. (2020). Experimental study on ultra-high performance concrete under triaxial compression. Construction and Building Materials, 263. https://doi.org/10.1016/j.conbuildmat.2020.120225

Yang, Y. (2019). Tensile behaviour of ultra-high-performance steel fiber reinforced concrete.

Yuan, W., Wang, X., Dong, Z., Zhou, P., & Wang, Q. (2022). Cyclic loading test for RC bridge piers strengthened with UHPC jackets in the corrosive environment. Soil Dynamics and Earthquake Engineering, 158. https://doi.org/10.1016/j.soildyn.2022.107290

Yuan, W., Wang, X., Guo, A., Li, C., Dong, Z., & Wu, X. (2022). Cyclic performance of RC bridge piers retrofitted with UHPC jackets: Experimental investigation. Engineering Structures, 259. https://doi.org/10.1016/j.engstruct.2022.114139

Zhang, Y., Yang, J., Li, T., & Deng, M. (2022). Mechanical behavior of RC columns strengthened with thin UHPC jacket under cyclic loads. Journal of Building Engineering, 49. https://doi.org/10.1016/j.jobe.2022.104065

Zhou, M., Song, J., Yin, S., Zhu, G., Lu, W., & Lee, G. C. (2023). Cyclic performance of severely earthquake-damaged RC bridge columns repaired using grouted UHPC jacket. Engineering Structures, 280. https://doi.org/10.1016/j.engstruct.2023.115615